# FERROELECTRIC DOMAIN STUDIES

## Period 31 January 1998 to 09 December 2001

## Final Report

OFFICE OF NAVAL RESEARCH
Contract No: N00014-98-0326

APPROVED FOR PUBLIC RELEASE –
DISTRIBUTION UNLIMITED

Reproduction in whole or in part is permitted for any
purpose of the United States Government

L. Eric Cross

THE MATERIALS RESEARCH LABORATORY
UNIVERSITY PARK, PA

20030418 047

# REPORT DOCUMENTATION PAGE

*Form Approved*
*OMB No. 0704-0188*

Public reporting burden for this collection of information is estimated to average 1 hour per response, including the time for reviewing instructions, searching data sources, gathering and maintaining the data needed, and completing and reviewing the collection of information. Send comments regarding this burden estimate or any other aspect of this collection of information, including suggestions for reducing this burden to Washington Headquarters Service, Directorate for Information Operations and Reports, 1215 Jefferson Davis Highway, Suite 1204, Arlington, VA 22202-4302, and to the Office of Management and Budget, Paperwork Reduction Project (0704-0188) Washington, DC 20503.

**PLEASE DO NOT RETURN YOUR FORM TO THE ABOVE ADDRESS.**

| 1. REPORT DATE *(DD-MM-YYYY)* | 2. REPORT DATE | 3. DATES COVERED *(From - To)* |
|---|---|---|
| | 3/10/2003 | Final Rpt 31-01-1998-12-09-2001 |

**4. TITLE AND SUBTITLE**
FERROELECTRIC DOMAIN STRUCTURES

**5a. CONTRACT NUMBER**
ONR Contract No. N 00014-98-0326

**5b. GRANT NUMBER**

**5c. PROGRAM ELEMENT NUMBER**

**6. AUTHOR(S)**
L. Eric Cross

**5d. PROJECT NUMBER**

**5e. TASK NUMBER**

**5f. WORK UNIT NUMBER**

**7. PERFORMING ORGANIZATION NAME(S) AND ADDRESS(ES)**
Materials Reseach Laboratory
The Pennsylvania State University
University Park PA 16802

**8. PERFORMING ORGANIZATION REPORT NUMBER**

**9. SPONSORING/MONITORING AGENCY NAME(S) AND ADDRESS(ES)**
Office of Naval Research
ONR 321 SS
Ballaston Centre Tower ONE
500 N. Quincy St.
Arlington Va 2217-5660

Office of Naval Research
Regional Office
536 S. Clark St. Rm 208
Chicago, Ill 60605-1580

**10. SPONSOR/MONITOR'S ACRONYM(S)**

**11. SPONSORING/MONITORING AGENCY REPORT NUMBER**

**12. DISTRIBUTION AVAILABILITY STATEMENT**

**13. SUPPLEMENTARY NOTES**

**14. ABSTRACT**

This program was designed to permit the ONR sponsored program in the Materials Research Laboratory at Penn State, now a component in the Materials Research Institute, to draw upon the expertise of Professor Jan Fousek an internationally respected authority on domain processes in ferroelectrics. The program has sponsored Dr. Fousek for 3 month visits to Penn State in 1999, 2000 and 2001. Dr. Fousek is deeply respected in the MRL and has been able to interact effectively and provide advice which is bearing fruit in both practical and fundamental studies now ongoing and also contemplated in future studies. Topics which have benefited most from the interaction are briefly discussed in the report and several publications which were greatly facilitated are included as appendices to this report.

**15. SUBJECT TERMS**

| 16. SECURITY CLASSIFICATION OF: | | | 17. LIMITATION OF ABSTRACT | 18. NUMBER OF PAGES | 19a. NAME OF RESPONSIBLE PERSON |
|---|---|---|---|---|---|
| a. REPORT | b. ABSTRACT | c. THIS PAGE | | | L.Eric Cross |
| UU | UU | UU | UU | | 19b. TELEPONE NUMBER *(Include area code)* 814-865-1181 |

# FERROELECTRIC DOMAIN STUDIES

L Eric Cross
The Pennsylvania State University
Materials Research Institute
187 Materials Research Laboratory
University Park, PA 16802
Phone: 814-865-1181
Fax: 814-863-7846
E-mail: lec3@psu.edu

Grant Number: N00014-98-0326

ONR Officer: Wallace A. Smith

## TABLE OF CONTENTS


ABSTRACT ..... 1

1. INTRODUCTION ..... 1

2. APPROACH ..... 2
   2.1 Domain Related Studies. ..... 2
   2.2 Strain Gradient Related Properties. ..... 3

3. SUMMARY OF SCIENCE AND TECHNOLOGY INITIATED 4

4. IMPACT/NAVY RELEVANCE ..... 5

5. PLANNED SCIENCE AND TECHNOLOGY ..... 5

6. TECHNOLOGY TRANSFER ..... 5

7. REFEREED PAPERS ..... 6

8. NON REFEREED PAPERS ..... 6

9. BOOKS OR BOOK CHAPTERS PUBLISHED ..... 6

10. BOOKS IN PRESS ..... 6

11. INVITED PRESENTATIONS ..... 7

12. TECHNICAL REPORTS ..... 8

13. INVENTION DISCLOSURE ..... 8

14. PATENTS GRANTED ..... 8

15. PATENTS PENDING ..... 8

16. PRESENTATIONS ..... 8

ABSTRACT

This program was designed to permit the ONR sponsored program in the Materials Research Laboratory at Penn State, now a component in the Materials Research Institute, to draw upon the expertise of Professor Jan Fousek an internationally respected authority on domain processes in ferroelectrics. The program has sponsored Dr. Fousek for 3 month visits to Penn State in 1999, 2000 and 2001. Dr. Fousek is deeply respected in the MRL and has been able to interact effectively and provide advice which is bearing fruit in both practical and fundamental studies now ongoing and also contemplated in future studies. Topics which have benefited most from the interaction are briefly discussed in the report and several publications which were greatly facilitated are included as appendices to this report.

## 1. INTRODUCTION

Domain wall processes are widely accepted to be of major importance in facilitating the performance of piezoelectric materials derived from oxygen octahedron type ferroelectrics with centric prototypic symmetrys as exemplified in the most widely used perovskites structure material families. The solid solution system between lead zirconate and lead titanate (PZT) is much the most widely used piezoelectric ceramic, and here the compositions of most interest cluster around the morphotropic phase boundary (MPB) between ferroelectric rhombohedral and ferroelectric tetragonal forms. Unfortunately at the 52% Zr/48% Ti composition of this phase boundary PZT has proven impossible to grow in single crystal form however, recently lead zinc niobate: lead titanate and lead magnesium niobate: lead titanate have been shown to have pseudo-morphotropic rhombohedral: tetragonal ferroelectric phase boundaries and both can be grown (with some difficulty) in effective single crystal form. Now with control of orientation of the field with respect to the crystal axes, the concepts of Domain Engineering and Domain Averaging could be examined with Fousek, the huge anisotropy in properties explained and massive anhysteretic strain capability rationalized.

A second area which has been most productive was the suggestion to explore flexoelectricity i.e. the generation of electric field/polarization by an elastic strain gradient. The work stemmed from discussions with Fousek concerning composites with oriented cone shaped inclusions which from the shape must be piezoelectric. We concluded the origin of the

charge separation must be the strain gradient induced by the cone shape and determined to explore gradient induced (flexoelectric) effects to see if useful properties could result which would be very different from conventional ceramics.

Throughout the full period of the grant, Fousek and Cross have cooperating in assembling material for a book on Domain Walls and Switching in Ferroic Materials. Unfortunately, the magnitude of the task of writing a truly authoritative work on this topic was originally grossly underestimated and the original proposed time scale has now expanded from 3 to 5 years. The whole significant new area of domain studies in thin films proved a major difficulty and we were fortunate to be joined by Dr. Alexander Tagantsev as a co-author. Now all chapters are undergoing second revisions and the deadline for submission of the manuscript is July 2003.

A third area of activity concerned the important task of completing the new IEEE standard on Ferroelectricity which involves a number of MRL/MRI faculty. The proper definition of polarization in a pyroelectric but non-ferroelectric polar crystal is non trivial but of significant importance as ferroelectrics can occur from polar prototypic groups. Dr. Fousek was of great assistance in removing the inconsistencies, which had vitiated the original standard.

## 2. APPROACH

### 2.1 DOMAIN RELATED STUDIES

The task for this program was not to complete specific studies, but rather to catalyze and explore new areas related to current MRL programs which could have strong relevance to navy needs. It was natural with the major database being generated on domains, domain walls and switching for the book, to be in discussion on the fascinating domain related properties of the important PZN:PT and PMN:PT single crystals being generated in the laboratory.

The publication "Engineering Multidomain Ferroic Samples" by Fousek and Cross (Appendix 1) was probably the first attempt to systematize the possibilities of controlling domain structure to provide regular spacial arrays we called domain geometry engineered samples where the domain is tuned to correspond to the k vectors of fields propagating through the sample and domain average engineered samples where the crystal is sub divided into a very large number of domains so as to yield on averaged "texture" symmetry. The concept is further refined in the letter "Domain Geometry engineering and domain average engineering of

ferroics." (Appendix 2) by Fousek, Litvin and Cross. Here the possibilities for generating a whole range of averaged symmetries for particular sub sets of domains are discussed.

The importance of the domain average engineered structure in the 001 field poled rhombohedral phase of the 0.955 lead zinc niobate 0.045 lead titanate for high strain actuation was underscored in the paper "Domain and Phase Change Contributions to Response in High Strain Piezoelectric Actuators" by Cross. (Appendix 3) Here there is no switching force on the domain walls in the 001 poled condition so that the induced strain is intrinsic and shown to be associated with a rotation of the 111 polarization vector in the domain towards the 001 field direction. The calculated titling of Ps was later confirmed by optical studies by Z. Ye (1).

A further extension of the symmetry arguments to consider explicitly the polar character of the domain is in the paper "Symmetry and antisymmetry in Electroceramics" by Newnham and Cross (Appendix 4) where the sample geometry is used to control modes of vibration and their interaction with the polar structure is a Domain Geometry Engineered context.

A fascinating study, triggered by interaction between Fousek and Cao concerned the characterizations of the strange S wall in Ferroelectrics (Appendix 5). The S walls refer to the domain walls whose orientations do not coincide with simple crystallographic planes but are planes of elastic strain compatibility and change with temperature. A simple continuum model is constructed to describe S wall structures in a proper ferroelastic ($m\bar{3}m \rightarrow mmm$ ferroelastic phase transition). This model describes local values of elastic strain components and the temperature dependence of the S wall orientation. Variation of strain across the S wall are also derived.

## 2.2 STRAIN GRADIENT RELATED PROPERTIES

The major area of activity on strain gradient effects in dielectrics, flexoelectricity was initiated through discussion with Dr. Fousek where we were looking for an explanation of the shape induced piezoelectricity in composites, discussed in Appendix 6. To determine practical feasibility of such a composite measurement of coefficients $\mu_{1111}$, $\mu_{1122}$, $\mu_{1212}$, in lead magnesium niobate: lead titanate ceramic Appendix 7 were initiated.

The very high values of the coefficient $\mu_{12}$ ($\mu_{1122}$) as compared to earlier measurements on polymers lead us to suspect the relaxor character in PMN:PT Appendix 8 and a strong role of micro-polar regions. Further studies on excellent $Ba_{0.7}Sr_{0.3}TiO_3$ ceramics however, revealed

constants even 10 times higher than in PMN:PT (Appendix 9). A very interesting feature of the $(BaSr)TiO_3$ data was a steep upturn in the measured $\mu_{12}$ in the 15° C region above but close to Tc where C departs from regular Curie Weiss behavior.

In further extension of these studies it was decided to explore an unpoled ferroelectric ceramic under very large flexing stress to see if it would be possible to induce piezoelectric poling (Appendix 10) using PZT 5 H obvious ferroelastic poling could be induced at the higher stress levels, and a clear softening of the modulus was evident suggesting the onset of ferroelastic wall motion. Closely coupled to this change was an obvious upturn in the flexoelectric coefficient from 0.5 μc/m to 2.0 μc/m strongly suggesting an extrinsic contribution to $\mu_{12}$ triggered by the ferroelastic wall motion.

We are excited that NUWC at Newport Rhode Island have excellent facilities for very high strain 4 point bending tests and are interested to cooperate in extending the flexoelectric studies to other ceramic and single crystal samples.

A third area, which was of considerable help, concerned the importance task of updating the IEEE standard on Ferroelectricity, a task taken on by the MRL faculty. Here the proper definition of polarization in a pyroelectric but no ferroelectric crystal is non trivial, but very important. The original standard was demonstrably wrong in this context, but with Fousek's help we were able to arrive at a physically consistent definition.

## 3. SUMMARY OF SCIENCE AND TECHNOLOGY INITIATED

The task for the visits of Professor Jan Fousek was not to complete studies on this program, but rather to initiate and advance important new concepts.

(i) Domain Geometry and Domain Average Engineering

Important MRL/MRI programs initiated in contact with Fousek are summarized in Appendixes 1-4. The first initiative in the laboratory on the theory of strange S walls in Appendix 5 opens the more complex topic of strange walls in ferroelectrics and the rubber like elasticity which can be generated.

(ii) Flexoelectricity: This whole exciting new mode of charge separation under strain gradient stems from Fousek's curiosity regarding shape induced piezoelectricity in composites. (Appendix 6-9). Clearly there is a need for more measurements in high permittivity high symmetry systems to understand the origins of the phenomenon and to provide reliable

theoretical underpinning. New measurements on unpoled high symmetry systems suggest that the DC flexoelectric effects may give us new modes for separating intrinsic and extrinsic domain related behaviors (Appendix 10).

(iii) The importance of a proper Ginsburg: Landau formulation for antiferroelectrics is highlighted in the works by Hatt and Gao. (Appendix 11, 12) Unlike earlier Landau formulations this approach permits the proper modeling of the group symmetry and of twin and antiphase boundaries.

(iv) Fousek's most effective help is in formulating vital parts of the new IEEE standard on ferroelectrics took a major load from MRL ONR related faculty and helped to clarify the thinking of both students and faculty in MRI.

## 4. IMPACT/NAVY RELEVANCE

Ferroelectric ceramic systems are very widely used in Navy undersea sonar systems. By its very nature the poled ferroelectric piezoelectric ceramic has strong local gradients in electric and elastic boundary conditions. Flexoelectric effects must be present and in many of the best "soft" compositions relaxor effects occur. We will be providing the quantitative background to understand the importance of these effects. In the newer single crystal transducers domain averaging is exploited in the ultra high coupling rhombohedral compositions. The complexity of possible averaging was ill appreciated.

## 5. PLANNED SCIENCE and TECHNOLOGY

It is anticipated that although the formal program was terminated in September 2001 personal contacts will continue with exchange of ideas on both fundamental and practical issues in ferroelectric crystals and ceramics.

## 6. TECHNOLOGY TRANSFER

A continuous flux of small and mid-sized companies are involved with material and device studies in MRI/MRL and afford many avenues for commercialization. For Navy needs close cooperation with ARL at Penn State is well established and joint programs are now extending to NUSC through Ewart and Amin.

7. REFEREED PAPERS

1 J. Fousek, L.E. Cross, "Engineering Multidomain Ferroic Samples", Ferroelectrics, Vol 252 pg 171-180, 2001

2. J. Fousek, D.B. Litvin, L.E. Cross. "Domain Geometry and domain average engineering of ferroics". J. Phys Condens. Matter 13 L 33, 2001.

3. J. Erhart, W. Cao, J. Fousek, "The Structures of S-Walls in $m\bar{3}m \rightarrow mmm$ Ferroelastics" Ferroelectrics 252 pp 137-144, 2001

4. J. Fousek, L.E. Cross, B. B. Litvin, "Possible piezoelectric composites based on the flexoelectric effect". Materials Letters 39, 287-291, 1999

5. Wenhiu Ma, L.E. Cross, "Observation of the flexoelectric effect in relaxor Pb ($Mg_{1/3}$ $Nb_{2/3}$) $O_3$ Ceramic". Applied Physics Letters 78, No 19 . 2920, 2001.

6. Wenhui Ma, L.E. Cross, "Large Flexoelectric Polarization in Ceramic lead Magnesium Niobate" Applied Physics Letters. 79, No. 26, 4420 4422 Dec 2001

7. W. Ma, L.E. Cross, "Flexoelectric polarization of barium strontium titanate in the paraelectric state" Applied Physic Letters 81 No 18 October 2002

8. R. A. Hatt, W. Cao, "Microscopic Origin of the Two-Sublattice Model for Antiferroelectric State" Ferroelectrics, Vol. 252 pp 129-136- 2001

9. R. A. Hatt, W. Cao, "Landau-Ginzburg model for antiferroelectric phase transitions based on microscopic symmetry" Physical Review B Vol 62 No 2 pp 818-823 July 2000

8. NON REFEREED PAPERS

1. L. E. Cross, "Domain and Phase Change Contributions to Response in High Strain Piezoelectric Actuators", Fundamental Physics of Ferroelectrics 2000 Aspen Winter Workshop, 1 56396-959-9 Edited by Cohen

9 BOOKS OR BOOK CHAPTERS PUBLISHED

1. R. E. Newnham, L.E. Cross, "Symmetry and Antisymmetry in Electroceramics" chapter in "The Art of Ceramics", N. Claussen, Editor, Techna Srl, 2001.

10. BOOKS IN PRESS

1. J. Fousek, L.E. Cross, A. Tagantsev, "Domains and Switching in ferroics" Elsevier; Final stages of assembly (July 2003)

11. INVITED PRESENTATIONS

1. L.E. Cross, S. Park, and S. Liu, "Simple Phenomenological Analysis of the Strain Behavior in Relaxor Ferroelectric Lead Zinc Niobate: Lead Titanate Single Crystals," *SPIE 6th Annual International Symposium on Smart Structures and Materials*, Newport Beach, California, (3-5 March 1999)
2. Xu, B., Yaohong Ye, and L. E Cross, "Dielectric Hysteresis Under Transverse Electric Fields in Sol-Gel Lead Zirconate Titanate Films Deposited on $ZrO_2$ Passivated Silicon," *ISIF 99*, Colorado Springs, Colorado (7-10 March 1999)
3. L. E. Cross, "High Strain Actuator Materials Current Status and Future Prospects: *U.S. Navy Workshop on Acoustic Transduction Materials and Devices*, State College Pennsylvania (13-15 April 1999)
4. L. E. Cross, "Phenomenology of the Elasto-Dielectric Response in the Field Forced Ferroelectric Phases of Lead Zinc Niobate: Lead Titanate (PZN:PT) Relaxor Ferroelectric Single Crystals", *Ferroelectric Workshop in Puerto Rico*, Guanica, Puerto Rico (12-14 May 1999)
5. L. E. Cross. "Electronic Ceramics: Current Progress and Prospects for the 21st Century, *IUMRS-ICAM 99*, Beijing China (13-19 June 1999)
6. L. E. Cross, "Piezoelectricity in Single Crystal Relaxor Ferroelectrics with Morphotropic Phase Boundaries Properties: Processing and Future Prospects", *1999 Annual Conference of British Association for Crystal Growth,* Cambridge, England (16-17 September 1999)
7. L. E. Cross, "New Materials for Smart Applications Progress in the USA", *US: Japan 2nd Collaboration Meeting,* Penn State University, University Park, Pennsylvania, (23 September 1999)
8. L. E. Cross, "New Relaxor Ferroelectric Piezoelectric and Electrostrictive Actuators and Sensors for Smart Materials", *Euromat* 99, Munich, Germany (27-30 September 1999)

9. L. E. Cross, "Current and Potential Future Developments in electrostrictive Actuator Materials", *ICAST 99*, Paris, France (11-13 October 1999)
10. L.E. Cross, "Phase switching perovskites for actuator applications", SPIE 7th Annual International Symposium on Smart Structures and Materials, March, Newport Beach, CA.
11. L.E. Cross, P. Hana, "Progress in the Thermodynamic Phenomenology for the Lead Zinc Niobate : Lead Titanate Solid Solution System", (VII.3), 2000 US Naval Workshop on Acoustic Transduction Materials and Devices, April, State College, PA.
12. L.E. Cross, "PNO38: Domain and phase change contributions to response in high strain ferroelectric materials", The 6th International Symp. On Ferroic Domains and Mesoscopic Structures (ISFD-6), May, Nanjing University.
13. L.E. Cross, "Overview of Active Materials", Aero Smart 2000, Texas A&M University, September, College Station, TX.
14. L.E. Cross, "Domain and Phase Change Contributions to Response in High Strain Piezoelectric Actuators", 3rd Asia Meeting on Ferroelectrics AMF3, December, Hong, Kong,
15. J. Fousek, "The role of soft Dielectric Energy in Poling Ceramics, Glass like systems and in Domain Average Engineering" Proc ISAF10, 2, 679, 2001
16. L. Eric Cross, "Single Domain and extrinsic domain wall contributions to response in ferroelectrics" ISAF10, August 2000, Hawaii

12. TECHNICAL REPORTS
None

13. INVENTION DISCLOSURE
None

14. PATENTS GRANTED
None

15. PATENTS PENDING
None

16. PRESENTATIONS
None

# APPENDIX 1

*Ferroelectrics*, 2001, Vol. 252, pp. 171-180
Reprints available directly from the publisher
Photocopying permitted by license only

© 2001 OPA (Overseas Publishers Association) N.V.
Published by license under the
Gordon and Breach Science Publishers imprint.
Printed in Malaysia

# Engineering Multidomain Ferroic Samples

J. FOUSEK[ab] and L. E. CROSS[b]

[a]*Dept. of Physics and International Center for Piezoelectric Research, University of Technology, Liberec, 46117 Czech Republic and* [b]*Materials Research Laboratory, The Pennsylvania State University, University Park, PA 16802, U.S.A.*

*(Received June 2, 2000)*

The existence of domains is essential in many practical applications of ferroics. Here we discuss devices in which a *fixed* spatial distribution of domains plays the significant role. Depending on the prevailing attributes of multidomain single crystals, three different possibilities can be distinguished. In *domain-geometry-engineered* samples the spatial distribution of domains is tuned to correspond to the *k*-vectors of fields propagating through the material. In *domain-average-engineered* samples the crystal is subdivided into a very large number of domains, representing a *limited* number of domain states. In *domain-wall-engineered* samples the characteristics of static walls can play an essential role in the averaged macroscopic properties. Examples illustrating these approaches are given.

*Keywords:* domain engineering; domain-geometry engineering; domain-average-engineering; domain-wall-engineering; multidomain ferroics; static domain pattern

## 1. INTRODUCTION

Practical applications of ferroics (undergoing a phase transition from the point group G to F) are of two basically different characters: those which rely on properties of single domain samples and those in which the presence of domains is essential. The latter can be categorized into

devices based on dynamical domain processes or those in which a static distribution of domains plays a significant role. Here we discuss the last mentioned case: general characteristics of multidomain samples with fixed spatial distribution of domains.

Depending on the prevailing attributes of multidomain single crystal samples, several possibilities can be distinguished. Those discussed in the following sections 2 to 4 differ in general features of the geometry of domains and it is assumed that domain walls are of negligible thickness. In the last considered case, the thickness of domain walls is finite and specimens exhibit large wall density. Aspects of preparation and properties of such samples are discussed in the section 5.

## 2. DOMAIN-GEOMETRY-ENGINEERED FERROIC SAMPLES

As early as in 1964, Miller[1] showed that a regular pattern consisting of $180^0$ domains in $BaTiO_3$ with a period corresponding to the coherence length could substantially increase the effectiveness of optical second harmonic generation. The idea is based on two factors: a) domain states differ in the sign of nonlinear optical coefficient, b) the width of domains is tuned to the coherence length. It was Feng Duan et al. [2] who succeeded in manufacturing a periodic domain pattern in $LiNbO_3$ and proved its efficiency in nonlinear optics. More recently, S. N. Zhu et al.[3] initiated an essential progress in this field by producing a domain pattern whose geometry corresponds to a Fibonacci superlattice and which makes it possible to realize second harmonic generation for multiple wavelengths. But the significance of domain patterns with engineered geometry was proved also in acoustics. Meeks at el.[4] produced tunable acoustic systems based on spatial modulation of elastic coefficients in a periodic domain pattern in $NdP_5O_{14}$ while Y. Y. Zhu et al.[5] succeeded in producing transducers up to 800 MHz based on spatial modulation of piezoelectric coefficients in multidomain $LiNbO_3$.

In all these applications the periodicity of domain patterns corresponds to $k$-vectors of propagating waves and the multidomain domain systems represent just two domain states. Up to now less than 10 ferroics have been utilized in this area, and in any of these materials the total number of domain states $\nu = |G| / |F| = 2$ (here $|G|$ and $|F|$ stand for the order of the parent and ferroic phase point groups, resp.). This is understandable since to produce a regular pattern in ferroics with $\nu > 2$ in which only two domain states are involved is not trivial.

To solve this task in particular cases experimentally is, however, possible. In fact the nature itself shows that patterns with a regular geometry of a limited number $\mu < \nu$ of domain states can be materialized. Several observations have been made of domain patterns with regular geometry, fulfilling this requirement. As an example, we refer to the Forsbergh's square-net pattern[6] shown in Fig.1, which has been repeatedly observed in $BaTiO_3$ single crystals as well as ceramic grains. It might be inspiring to examine its macroscopic properties for external fields with both $k = 0$ and $k \neq 0$, based on its symmetry characteristics.

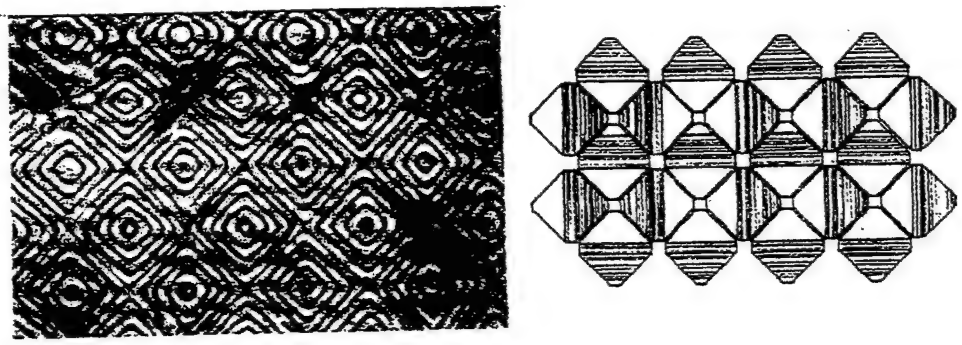

FIGURE 1 Example of a "natural" multiaxial domain-geometry engineered system: the Forsbergh's square-net pattern in tetragonal $BaTiO_3$. Left: microscopic picture; right: arrangement of tetrahedral building blocks. From Ref. [6].

Several other multiaxial threedimensional and reproducible patterns have been observed under natural conditions and there is little doubt that they could be produced artificially. To mention just one more example, we refer to the Arlt's[7] patterns $\alpha$ and $\beta$; till now they have been observed only in ceramic grains but very probably they could be created in crystals under properly designed external forces. Again, in order to deliberate about their properties, the symmetry analysis would be the first step to take.

Indeed, regular domain systems can offer unexpected symmetry properties. Thus, for instance, the well known Hallbach array of magnets with asymmetric distribution of magnetic field can have a simple analogy in thin ferroelectric plates containing a regular system of $90^0$ domain pairs. While in the latter case, because of the existence of free charges, we do not expect pronounced external depolarizing field

effects, macroscopic properties of the array could offer new applicable aspects.

## 3. DOMAIN-AVERAGE-ENGINEERED FERROIC SAMPLES

In contrast to the previous cases, in *domain-average-engineered* samples of ferroic crystals the specimen is subdivided into a very large number of domains, representing just $\mu < \nu$ domain states. Such situations can be achieved by cooling samples through their phase transition temperatures under properly oriented stresses, electric fields or their combinations. The geometry of domains is irregular. The sample's response to external fields is roughly described by tensorial properties averaged over all involved domain states. Thus, e.g. for the piezoelectric response we can write in the zeroth approximation

$$\bar{\varepsilon}_{jk} = \bar{d}_{ijk}\bar{E}_i, \quad \bar{d}_{ijk} = \frac{1}{V}\sum_{\alpha=1}^{\mu} d_{ijk}^{(\alpha)} V^{(\alpha)}.$$

Here $V(\alpha)$ denotes the volume occupied by the domain state $\alpha$.

In recent years, Park et al.[8,9], Yin and Cao[10] and other authors considered a case of this character to discuss piezoelectric properties of PZN-PT single crystals poled along one of the {001} directions. Assuming that the material went through the phase transition from G = $m\bar{3}m$ to F = $3m$, the poling along [100] supports the coexistence of four domain states with spontaneous polarization along the directions [111], [$1\bar{1}1$], [$11\bar{1}$] and [$1\bar{1}\bar{1}$], with equal probability. In this statement, it is assumed that the domain wall orientation aspects (e.g. mechanical compatibility) can be neglected. In fact, in samples of ferroelastic crystals strictly speaking, only one set of mechanically permissible parallel domain walls is allowed[11] while in real samples walls of various orientations coexist connected with additional elastic strains, paid by increased elastic energy.

The symmetry aspects of domain–average–engineered samples can be discussed in a general way. The task is to determine the average point symmetry H, i.e. the symmetry of the subset of domain states contained in the multidomain sample. This was addressed by Fousek et al.[12] and the procedure can be facilitated by the use of the computer programme of Schlesmann and Litvin.[13]

As an example, in Fig.2 we reproduce[12] the average symmetry groups H of six selected subsets of domain states (out of 13 leading to

different symmetries F) which arise in the phase transition specified above (here $\mu = 8$). States are represented by self-explanatory numbers and dots indicating the directions of $\mathbf{P}_S$ vectors.

| Representative subset | Subset symmetry H |
|---|---|
| [1] 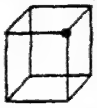 | $3_{xyz}\, m_{\bar{x}y}$ |
| [13] 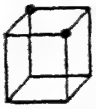 | $m_{xy}\, m_{\bar{x}y}\, 2_z$ |
| [15] 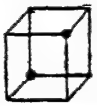 | $\bar{3}_{xyz}\, m_{\bar{x}y}$ |
| [136] 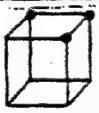 | $m_{xy}$ |
| [1356] 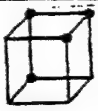 | $2_{\bar{x}z}$ |
| [1368] | $4_z m_x m_{xy}$ |

FIGURE 2 Examples of subsets of domain states corresponding to the transition $m\bar{3}m - 3m$ and their symmetries.

Taking into account the distribution of polar vectors and corresponding strain tensors, one can determine which external forces should be applied in order to obtain any of the domain-average-engineered systems. The trivial example is the subset [1] produced by the electric field **E** along [111]. The subset [1368], discussed[8-10] before, will be produced by the field along [001] while the combination [15] requires the application of a uniaxial stress along [111]. The subset [13] calls for the application of both electric field along [001] and uniaxial stress along [$\bar{1}$10].

In addition to the applied fields, electrical or mechanical, there are other approaches which can eliminate particular domain states in a

given ferroic material. The stimulating example is based on chiral dopants. Keve et al.[14] showed that doping TGS with $L$-α-alanine prefers just one of the two domain states with antiparallel $\mathbf{P}_S$. Zikmund and Fousek[15,16] generalized this approach and showed that chiral substitients can reduce the number of domain states by a factor of two in a number of ferroic species.

It is understood that in the mentioned approaches we leave behind the problems of domain coexistence connected with their mechanical compatibility. It seems obvious that domain average engineering can succesfully lead to formation of crystalline systems with new desired properties in particular in crystals where the domain size is small. Crystalline systems exhibiting tweed microstructures similar to those observed in La-modified lead titanate[17] or PLZT[18] might serve as candidates for this approach.

## 4. PHASE- AND- DOMAIN-AVERAGE ENGINEERED FERROICS

The domain-average-engng concept can be generalized to systems in which the prescribed domain states represent two or more ferroic species. Such multiphase situations occur in PZT ceramics near the morphotropic boundary and originate[19] in concentration gradients as well as in the independent nucleations of the ferroic phases since the transition is of the 1st order. It appears that PZN-PT single crystals with a pronounced piezoelectric response contain blocks of both tetragonal and rhombohedral symmetry[20]. In the basic approximation, the piezoelectric coefficient of a properly poled sample is then described by

$$\bar{d}_{ijk} = \frac{1}{V_1}\left[\sum_{\alpha=1}^{\mu 1} d_{ijk}^{(\alpha)} V^{(\alpha)}\right] + \frac{1}{V_2}\left[\sum_{\beta=1}^{\mu 2} d_{ijk}^{(\beta)} V^{(\beta)}\right] + \\ + \Delta d_{ijk}(walls) + \Delta d_{ijk}(phase\ bndrs)$$

where μ1 and μ2 are numbers of domain states represented in the phase 1 and 2, resp., after poling. The high piezoelectric response of PZN-PT single crystals originates in the combination of intrinsic coefficients $d_{ijk}^{(\alpha)}$, $d_{ijk}^{(\beta)}$ as well as in the extrinsic contributions due to the motion of domain walls and phase boundaries. The question what role is played by any of these contributions is still to be solved.

When addressing the problem of average symmetries of phase-and-domain-average-engineered samples one can follow[21] a similar approach as mentioned above. Consider that two species coexist, namely $m\bar{3}m$–$3m$ and $m\bar{3}m$–$4mm$. It can be shown that when poling along principal directions, i.e. **E** ∥ [001] or **E** ∥ [011] or **E** ∥ [111], regions of the two species differ in the systems of $\mathbf{P}_S$ vectors but are of the same averaged symmetries $4mm$, $mm2$ or $3m$, resp.

It has to be stressed that in both domain-average enginnered and phase-and-domain-average engineered systems, electrical and mechanical compatibility conditions play, in the energy evaluations, a significant role. It is beyond the scope of this presentation to discuss these problems in detail and the subject will be addressed in another paper.

## 5. DOMAIN-WALL-ENGINEERING

In the last considered case, the thickness of domain walls is finite and the specimens exhibit large wall density. As before, the representation of specific walls can be influenced by external forces. In such *domain-wall-engineered* samples the characteristics of static walls can play an essential role in the averaged macroscopic properties.

It was predicted by Walker and Gooding[22] that Dauphiné domain walls in nonpolar quartz can carry a dipole moment and this was later demonstrated experimentally by Snoeck et al.[23], in the incommensurate phase of $SiO_2$. In fact it is easy to demonstrate this possibility for ferroelastic walls. If in the free energy function the invariant $\mu_{ijkl}(\partial\varepsilon_{ij}/\partial x_k)E_l$ is allowed by symmetry, a ferroelastic wall will carry polarization

$$P_l = \mu_{ijkl}\frac{\partial\varepsilon_{ij}}{\partial x_k}.$$

Here the $\mu$-tensor describes the flexoelectric effect. As an example, consider the species $m\bar{3}m - 4/mmm$ represented by crystals of $SrTiO_3$, or $CsPbCl_3$ and the species $m\bar{3}m - 4mm$ describing the properties of $BaTiO_3$. In both cases, ferroelastic walls ($90^0$ wall in the latter case) are, by symmetry, allowed to carry polarization

$$P_x = P_z = (\mu_{1111} - \mu_{3311})\frac{\partial\varepsilon_{xx}}{\partial x};$$

this is demonstrated in Fig. 3. Symmetries of nonferroelastic domain walls from which their possible macroscopic properties can be envisaged have been discussed by Přívratská and Janovec[24].

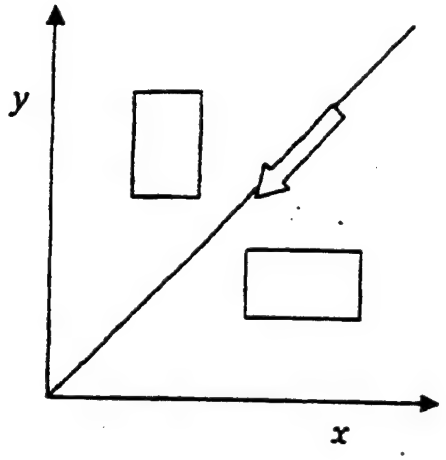


FIGURE 3 Due to flexoelectricity, domain wall separating two ferroelastic domains of species $m\bar{3}m$ – $4/mmm$ or $m\bar{3}m$ – $4mm$ can carry polarization represented by the arrow.

Should macroscopic properties of domain walls play a non-negligible role in the properties of a ferroic sample, they have to occupy a sizable volume. Realistic values of domain width and domain wall thickness are $d_{domain}$ = 1 to 10 μm and $t_w$ = 3 nm, resp. Suppose that the required relative volume occupied by domain walls is 10% and that there so no way how to increase the wall thickness. Then we look for methods how to reduce the average domain width to about 30 nm, i.e. how to increase the wall density 30 times or more.

It appears that there is a significant number of experimental methods which could address this problem. Here we mention in passing only some of those which might be considered. The density of defect-induced order parameter gradients could be increased at crystal growth[2]. The size of AFM-written domains[25] could be further reduced, their density increased. Attempts to freeze-in high density tweed structures[26] in some ferroelastics close above $T_C$ or high density pattern of discommensurations in modulated phases close above the lock-in temperatures[27] appear attractive. Fixing photorefractive gratings by domains[28] in ferroelectrics with small $P_S$ (small defect-

assisted nucleation energies to produce domains in real time) looks also promissing.

## 6. CONCLUSIONS

Till now, the field of domain geometry engineering has been succesfully developed and applied to ferroics representing five species of ferroelectrics and one species of ferroelastics, all with two domain states. Such specimens proved to be competitive in the field of nonlinear optics and promissing in the field of ultrasonic generation and detection. But much more complex domain systems are obtainable and have not yet been considered and investigated.

Two new areas of research appear to be very promissing. Domain- and phase-average engineered systems offer increased values of macroscopic properties, probably strengthened by domain wall and/or phase boundary induced motions. We still miss detailed data about the real structure of existing compounds like PZN-PT as well as theoretical analysis of multiple domain states compatibility, the more so for multiple phase systems. Domain-wall engineered samples with high density of walls also promise a new interesting research and application area. At present, particular systems useful in selected applications could be specified and methods to produce high density domain patterns investigated experimentally.

***Acknowledgments***

J.F. appreciates the support of the Ministry of Education of the Czech Republic (Project VS 96006) and the assistance of the Materials Research Laboratory, The Pennsylvania State University.

### *References*

[1] R. C. Miller. *Phys. Rev.* **134,** A1313 (1964).
[2] D. Feng, N. B. Ming, J. F. Hong, Y. S. Yang, J. S. Zhu, Z. Yang and Y. N. Wang, *Appl. Phys. Lett.* **37,** 607 (1980).
[3] S. N. Zhu, Y. Y. Zhu, Y. Q. Qin, H. F. Wang, C. Z. Ge and N. B. Ming, *Phys. Rev. Lett.* **78,** 2752 (1997).
[4] S. W. Meeks, L. Clarke and B. A. Auld, IEEE Ultrasonics Symposium, San Francisco, CA (1985).
[5] Y. Y. Zhu, N. B. Ming, W. H. Jiang and Y. A. Shui. *Appl. Phys. Lett.* **53,** 1381 (1988).
[6] P. W. Forsbergh, Jr., *Phys. Rev.* **76,** 1187 (1949).
[7] G. Arlt and P. Sasko. *J. Appl. Phys.* **51,** 4956 (1980).
[8] Seung-Eek Park and T. R. Shrout. *J. Appl. Phys.* **82,** 1804 (1997).
[9] Seung-Eek Park. S. Wada. P. W. Rehrig, Shi-Fang Liu, L. E. Cross and T. R. Shrout, "Crystallographic Engineering in High-performance Piezoelectric Crys tals." Paper presented at SPie Smart tructures and Materials (New Port Beach. 1999).

[10] Jianhua Yin and W. Cao, *J. Appl. Phys.* **87,** 7438 (2000).
[11] J. Fousek and V. Janovec, *J. Appl. Phys.* **40,** 135 (1969).
[12] J. Fousek, D. B. Litvin and L. E. Cross, submitted.
[13] J. Schlessman and D. B. Litvin, *Acta Cryst.* **A51,** 947 (1995).
[14] E. T. Keve, K. L. Bye, P. W. Whipps and A. D. Annis, *Ferroelectrics* **3,** 39 (1971).
[15] Z. Zikmund and J. Fousek, *Ferroelectrics* **79,** 73 (1988).
[16] Z. Zikmund and J. Fousek, *phys. stat. sol. (a)* **112,** 625 (1989) and **118,** 539 (1990).
[17] G. A. Rossetti, Jr., W. Cao and C. A. Randall, *Ferroelectrics* **158,**343 (1994).
[18] C. A. Randall, G. A. Rossetti, Jr. and W. Cao, *Ferroelectrics* **150,**163 (1993).
[19] V. A. Isupov, *Ferroelectrics* **46,** 217 (1983).
[20] K. Fujishiro, R. Vlokh, Y. Uesu, Y. Yamada, J.-M. Kiat, B. Dkhil and Y. Yamashita, *Jpn. J. Appl. Phys.* **37,** 5246 (1998).
[21] J. Fousek, D. B. Litvin and L. E. Cross, to be published.
[22] M. B. Walker and R. J. Gooding, *Phys. Rev. B* **32,** 7408 (1985).
[23] E. Snoeck, P. Saint-Gregoire, V. Janovec and C. Roucau, *Ferroelectrics* **155,** 371 (1994).
[24] J. Přívratská and V. Janovec, *Ferroelectrics* **191,** 17 (1997).
[25] L. M. Eng, M. Bammerlin, Ch. Loppacher, M. Guggisberg, R. Bennewitz, R. Lüthi, E. Meyer, Th. Huser, H. Heinzelman and H.-J. Güntherodt, *Ferroelectrics* **222,** 153 (1998).
[26] A. M. Bratkovsky, E. K. H. Salje and V. Heine, *Phase Transitions* **52,** 77 (1994).
[27] V. Novotna, H. Kabelka, J. Fousek, M. Havrankova and H. Warhanek, *Phys. Rev. B* **47,** 11019 (1993).
[28] J. Fousek, M. Marvan and R. S. Cudney, *Appl. Phys. Letters* **72,** 430 (1998).

# APPENDIX 2

INSTITUTE OF PHYSICS PUBLISHING JOURNAL OF PHYSICS: CONDENSED MATTER

J. Phys.: Condens. Matter 13 (2001) L33–L38 www.iop.org/Journals/cm PII: S0953-8984(01)17769-6

LETTER TO THE EDITOR

# Domain geometry engineering and domain average engineering of ferroics

**J Fousek[1,2], D B Litvin[3] and L E Cross[2]**

[1] Department of Physics and International Centre for Piezoelectric Research, Liberec University of Technology, Liberec, CZ 46117, Czech Republic
[2] Materials Research Laboratory, The Pennsylvania State University, University Park, PA 16802, USA
[3] Department of Physics, The Pennsylvania State University, Berks Campus, Reading, PA 19610, USA

Received 5 October 2000

**Abstract**

Multidomain samples of ferroics (ferroelectrics, ferroelastics, and related materials) with *fixed* geometrical distribution of domains can offer new macroscopic properties required for particular applications. Two extreme cases of such applications are defined. In *domain-geometry-engineered* samples of ferroic crystals, the spatial distribution of domains and thus the spatial distribution of tensorial properties is tuned to correspond to the $k$-vectors of applied electric, optical or acoustic fields. For a given wavelength, the size, geometry, and distribution of domains give rise to a qualitatively new kind of response specified by the symmetry of the multidomain system. In *domain-average-engineered* samples of ferroic crystals, the specimen is subdivided into a very large number of domains, representing $\mu$ domain states where $\mu$ is smaller than the theoretically allowed maximum number, and forming a regular or irregular pattern. Its response to external fields is roughly described by tensorial properties averaged over all of the domain states involved. The effective symmetry of the domain-average-engineered system is given by a point group $H$ and we show how it can be determined. As an example, all groups $H$ are specified for domain-average-engineered samples which can arise in a material undergoing the phase transition with symmetry change from $m\bar{3}m$ to $3m$.

Ferroic materials (and here we concentrate on non-magnetic materials, i.e. on ferroelectrics, ferroelastics, and higher-order ferroics) play an essential role in a number of technical applications. In some of them, dynamic domain processes are essential (e.g. thin-film memories, electron emitters) while in others the static distribution domains in the sample play the crucial role. In this contribution we concentrate on the latter case and wish to specify a clear distinction between two kinds of such static multidomain system.

We have in mind materials undergoing a structural phase transition from the parent phase of point group $G$ into the ferroic phase of symmetry $F \subset G$ (such a material is referred to

0953-8984/01/010033+06$30.00 © 2001 IOP Publishing Ltd Printed in the UK 

as belonging to the species $G - F$). This leads necessarily to the possibility of a coexistence of $\nu$ domain states [1]; $\nu = |G|/|F|$ where $|A|$ is the order of the group $A$. Assuming that domain walls are of negligible thickness compared with the size of the domains, there are two different ways of specifying—and utilizing—properties of a multidomain sample with a *fixed* distribution of domains; we propose to refer to them as *domain geometry engineering* and *domain average engineering*, respectively. It is the purpose of this contribution to give their definitions and in particular to specify symmetry properties of domain-average-engineered multidomain samples.

First, we consider *domain geometry engineering*. Consider a multidomain sample for which the geometry of the spatial distribution of domains and therefore that of the tensorial material coefficients is specified. Macroscopic responses of such samples to external fields (forces) of defined frequency are determined by this distribution. If the applied fields are static, the response of a multidomain sample is primarily determined by the spatial distribution of tensorial properties (domains) and of the applied field, and codetermined by the boundary conditions along domain walls. (Only in cases of the simplest geometry of domains, namely a single system of parallel domain walls in the case of ferroelastic species, can the latter be eliminated.) As an example, consider a multidomain piezoelectrically active sample. The spatial distribution of strain is

$$\varepsilon_{jk}(r) = d_{ijk}(r)E_i(r) \tag{1a}$$

$$d_{ijk}(r) = d_{ijk}^{(\alpha)} f^{(\alpha)}(r) \tag{1b}$$

where $d_{ijk}$ stands for the piezoelectric tensor, the factor $f^{(\alpha)}(r) = 0$ or 1, and $\alpha$ denotes the domain state: $\alpha = 1, 2, \ldots, \mu$ with $\mu \leqslant \nu$. Domain geometry engineering related to *dynamic external fields* is of particular interest. The $k$-vector of the applied fields defines the wavelength whose magnitude is chosen to be appropriately related to the size of domains and whose direction is correlated with the domain geometry. For a given wavelength, the size, geometry, and distribution of domains give rise to a qualitatively new kind of response specified by the symmetry of the multidomain system. In the example specified above, we expect the presence of new piezoelectric resonance frequencies. It was this case which was suggested by Newnham *et al* [2], offering new resonance modes of a two-domain sample. Recently, more involved multidomain piezoelectric systems were suggested and realized [3] in crystals of $LiNbO_3$ and $LiTaO_3$. Referred to as acoustic superlattices, they can be used to generate and detect ultrasonic waves with frequencies in the range up to several hundreds of MHz. Another example, which has received unusual attention, is quasi-phase-matched optical multipliers. When the conventional phase-matching condition ($n_{2\omega} = n_\omega$) cannot be realized in a particular material because of unsuitable dispersion of refractive indices, often a quasi-phase-matched system can be constructed which offers a high integrated non-linear optical response leading to frequency doubling [4]. This requires that a periodic domain pattern be fabricated with a period twice the coherence length $l_c$. Such domain-shape-engineered systems are now widely used. An even more intricate geometry-engineered domain pattern has been designed [5] in which two geometrically different building blocks A, B, each containing two domains with antiparallel spontaneous polarizations, are arranged to form a Fibonacci sequence. This leads to the possibility of second-harmonic light generation simultaneously for several optical frequencies.

While domain-geometry-engineered systems have been repeatedly realized and theoretically analysed, the alternative approach to studying and utilizing multidomain ferroic samples with static chaotic distribution of domains has only recently become extremely attractive. By the term *domain average engineering* we mean a situation in which the ferroic sample is subdivided into a very large number of domains, representing $\mu$ domain states where

$\mu < \nu$, and forming a regular or irregular pattern. Ideally, the domain size is expected to be much smaller than the wavelength of externally applied fields. Here, in contrast to the case for domain shape engineering, the spatial distribution of tensorial material coefficients is not defined or is irrelevant. The response of the sample can be to some approximation described by tensorial properties averaged over all domain states involved. Considering, as an example, again a sample consisting of piezoelectrically active domains, we expect for the multidomain sample

$$\bar{\varepsilon}_{jk} = \bar{d}_{ijk}\bar{E}_i \tag{2a}$$

$$\bar{d}_{ijk} = \frac{1}{V}\sum_{\alpha=1}^{\mu} d_{ijk}^{(\alpha)} V^{(\alpha)} \qquad \mu < \nu. \tag{2b}$$

Both equations (1), (2) can be easily generalized for tensors of higher order.

Recently, a case of this character was considered [6–8] to allow discussion of piezoelectric properties of PZN-PT single crystals poled along one of the {001} directions. Assuming that the material went through the phase transition from $G = m\bar{3}m$ to $F = 3m$, poling along [100] supports the coexistence of four domain states with spontaneous polarization along the directions [111], [$1\bar{1}1$], [$11\bar{1}$], and [$1\bar{1}\bar{1}$], with equal probability. In this statement, it is assumed that the domain wall orientation (i.e. mechanical compatibility) aspects can be neglected. In fact, in samples of ferroelastic crystals, strictly speaking, only one set of mechanically permissible parallel domain walls is allowed [9] while in real samples walls of various orientations coexist connected with additional elastic strains, paid for by increased elastic energy [10].

We now discuss the symmetry of *domain-average-engineered* samples in which the volumes of the domain states represented are identical, i.e. $V(\alpha) = V/\mu$. Such situations can be achieved by cooling samples through their phase transition temperatures under properly oriented stresses, electric fields or combinations of these. We introduce a classification of domain-average-engineered ferroic samples and determine their average point symmetries. This average symmetry is taken to be the symmetry of the subset of domain states contained in the multidomain ferroic sample.

Consider the phase transition from $G$ to $F$. The symmetry analysis is based on the coset decomposition of the point group $G$ with respect to its subgroup $F$, i.e.

$$G = F + g_2F + g_3F + \cdots + g_\nu F$$

where the elements $g_i$ are the coset representatives of the decomposition and $g_1 = 1$. We denote the $\nu$ domain states which may arise at the transition as $S_1, S_2, \ldots, S_\nu$. The symmetry groups $F_i$ of the domain states and the relative orientations of the domain states and their polarizations $P_i$ are all determined by the coset representatives, i.e. $F_1 = F$, $F_i = g_iF_1g_i^{-1}$, $S_i = g_iS_1$, and $P_i = g_iP_1$, $i = 2, 3, \ldots, \nu$. The closure of the group $G$ under multiplication implies a permutation of the cosets of the coset decomposition and in turn a permutation of the domain states $S_i$ under elements $g$ of $G$. The action of an element $g$ of $G$ on $S_i$ is defined as $gS_i = gg_iS_1 = g_jfS_1 = g_jS_1 = S_j$, where $f$ is an element of $F$, and the domain state $S_i$ is transformed by the element $g$ into the domain state $S_j$. The action of an element $g$ of $G$ on a subset of domains is denoted by $g\{S_1, S_2, \ldots, S_\mu\} = \{gS_1, gS_2, \ldots, gS_\mu\}$.

Two subsets of domains $\{S_1, S_2, \ldots, S_\mu\}$ and $\{S'_1, S'_2, \ldots, S'_\mu\}$ are said to belong to the same class of subsets of domains if there exists an element $g$ of $G$ such that $g\{S_1, S_2, \ldots, S_\mu\} = \{gS_1, gS_2, \ldots, gS_\mu\} = \{S'_1, S'_2, \ldots, S'_\mu\}$. The symmetry group $H$ of a subset of domains $\{S_1, S_2, \ldots, S_\mu\}$ is defined as the group of all elements $g$ of $G$ which leave the set invariant, i.e. $g\{S_1, S_2, \ldots, S_\mu\} = \{S_1, S_2, \ldots, S_\mu\}$. The group $H$ represents the effective symmetry of the domain-average-engineered system consisting of the subset of domains $\{S_1, S_2, \ldots, S_\mu\}$.

As an example, we consider the phase transition from $G = m\bar{3}m$ to $F = 3_{xyz}m_{\bar{x}y}$. Here $\nu = 8$. The indexing of the domain states, the corresponding coset representatives of the coset decomposition of $G$ with respect to $F$, the symmetry groups, and the corresponding polarizations in each domain state are given in table 1.

**Table 1.** Domain state index, coset representative, symmetry group, and polarization.

| Index $i$ | Coset representative $g_i$ | $F_i = g_i F_1 g_i^{-1}$ | $P_i = g_i P_1$ |
|---|---|---|---|
| 1 | 1 | $3_{xyz}m_{\bar{x}y}$ | $(A, A, A)$ |
| 2 | $2_x$ | $3_{\bar{x}yz}m_{\bar{y}z}$ | $(A, -A, -A)$ |
| 3 | $2_z$ | $3_{xy\bar{z}}m_{\bar{x}y}$ | $(-A, -A, A)$ |
| 4 | $2_y$ | $3_{x\bar{y}z}m_{\bar{x}z}$ | $(-A, A, -A)$ |
| 5 | $\bar{1}$ | $3_{xyz}m_{\bar{x}y}$ | $(-A, -A, -A)$ |
| 6 | $m_x$ | $3_{\bar{x}yz}m_{\bar{y}z}$ | $(-A, A, A)$ |
| 7 | $m_z$ | $3_{xy\bar{z}}m_{\bar{x}y}$ | $(A, A, -A)$ |
| 8 | $m_y$ | $3_{x\bar{y}z}m_{\bar{x}z}$ | $(A, -A, A)$ |

All subsets of these domain states have been classified into classes as defined above. In table 2 we list one subset of domain states from each class. Each subset is denoted by listing, between square brackets, the indices of the domain states contained in that subset, the indices having been given in table 1, e.g. the subset $\{S_1, S_3, S_5\}$ is denoted by [135]. In the right-hand column is the subgroup $H$ of elements of $G$ which leave the corresponding subset invariant. This table, in fact, represents the list of domain-average-engineered systems which can arise in a material undergoing a phase transition from $m\bar{3}m$ to $3m$.

**Table 2.** Representative subsets of domain states for the species $m\bar{3}m - 3m$ and the subgroups of $m\bar{3}m$ which leave them invariant.

| Representative subset | Symmetry $H$ of the subset |
|---|---|
| [1] or [2345678] | $3_{xyz}m_{\bar{x}y}$ |
| [13] or [245678] | $m_{xy}m_{\bar{x}y}2_z$ |
| [15] or [234678] | $\bar{3}_{xyz}m_{\bar{x}y}$ |
| [16] or [234578] | $m_x m_{\bar{y}z}2_{yz}$ |
| [123] or [45678] | $3_{xyz}m_{xz}$ |
| [135] or [24678] | $m_{\bar{x}y}$ |
| [136] or [24578] | $m_{xy}$ |
| [1234] | $\bar{4}3m$ |
| [1235] | $m_{\bar{x}z}$ |
| [1238] | $3_{x\bar{y}z}m_{\bar{x}z}$ |
| [1356] | $2_{\bar{x}z}$ |
| [1357] | $m_{xy}m_{\bar{x}y}m_z$ |
| [1368] | $4_z m_x m_{xy}$ |

In figure 1, for each subset listed in table 2, we schematically represent the array of domain states and their polarizations associated with the domain states of each subset. Each domain state is denoted by a heavy dot at a corner of the cube. This represents a polarization from the centre of the cube to that corner—that polarization given in table 1 associated with the corresponding domain state. Subfigure [1] denotes the single-domain state with polarization

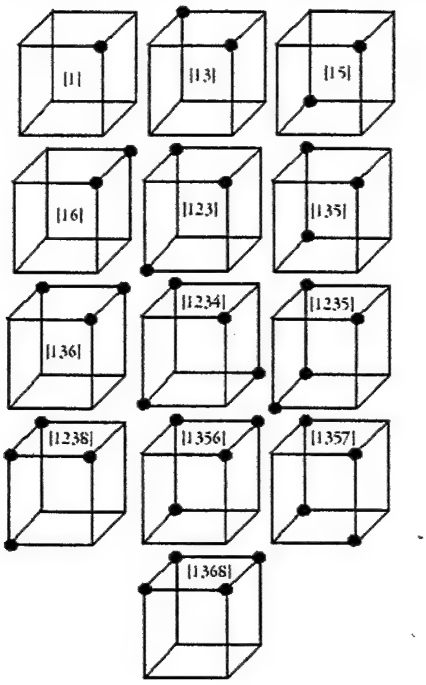


**Figure 1.** Graphical representation of the subsets of domain states whose symmetries are specified in table 1. Points at the cube vertices represent spontaneous polarization vectors; the origin is in the centre of the cube. The numbering is that of the indices of the domains and polarizations given in table 1.

in the [111] direction. The figure denoted by [1368], e.g., denotes a multidomain sample in which the following polarization vector directions are equally represented: [111], $[\bar{1}\bar{1}1]$, $[1\bar{1}1]$, and $[\bar{1}11]$. The corresponding symmetry groups of all these multidomain systems are listed, as already pointed out, in the right-hand-side column of table 2.

Taking into account the distribution of polarization vectors and corresponding strain tensors, one can determine which external forces should be applied in order to obtain any of the domain-average-engineered systems listed in table 1. The trivial example is the system [1] produced by the electric field $\boldsymbol{E}$ along [111]. The system [1368], discussed above (see references [6–8]) will be produced by the field along [001] while the system [16] requires the application of the field along [011]. The combination [15] requires the application of a uniaxial stress along [111] while the system [13] calls for the application of both an electric field along [001] and a uniaxial stress along $[\bar{1}10]$.

It is understood that in this symmetry approach we leave behind problems of coercive fields and stresses as well as, as already mentioned, problems of domain coexistence connected with their mechanical compatibility. It seems obvious that domain average engineering can successfully lead to the formation of crystalline systems with new desired properties, in particular in crystals where the domain size is small.

Each of the methods of domain engineering specified above can open a new vista of materials research possibilities in the area of ferroic materials and lead to multidomain assemblies with new desired properties.

JF appreciates the support of the Ministry of Education of the Czech Republic (Project No VS96006) and the assistance of the Materials Research Laboratory, The Pennsylvania State University; DBL acknowledges the hospitality of Dr V Kopsky and the Institute of Physics of the Czech Academy of Sciences, and the support of the Czech Ministry of Education under Grant ME336(1999) and of the National Science Foundation under Grants No DMR-9722799 and No DMR 0074550.

## References

[1] Aizu K 1970 *Phys. Rev.* B **2** 754–72
[2] Newnham R E, Miller C S, Cross L E and Cline T W 1975 *Phys. Status Solidi* a **32** 69–78
[3] Chen Y F, Zhu A N, Zhu Y Y, Ming N B, Jin B B and Wu R F 1997 *Appl. Phys. Lett.* **70** 592–4
[4] Duan F, Ming N B, Hong J F, Yang Y S, Zhu J S, Yang Z and Wang Y N 1980 *Appl. Phys. Lett.* **37** 607–9
[5] Zhu S N, Zhu Y Y, Qin Y Q, Wang H F, Ge C Z and Ming N B 1997 *Phys. Rev. Lett.* **78** 2752–5
[6] Park S E and Shrout T R 1997 *J. Appl. Phys.* **82** 1804–11
[7] Wada S, Park S E, Cross L E and Shrout T R 1999 *Ferroelectrics* **221** 147–55
[8] Yin J and Cao W 2000 *J. Appl. Phys.* **87** 7438–41
[9] Fousek J and Janovec V 1969 *J. Appl. Phys.* **40** 135–42
[10] Salje E K H and Ishibashi Y 1996 *J. Phys.: Condens. Matter* **8** 8477–95

# APPENDIX 3

# Domain and Phase Change Contributions to Response in High Strain Piezoelectric Actuators

L. Eric Cross

Evan Pugh Professor Emeritus of Electrical Engineering
Materials Research Laboratory
The Pennsylvania State University
University Park, PA 16802 USA

**Abstract.** Current solid state actuators are briefly compared to traditional actuator technologies to highlight the major need for enhanced strain capability. For the ferroelectric piezoelectric polycrystal ceramics, the balance of evidence suggests a large entrinsic contribution to the field induced strain from ferroelectric-ferroelastic domain wall motion. Here-to-fore the intrinsic single domain contribution has been derived indirectly from phenomenological analysis. Now, new evidence of a stable monoclinic phase at compositions very close to the MPB suggest that the previous assessment will need to be revised.

Actuator behavior in the new lead zinc niobate-lead titanate (PZN:PT) single crystal shows most unusual anisotropic behavior. For 111 oriented field poled crystals in the rhombohedral phase normal low induced strain is observed. For 001 field poled crystals however massive (0.6%) quasi-linear anhysteritic strain can be induced. Since the 001 oriented field in the rhombohedral phase can not drive ferroelastic domain walls it is suggested that the strain must be intrinsic. The suggestion is that it is due to an induced monoclinic phase in which the Ps vector tilts under increasing field up to more than 20° from 111, before the vector switches to the tetragonal 001 direction. Such a polarization rotation mechanism has also been suggested by Fu and Cohen [1]. Calculations of induced single domain strain using measured electrostriction constants agree well with observed behavior.

Recent measurements by Park et al [2] and Wada et al [3] on single crystal $BaTiO_3$ show strongly enhanced piezoelectricity at temperatures near the ferroelectric phase transitions. Of particular relevance is the inverse experiment forcing the tetragonal over to the rhombohedral phase with high 111 oriented field. From this result it is suggested that both cubic and dodecahedral mirrors participate in the reorientation through orthorhombic to the rhombohedral state giving rise to different value of the induced $d_{33}$ at different field levels.

CP535, *Fundamental Physics of Ferroelectrics 2000: Aspen Center for Physics Winter Wkshp.*, edited by R. E. Cohen
© 2000 American Institute of Physics 1-56396-959-9/00/$17.00

# INTRODUCTION

Characteristics of stress levels, strain capability and efficiency for a number of actuator systems are summarized in Table 1. Traditional electromagnetic, pneumatic and hydraulic systems have high efficiency good stroke (strain levels) and adequate force. They are however bulky, rather slow, and require extensive backup generator equipment. Solid state electrical piezoelectric, electrostrictive and phase switching actuators clearly have adequate force, tolerable efficiency, however the stroke permitted by induced strain levels is miniscule. These materials are still important as the actuation can be very fast, inertia is low and compact systems can be engineered, however there is still a major need for enhanced strain capability.

In this paper, the mechanisms responsible for strain in the polycrystal ferroelectric ceramics will be discussed. Currently the balance of evidence points to a major contribution from ferroelastic domain wall motion particularly in the soft PZTs, but the discovery of a new monoclinic phase, just at the critical morphotropic phase boundary composition requires a re-assessment of the intrinsic contribution to response. Evidence from the new lead zinc niobate:lead titnate (PZN:PT) single crystals suggests that the ultra high strain in 001 field poled crystals may be dominantly intrinsic involving the field induction of a monoclinic phase in which $P_s$ is strongly tilted in the dodecahedral mirror plane before finally switching to the 001 polar tetragonal form. Recent experiments on $BaTiO_3$ where the inverse experiment, forcing the tetragonal over to rhombohedral symmetry by high (111) oriented E-field at room temperature lends further support for a monoclinic mechanism for the switching, but now involving both cubic and dodecahedral mirrors.

## *Polarization and Strain Mechanisms*

For the simple linear nonferroelectric insulator the induced deformation under electric field may be described by

$$x_{ij} = s_{ijkl}X_{ij} + d_{mij}E_m + M_{mnij}E_mE_n \qquad (1)$$

where $x_{ij}$ are components of induced strain, $X_{ij}$ components of applied stress $E_m$, $E_n$ components of electric field $s_{ijkl}$ the elastic compliance, $d_{mij}$ the piezoelectric tensor and

$M_{mnij}$ the electrostriction coefficients. Obviously if the $d_{mij}$ are non zero, in the absence of stress

$$x_{ij} = d_{mij}E_m \qquad (2)$$

TABLE 1. Salient Features of Traditional and Solid State Actuators

*TRADITIONAL TECHNOLOGIES*

| | Stress (MPa) | Strain | Efficiency |
|---|---|---|---|
| Electromagnetic | 0.02 | 0.5 | 90% |
| Hydraulic | 20 | 0.5 | 80% |
| Pneumatic | 0.7 | 0.5 | 90% |

*SOLID STATE ACTUATORS*

| | Stress (MPa) | Strain | Efficiency |
|---|---|---|---|
| Shape Memory Alloys | 200 | 01 | 3% |
| Piezoelectric | 35 | 0.002 | 50% |
| Electrostrictive | 50 | 0.002 | 50% |
| Phase Switching Electroceramic | 50 | 0.004 | ? |
| Electrostrictive Polyurethane | 0.1 | 0.10 | 20% |
| Contractile Polymer | 0.3 | 0.5 | 30% |
| Muscle | 0.35 | 0.2 | 30% |

which is the piezoelectric actuation function and if the $d_{mij}$ are zero by symmetry

$$x_{ij} = M_{mnij}E_mE_n \tag{3}$$

and the system will be electrostrictive.

In a polycrystal ensemble, as for the randomly axed ceramic, the system is much more complex. With any symmetry in the crystallites (fig. 1a) the random axial arrangement will introduce two infinite fold rotation axes ($\infty\infty$) in the macro-ensemble symmetry wiping out all piezoelectricity. One of the few way out of this dilema is to consider a ferroelectric crystallite where in the ferroelectric state spontaneous electric polarization is distributed in domains with different equivalent orientation states that can be reoriented by an external poling field (fig. 1b). The remanent polar vector drops the macro-symmetry to conical ($\infty m$) which is piezoelectric with non zero $d_{31} = d_{32}$, $d_{33}$, $d_{15} = d_{24}$.

All practical polycrystal ceramic actuators use compositions in the lead zirconate:lead titanate (PZT) solid solution system (fig. 1c). The reason for the infatuation with PZT is the near vertical (morphotropic) phase boundary close to the 52:48 Zr/Ti cation ratio, separating tetragonal and rhombohedral ferroelectric phases. Qualitatively two clear advantages stem from working with compositions near this boundary, and this is where most practical systems are pitched.

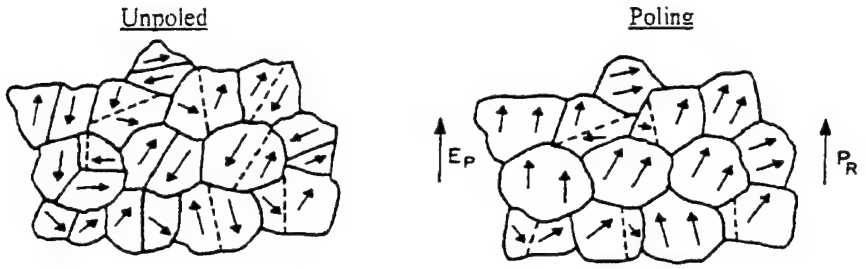


(a) the symmetry is ∞∞∞m which is centric and forbids piezoelectricity

(b) the symmetry is ∞m which is non centric (polar) and permits piezoelectricity.

*Macro Symmetry and the importance of poling of a ferroelectric species.*

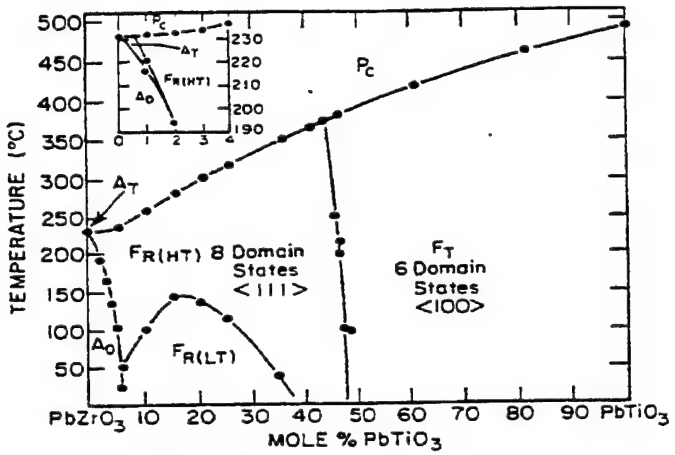


(c) Lead zirconate titanate phase diagram.

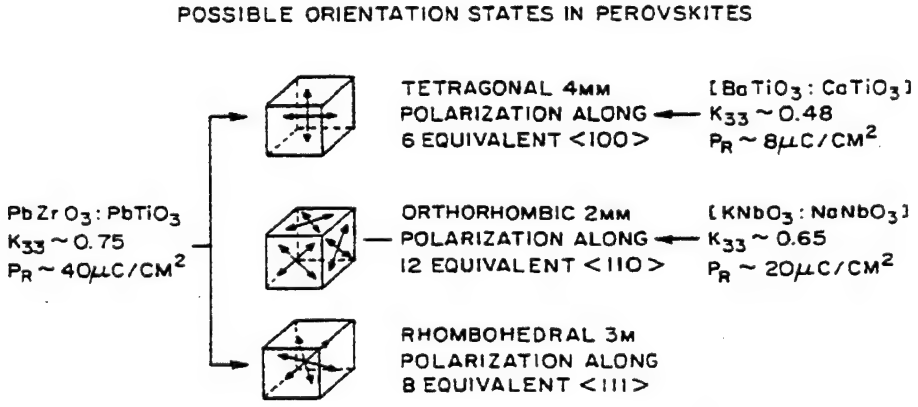


(d) Importance of many orientation states for polycrystal polability and performance.

**FIGURE 1.** Important features in piezoelectric polycrystal ceramic materials.

Firstly, the MPB is a first order phase change, so that in the co-existence region for the two phases it is possible in the poling process to make use of 14 domain orientation states (fig. 1d) leading to more complete poling. Secondly, for properly chosen compositions one can stay close to the phase boundary over a wide temperature range and use its destabilizing influence to enhance the intrinsic polarizability of the single domain states.

From these basic advantages stem two fundamental problems in understanding the behavior. Firstly, what is the balance between intrinsic single domain and extrinsic contributors to response; and secondly, what exactly is the nature of the dominant extrinsic contributor.

In the randomly axed polycrystal ceramic, ferroelectric domain wall motion is essential to permit the induction of strong remanent polarization essential for piezoelectricity. For the quasi-reversible behavior working about this induced remanent polar state the question is to what extent are ferroelastic:ferroelectric wall motions the primary extrinsic contributor to both dielectric and piezoelectric response.

No practical PZTs are in fact pure lead zirconate titanate solid solutions, all are modified by aleovalent cation additions (fig. 2). We speak of excess charge cation added or donor doped soft PZTs, and of charge deficient cation or Acceptor doped hard PZTs. The terminology "hard" versus "soft" is derived from magnetism and clearly implying difficult or easy domain wall motion as in the magnetic counterparts. For the hard PZTs however, there is compelling evidence [4,5], that stabilization by weakly mobile oxygen vacancy:defect dipole pairs is of the whole domain not just the wall. A mechanism that has no counterpart in magnetism but does however indirectly make the walls more difficult to move.

In soft donor doped PZTs, there is very strong evidence for enhanced extrinsic response in both dielectric and piezoelectric behavior, however evidence that it is associated with domain wall motion is indirect. It is clear that at fields well below the coercivity, the response is hysteritic [6] and can be well described by the Rayleigh law [7] suggesting a domain wall origin. There is however also evidence from transmission electron microscopy that the donor dopants tend to break-up the normal domain structure leading to tweed like and micro-polar relaxor like structures [8].

Earlier a rather complete phenomenology has been presented for the whole PZT family [9-13] from which single domain intrinsic values can be dervied for both tetragonal and rhombohedral phases adjacent to the MPB and averaged values for permittivity and piezoelectric response derived. It was on this basis that some 80% of dielectric response in hard PZTs, but only of order 30% of response in soft PZTs was predicted to be intrinsic (fig. 3).

Very recently the whole basis for evaluating both contribution to response has been changed by the discovery using very precise x-ray analysis [14,15] of a new monoclinic phase just on the rhombohedral side of the MPB (fig. 4). In this phase, the axial components of spontaneous polarization Ps are

$$P_1^2 = P_2^2 \neq 0 \qquad P_3^2 \neq 0 \quad but \quad P_1^2 \neq P_3^2 \tag{4}$$

**(a)**

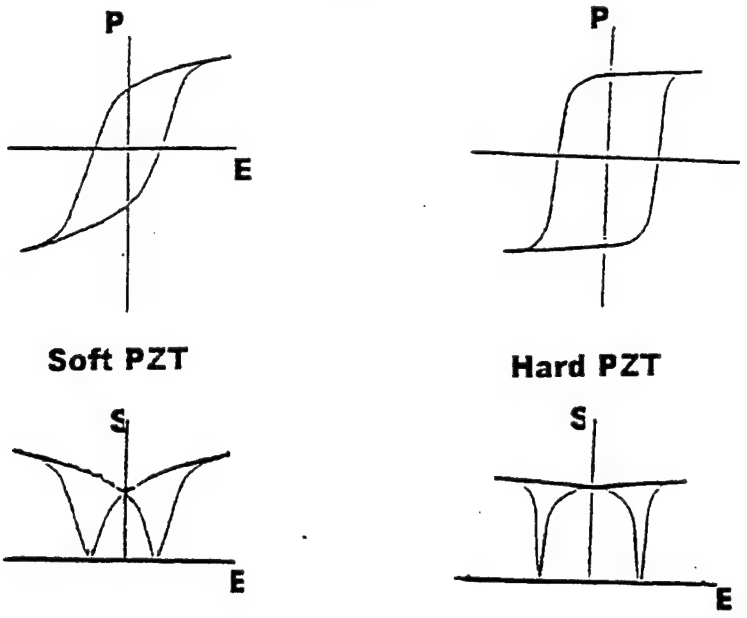


**(b)**

| DONOR ADDITIVES | | ACCEPTOR ADDITIVES |
|---|---|---|
| $Nb_2O_5$ | $PbNb_2O_6$ | $Fe_2O_3$ |
| $Ta_2O_5$ | $PbTa_2O_6$ | $Al_2O_3$ |
| $WO_3$ | | $Cr_2O_3$ |
| $Bi_2O_3$ | | $MnO_2$ |
| $Sb_2O_3$ | | MgO |
| $La_2O_3$ | | NiO |

**(c)**

| Wall Motion Promoters | | Wall Motion Inhibitors |
|---|---|---|
| $d_{33}$ | 593 pC/N | 150 pC/N |
| $d_{31}$ | 273 pC/N | 60 pC/N |
| Tc | 195°C | 350°C |
| $\varepsilon 3$ | 3.450 | 1,000 |
| Kp | 0.69 | 0.52 |
| Tan $\delta$ | 0.02 | 0.004 |
| $E_c$ | 6 Kv/cm | 15 Kv/cm |

FIGURE 2. (a) Typical polarization and strain curves. (b) Donor and Acceptor Dopants. (c) Dielectric and Piezoelectric Parameters

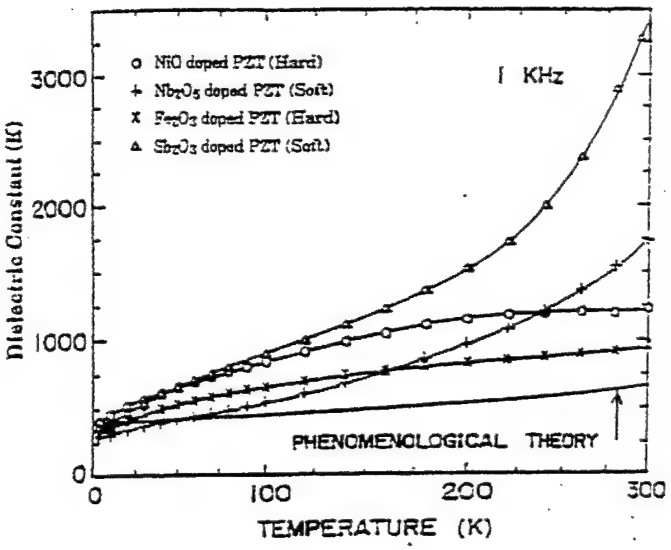


FIGURE 3. Dielectric response for Soft and Hard PZTs vs Temperature (4.2K to 300K) intrinsic response derived from Phenomenological Theory.

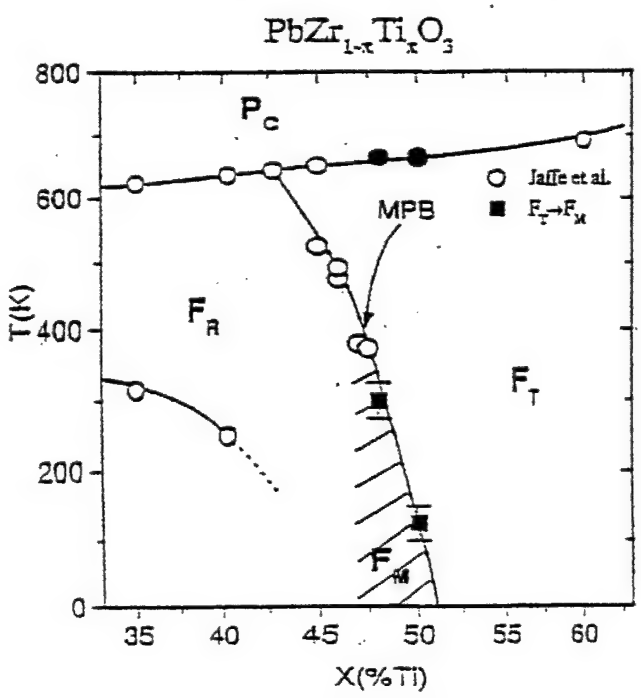


FIGURE 4. Modified PZT phase diagram after Noheda [2].
The open symbols represent the PZT phase diagram after Jaffee et al.
Note: The temperature axis is in degrees K not celcius as in the original studies.

The polar vector lies within the dodecahedral mirror plane of the prototype m3m and there are 24 orientation states for this species. From symmetry, the transitions rhombohedral 3m ↔ monoclinic m and tetragonal mm 2 ↔ monoclinic m may be either first or second order.

The presence of this newly discovered phase does require a revision of the phenomenology, as in the earlier treatment all phases other than tetragonal and rhombohedral were chosen to be metastable in the composition range of the MPB. Similarly the possible extrinsic contributions to response now need further consideration. The possibility for the E-field to drive phase boundary motion of a weakly hysteritic first order 3m ↔ m or 4mm ↔ m phase change could contribute here-to-fore unimagined extrinsic response that could mimic domain wall motion but contribute very strongly to elastic strain and piezoelectricity. Either intrinsic or extrinsic contributions from this very narrow insert of monoclinic phase could explain the very sharp peaking of $k_{33}$ near the MPB that is evident in pure PZTs and has been most difficult to explain on earlier theories.

## *Alternative Single Crystal Systems*

The complexity of the elasto-dielectric behavior of the polycrystal PZTs highlight the need for single crystal and single domain studies to properly explore the phenomena in lead based perovskite structures. PZT has proven markedly intractable for crystal growth, but more recent studies of the lead zinc niobate:lead titanate PZN:PT, and lead magnesium niobate:lead titanate (PMN:PT) have yielded "respectable" crystals for compositions close to the pseudo-morphotropic boundaries between rhombohedral and tetragonal phases in both systems [16,17,18].

Dielectric and piezoelectric properties have been well characterized [19,20] and the massive anisotropy in response between 111 and 001 E-field poled crystals in the rhombohedral phase underscored. The piezoelectric $d_{33} > 2000$ pC/N, $k_{33} > 92\%$, $\varepsilon_{33}^{T} > 5{,}000$ for 001 E-field rhombohedral phase crystal at composition close to the MPB are of strong practical interest. Of major concern here is the actuator performance where it has been shown that in 001 field poled PZN:PT strains up to 1.7% can be induced at high fields (fig. 5a).

There is good evidence that at the highest field levels the crystal is switched over into the tetragonal phase through a field induced first order phase change that is necessarily hysteritic. Of special interest is the long quasi-linear anhysteritic strain, up to 0.6% (fig. 5b) and polarization change 10 $\mu c/cm^2$ (fig. 5c) that can be induced by fields up to 60 Kv/cm.

It is suggested that the sequence of phase changes induced by the 001 high E-field is as in fig. 6. In the virgin state, the crystal is a relaxor with presumable a largely frozen rhombohedral nano/micro domain structure (fig. 6a). On first poling with 001 oriented field the $P_r$ which is almost exactly $1/\sqrt{3}$ of the rhombohedral states, i.e. *111. $\bar{1}11$. $1\bar{1}1$, and $11\bar{1}$* oriented polarizations have been induced (fig. 6b). Note that this

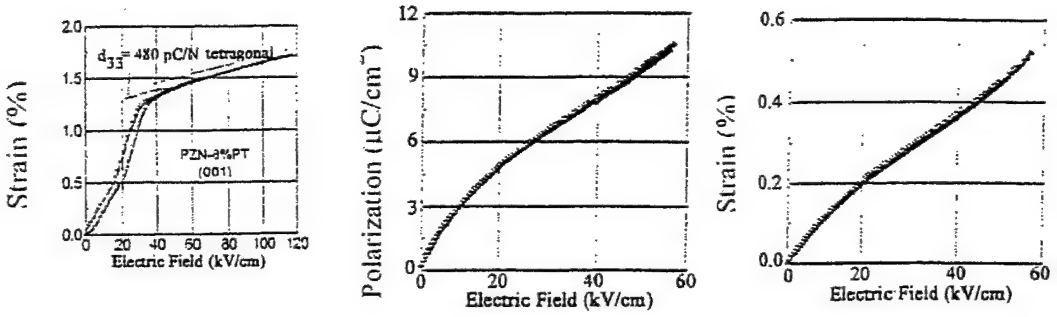


(a) $E_3$ field induced longitudinal strain in 001 Poled PZN 92:PT8.

(b) Electric Field induced polarization under 001 field in poled rhombohedral PZN 95.5 PT 4.5.

(c) Electric Field Induced Strain in 001 field Poled PZN 95.5 PT 4.5 anhysteritic for repeated field application.

**FIGURE 5.** Actuator behavior of 001 electric field poled rhombohedral PZN:PT single crystal.

structure requires a high concentration of charged walls, and gives rise to a domain averaged tetragonal 4mm macro symmetry. Since the high 001 field will change the energy of each of the 4 symmetry equivalent domains in the same way, there is no driving force to move the ferroelastic walls between the remaining domain states. Obviously the high field will induce a tilting of the Ps vector of the domain into the appropriate dodecahedral mirror plane givng rise to monoclinic domain states (fig. 6c) in which

$$P_1^2 = P_2^2 \neq 0 \qquad P_3^2 \neq 0 \qquad P_3^2 > P_1^2 \tag{5}$$

Again the monoclinic domains will average to macro 4mm symmetry. Eventually one expects the field to induce a true tetragonal monodomain state in which macro and micro symmetries coincide (fig. 6d).

An interesting question is whether the proposed sequence of changes can account for the observed large strain changes without extrinsic domain wall contribution.

Since intrinsic shape changes are electrostrictive it is only necessary to know the total polarization and the electrostrictive coefficients $Q_{11}$, $Q_{12}$, and $Q_{44}$. For m3m, it is simple to show that the volume strain $s_v$ in all possible ferroelectric phases is given by

$$s_v = (Q_{11} + 2Q_{12})P_{Total}^2 \tag{6}$$

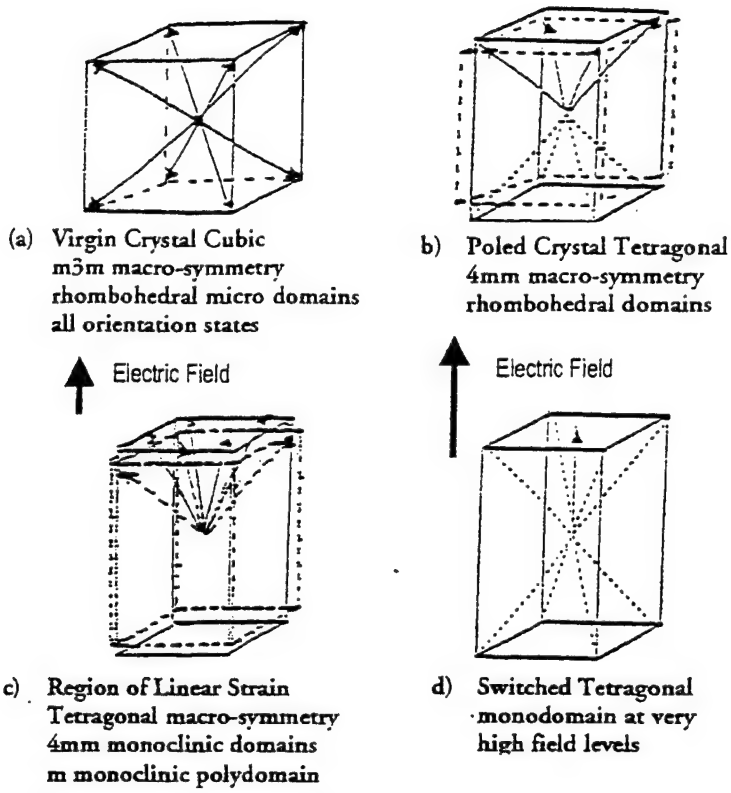


**FIGURE 6.**

Sequence of states in high 001 field poled rhombohedral PZN 95.5 PT 4.5 under increasing 001 E-field.

Measurements by Park [20] show that over the linear strain range up to 35 Kv/cm the volume change in PZN 0.95.5 PT 0.045 is less than 0.05%. Taking as a first aproximation $s_v = 0$, the polarization vector is just rotating under field and from fig. 5c the tilt angle in the induced monoclinic phase can be deduced and is presented in Table 2.

Taking $Q_{11}$ from the total strain and total polarization in the induced tetragonal monodomain state

$$\begin{aligned} Q_{11} &= 0.0535 \\ \text{taking } Q_h &= 0 \quad \text{then yields} \\ Q_{12} &= 0.0267. \end{aligned}$$

In the field induced monoclinic phase

$$\begin{aligned} s_1 &= (Q_{11} + Q_{12})P_1^2 + Q_{12}P_3^2 \\ s_2 &= (Q_{11} + Q_{12})P_1^2 + Q_{12}P_3^2 \\ s_3 &= (Q_{11} + P_3^2) + 2Q_{12}P_1^2 \end{aligned} \tag{7}$$

**TABLE 2.** Tilt angle and polarization components under increasing 001 $E_3$ field in rhombohedral PZN:95.5 PT 4.5 single crystal. Tilt is measured from the 001 axial direction.

| Field kV/cm | Polarization $P_3$ $\mu c/cm^2$ | Angle θ | Polarization $P_1$ $\mu c/cm^2$ |
|---|---|---|---|
| 5 | 27.8 | 50.1 | 23.47 |
| 10 | 29.8 | 46.5 | 22.21 |
| 15 | 31.4 | 43.4 | 21.04 |
| 20 | 33 | 40.34 | 19.82 |
| 25 | 34.3 | 37.5 | 18.64 |
| 30 | 35.6 | 34.6 | 17.42 |
| 35 | 36.75 | 31.9 | 16.19 |
| 40 | 37.85 | 29.1 | 14.87 |

From equation 7 and the known $P_1$ and $P_3$, components of the strains $s_1$, $s_2$, $s_3$ can be computed for the induced monoclinic phase in the anhysteritic range up to 35 Kv/cm $E_3$ field (fig. 7). Clearly the intrinsic strains in the monoclinic form are adequate to describe the induced total deformation.

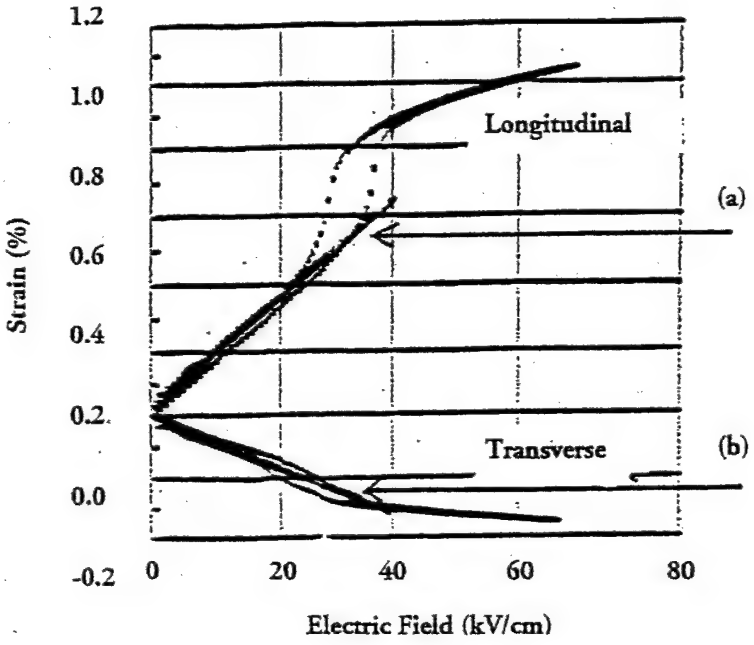


**FIGURE 7.** Calculated intrinsic strain in the field induced monoclinic phase (a) $S_3$ (b) $S_1$.

If this proposed explanation for high strain behavior is valid it should be expected that other peroskite structure ferroelectrics would show high intrinsic strain effects at temperatures close to phase boundaries. Strong enhancement of $d_{33}$ at temperatures below but close to both rhombohedral/orthorhombic and orthorhomic/tetragonal phase changes in $BaTiO_3$ single crystals have been demonstrated [2]. Of particular relevance is the study by Wada et. al. [3] of the inverse transition, i.e. tetragonal to rhombohedral in 111 cut $BaTiO_3$ crystal under increasing 111 oriented electric field. The sequence of changes taken from their paper is depicted schematically in fig. 8. The 111 poling field first induces 100, 010, and 001 orientation of $P_s$ in the tetragonal state. Under this condition for fields below 5 Kv/cm at 0.1 Hz a monoclinic phase is induced with intrinsic $d_{33} \sim 203$ pC/N (fig. 8a).

At higher fields, the system becomes hysteritic and the family of 110, 101, and 011 orthorombic domain orientations is finally induced (fig. 8b).

A new linear regimen of strain is evident for fields up to 45 Kv/cm, again exhibiting monoclinic symmetry, until the system moves by a hysteritic first order change to rhombohedral symmetry (fig. 8c). It is interesting to note that the second linear strain range has a different slope corresponding to a $d_{33} \sim 295$ pC/N.

We suggest (fig. 8) that because of the closeness to room temperature of the 4mm/mm2 change in $BaTiO_3$, the polarization vector under 111 field first moves out into the cube mirror ($m_1$) catalyzing the change to mm2 symmetry, but then at higher field must move in the dodecahedral mirror ($m_2$) to achieve the rhombohedral orientation. After achieving the rhombohedral state, it would appear the $P_s$ chooses to stay in the dodecahedral mirror which connects directly to the tetragonal state. Since the two monoclinic phases accessible from m3m are quite distinct this would account for the different piezoelectric slopes measured in the experiment.

Since there is a very complete Gibbs Free Energy Function for $BaTiO_3$ [21] it should be a simple matter to do the full three dimensional energy plots, to calculate the lowest energy trajectories for the polarization change and thus to verify the major role of the E•P term in Energy for these "soft" ferroelectric perovskites.

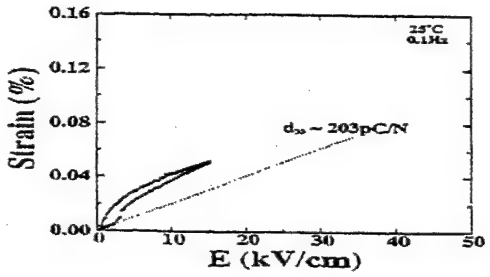


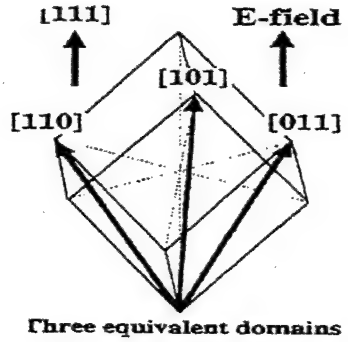


(a) **Strain vs electric-field curve for [111] oriented $BaTiO_3$ crystal under unipolar electric field below 5kV/cm with 0.1 Hz at 25°C.**

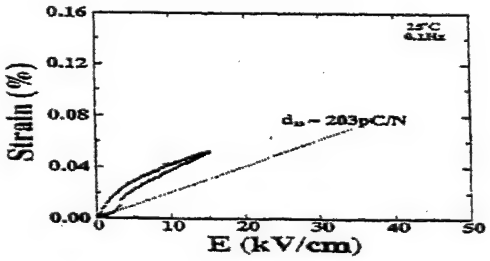


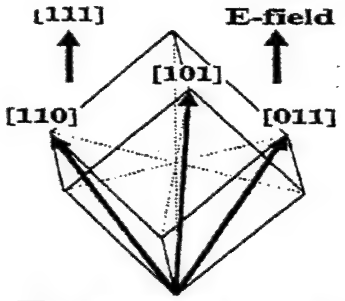


(b) **Strain vs electric-field curve for [111] oriented $BaTiO_3$ crystal under unipolar electric field below 16 kV/cm with 0.1 Hz at 25°C.**

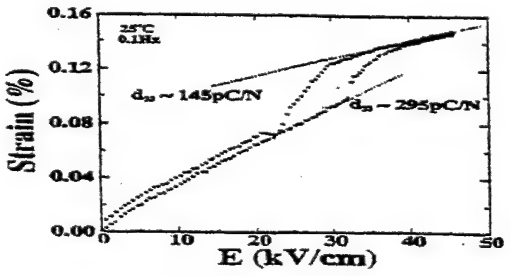


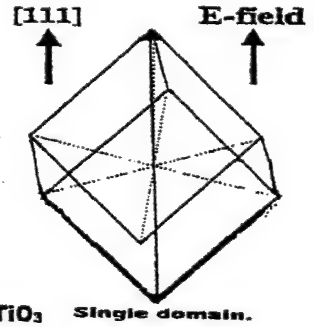


(c) **Strain vs electric-field curve for [111] oriented $BaTiO_3$ crystal under unipolar electric field below 45 kV/cm with0.1 Hz at 25°C.**

FIGURE 8. Sequence of domain and strain changes in 111 poled $BaTiO_3$ crystal at room temperature after Wada et. al. (2).

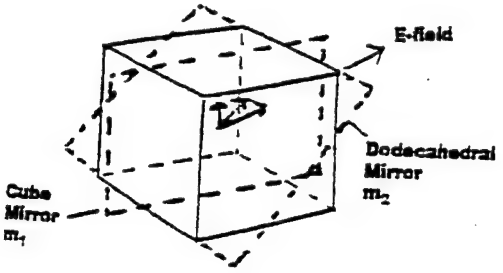


| | | | |
|---|---|---|---|
| $P_3^2 \neq 0$ | $P_1^2 = P_2^2 = 0$ | | Tetragonal |
| $P_3^2 \neq 0$ | $P_2^2 \neq 0$ $P_3^2 \neq P_2^2$ | $P_1^2 = 0$ | monoclinic (cube m) |
| $P_3^2 = P_2^2 \neq 0$ | $P_1^2 = 0$ | | Orthorhombic |
| $P_3^2 = P_2^2 \neq 0$ | $P_1^2 \neq 0$ | $P_1^2 \neq P_3^2$ | monoclinic (Dodecahedron m) |
| $P_3^2 = P_2^2 = P_1^2 \neq 0$ | | | Rhombohedral |

$E_{111}$

**FIGURE 9.** Suggested model for the inverse field induced transition from 4mm ⇒ 3m in single crystal $BaTiO_3$ at 25°C.

## Conclusions

In polycrystal ceramic PZT piezoelectrics the current balance of evidence still suggests a strong contribution to dielectric and piezoelectric responses from ferroelastic:ferroelectric domain wall motion. New evidence of a stable monoclinic phase just on the rhombohedral side of the MPB does however require revision of the earlier thermodynamic phenomenology to describe the intrinsic single domain responses and also contributes the possibility of previously unimagined new extrinsic contributions to response.

For the single crystal lead zinc niobate lead titanate at the 4.5% lead titanate composition the very high linear anhysteritic strain induced by 001 oriented E-field is suggested to be intrinsic and to result from the induction of a monoclinic phase in which $P_S$ is substantially tilted from 111. In $BaTiO_3$ for the "inverse experiment" forcing tetragonal to rhombohedral symmetry at room temperature it is suggested that with increasing E-field $P_S$ moves first in the cube mirror to orthorhombic, then in the doecahedral mirror towards rhombohedral symmetry, but at very high field may chose to accomplish complete switching in the alternative dodecahedral mirror.

# References


[1] Fu, H., and Cohen, R.E., *Nature* 403, 281-283 (2000).

[2] Park, S.-E., Wada, S., Cross, L.E., and Shrout, T.R., *J. Appl. Phys.* **86** (5), 2746 (1999).

[3] Wada, S., Suzuki, S., Nomura, T., Suzuki, T., Osada, M., Kakihana, M., Park, S., Cross, L.E., and Shrout, T.R., *Jpn. J. Appl. Phys.* **38**, 5505 (1999).

[4] Carl, K., and Hardtl, K.H., *Ferroelectrics* **17**, 472 (1978).

[5] Dederichs, D., and Arlt, G., *Ferroelectrics* **68**, 281 (1986).

[6] Kugel, V.D., and Cross, L.E., *J. Appl. Phys.* **84**, 2815 (1998).

[7] Damjanovic, D., Demarlin, M., Shulman, H.S., Testorf, M., and Setter, N., *Sensors and Actuators A* **353** (1996).

[8] Tan, Q., Li, J.F., and Viehland, D., *Ferroelectrics* **206**, 275 (1998).

[9] Haun, M.J., Furman, E., Jiang, S.J., and Cross, L.E., *Ferroelectrics* **99**, 13 (1989).

[10] Haun, M.J., Furman, E., McKinstry, H.A., and Cross, L.E., *Ferroelectrics* **99**, 27 (1989).

[11] Haun, M.J., Zhuang, Z.Q., Furman, E., Jang, S.J., and Cross, L.E., *Ferroelectrics* **99**, 45 (1989).

[12] Haun, M.J., Furman, E., Halemane, T.R., and Cross, L.E., *Ferroelectrics* **99**, 55 (1989).

[13] Haun, M.J., Furman, E., Jang, S.J., and Cross, L.E., *Ferroelectrics* **99**, 63 (1989).

[14] Noheda, B., Cox, D.E., Shirane, G., Gonzalo, J.A., Cross, L.E., and Park, S.-E., *Appl. Phys. Letters* **74**, 2059 (1999).

[15] Noheda, B., Gonzalo, J.A., Guo, R., Park, S.-E., Cross, L.E., Cox, D.E., and Shirane, G., "The monoclinic phase in PZT: new light on morphotropic phase boundaries," *Proceedings Workshop on Fundamental Physics of Ferroelectrics*, Aspen, Colorado (February 2000).

[16] Kuwata, J., Uchino, K., and Nomura, S., *Jpn. J. Appl. Phys.* **21**, 1298 (1982).

[17] Park, S.-E., and Shrout, T.R., *Science* **275**, 1878 (1997).

[18] Park, S.-E., and Shrout, T.R., *Mat. Res. Innovation* **1**, 20 (1997).

[19] Park, S.E., and Shrout, T.R., *IEEE Trans. UFFC* **44**, 1140 (1997).

[20] Liu, S.-F., Park, S.-E., Shrout, T.R., and Cross, L.E., *J. Appl. Phys.* 85, 2810 (1999).

[21] Bell, A.J., and Cross, L.E., *Ferroelectrics* **59**, 197 (1984).

# APPENDIX 4

The Art of Ceramics
*The Blend of Art and Science in Technology*
N. Claussen (Editor)
© Techna Srl, 2001


# SYMMETRY AND ANTISYMMETRY IN ELECTROCERAMICS

Robert NEWNHAM and Eric CROSS
The Pennsylvania State University, University Park, PA, USA

*Many types of symmetry are utilized in ceramic art and in ceramic science. In addition to the common mirror, rotation, inversion and translation symmetry elements observed in crystals and textured ceramics, artists and engineers often make use of the antisymmetry elements involved in color groups. We illustrate the application of color symmetry in controlling the vibration modes in ferroelectric and ferromagnetic ceramics prepared as spheres, hemispheres, and rings conforming to black-and-white Curie groups.*

## SYMMETRY IN ART AND SCIENCE

While visiting the city of Kütahya, one of the great centers for traditional ceramic tiles and porcelain products, we had the opportunity to view contemporary Turkish artwork. Islamic art has long been famous for its geometric patterns, but we were especially fascinated with the porcelains made by Kervan Chini, who incorporates many interesting symmetries into his pottery. The colorful dish shown in Fig. 1 contains a number of the symmetries and broken symmetries observed in electroceramic materials and devices: polar symmetry, chiral symmetry, symmetry of scale, quasisymmetry, the pseudosymmetry of incommensurate phases, and the antisymmetric elements of color symmetry groups.

Piezoelectric ceramics, pyroelectric glass ceramics, and certain functionally-graded ceramics have polar symmetry like that of a concave-shaped disk (Fig. 2a). Chiral symmetry is present in the porcelain dish as well (Fig. 2b). The leaf pattern of the flowers and the sleeping sheep near the edge are both arranged in a counterclockwise fashion leading to handedness. Chiral phenomena such as optical activity, acoustic activity, and the Faraday Effect are well known in crystal physics. Symmetry of scale is important in all classes of materials. The pattern in Fig. 1 violates the self-similarity principle introduced by Benoit Mandelbrot to describe fractal geometry. Beginning at the center, the porcelain dish shows 5-fold then 9-fold, 10-fold, and 19-fold rotational symmetry. Five-fold symmetry is characteristic of quasicrystals and the circle possesses a $\infty$-fold axis, one of Curie group symmetries found in textured polycrystalline ceramics. The change in symmetry with scale is illustrated in Fig. 2c.

The symmetry of scale is an important one in many electronic systems as component sizes become smaller and smaller. Current trends in multilayer capacitors are shown in Fig. 3 and 4. The lateral dimensions in MLC chips are now about 1 mm, approaching the limit for many of the pick-and-place machines used in assembling circuits. Layer thicknesses and grain sizes are also a concern. Ceramists are now testing $BaTiO_3$ MLCs with layers of 1 μm thickness which is pressing the limits of tape-casting technology. Particle sizes are in the 0.1 μm range which raises some fundamental questions regarding size effects in ferroelectrics. In large grain size, say 1 μm and larger, each grain contains many domains. The number of domains and the type of domain walls change as grain size drops below a micron. Eventually each grain becomes a single domain with profound changes in dielectric constant and switching behavior. In the nm range the ferroelectric phase transition becomes diffuse and the symmetry of $BaTiO_3$ appears pseudocubic. Size effects in primary ferroics are illustrated schematically in Fig. 5. Dielectric constants drop substantially for grain sizes less than 0.1 μm.

Returning to the porcelain plate in Fig. 1, the outer portions of plate provide an excellent illustration of pseudosymmetry or "almost" symmetry. In the central leaf pattern there are 10 leaves and between neighboring leaves are 10 flowers. Near the outside rim of the plate are red hearts which, at first glance, appear to be in register with the 10 leaves and with the 10 flowers, but such is not in the case. The artist has made a subtle change in symmetry with only 19 hearts instead of 20 (Fig. 2d). Many ferroelectric and ferrimagnetic oxides possess incommensurate structures in which the local polarization or magnetization vectors are out of register with the lattice periodicity (Fig. 6). These so-called incommensurate phases often exhibit unusual physical properties because of their abnormal symmetry.

## FERROIC CRYSTALS AND ANTISYMMETRY ELEMENTS

The symmetry elements discussed thus far are purely spatial transformations such as mirror planes, rotation axes, and inversion centers. Spatial symmetry elements are all that are required for the usual crystallographic and limiting point groups, but additional symmetries occur in ferroic electroceramics. These additional symmetries can be described by color symmetry. The ceramic dish from Turkey possesses decagonal color symmetry in which the flower rotates by 36° and changes color (Fig. 2e). In this paper we discuss color groups and the antisymmetry elements found in ferroic ceramics with complex domain patterns. The 10′ antisymmetry element in Fig. 2e belongs to this type of color group.

More than a century ago, the basic relationships between symmetry and physical properties were established by Neumann and the brothers Cu-

rie, and systematized in Woldemar Voigt's monumental "Lehrbuch der Kristallphysik." (Voigt,1928) Using Neumann's Principle, the symmetry restrictions for piezoelectricity, magnetostriction, and other linear and nonlinear tensor properties have been enumerated, and have led to the development of many types of sensors, actuators, and transducers. For single crystals, the properties are governed by the 32 crystallographic point groups, and for textured polycrystalline materials, we use the seven limiting groups first described by Pierre Curie. In 1974 we extended these symmetry arguments to ferroic crystals, laying out the symmetry changes involved in the phase transformations leading to the hysteretic phenomena created by domain wall motion (Newnham, 1974). There are, for example, 15 symmetry changes consistent with pure ferroelastoelectric behavior in which adjacent domains differ only in the orientation of third rank polar tensor properties. A "pure" ferroelastoelectric does not exhibit any other primary or secondary ferroic behavior (Newnham and Cross, 1974).

In crystals with long range magnetic order, the addition of a time reversal operator leads to the generation of the 90 magnetic point groups used to describe ferromagnetic, ferrimagnetic, and antiferromagnetic substances (Birss, 1964). Introduction of the antisymmetric spin reversal operator makes it possible to apply Neumann's Principle to magnetic crystals and classify the symmetry restrictions for magnetic properties such as magnetoelectricity, pyromagnetism and piezomagnetism. All three of these cross-coupled phenomena are axial tensor properties and since spin reversal corresponds to the reversal of an axial vector, all three properties are strongly influenced by the antisymmetry operator.

In this paper we introduce antisymmetry elements for other types of ferroic materials with movable domain walls. Ferroelectricity, ferroelasticity, and the six types of secondary ferroics are also controlled by tensorial antisymmetry operators (Table 1). For a ferroelectric, polarization - a polar vector - is the key operator, since ferroelectricity is defined by polarization reorientation between symmetry related states. For a ferroelastic, the key operator is strain - a second rank polar tensor - since ferroelasticity is defined by strain reorientation between symmetry related states. For a ferrobielastic secondary ferroic, the key operator is a fourth rank tensor, etc.

The procedure will adopt for introducing these antisymmetry elements is as follows. Each operator is combined with the spatial symmetry elements of the 32 crystallographic point groups or to the seven Curie groups to generate a family of antisymmetric groups analogous to the 90 magnetic point groups. Having determined the relevant symmetries, Neumann's Principle is then applied to determine the polar and axial property matrices, enabling one to predict the useful symmetries that will optimize the material for a given

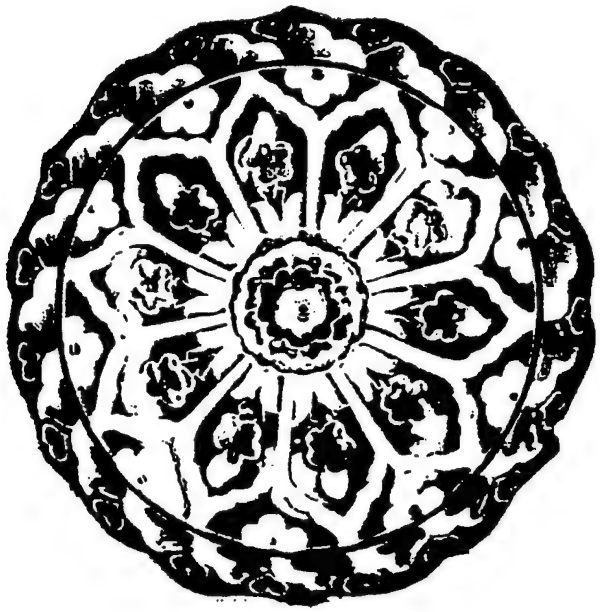

*FIGURE 1 - A ceramic dish made by Kervan Chini which illustrates many types of unusual symmetry.*

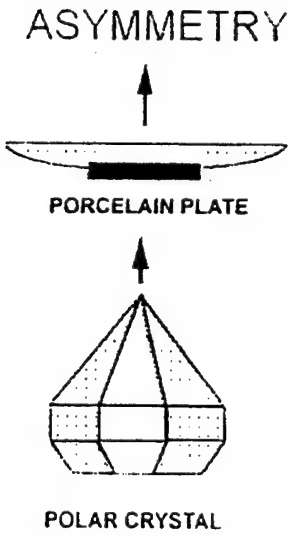


PYROELECTRICITY

*FIGURE 2a - Polarity.*

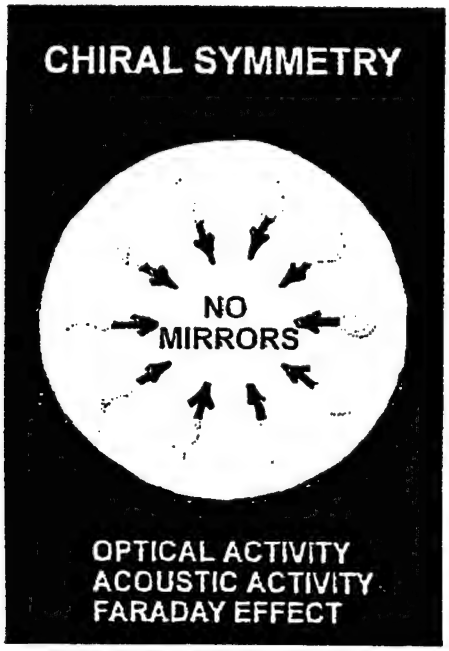


*FIGURE 2b - Handedness.*

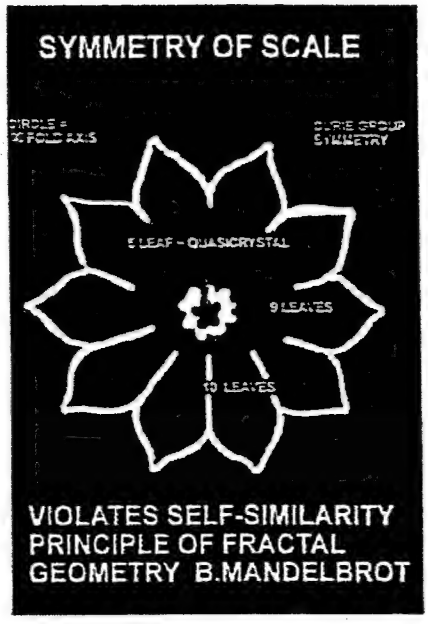


*FIGURE 2c - Size effects.*

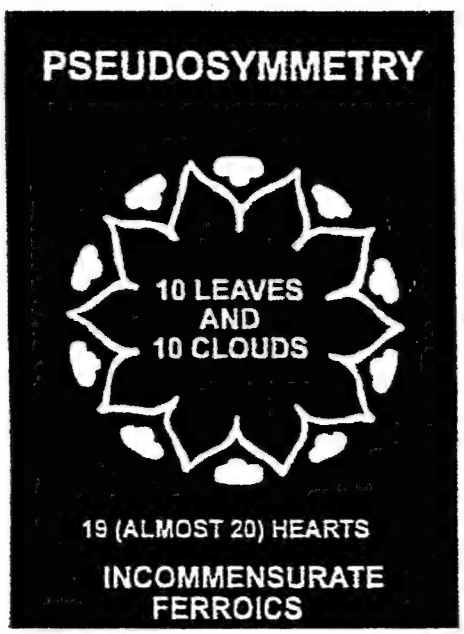


*FIGURE 2d - Aperiodicity.*

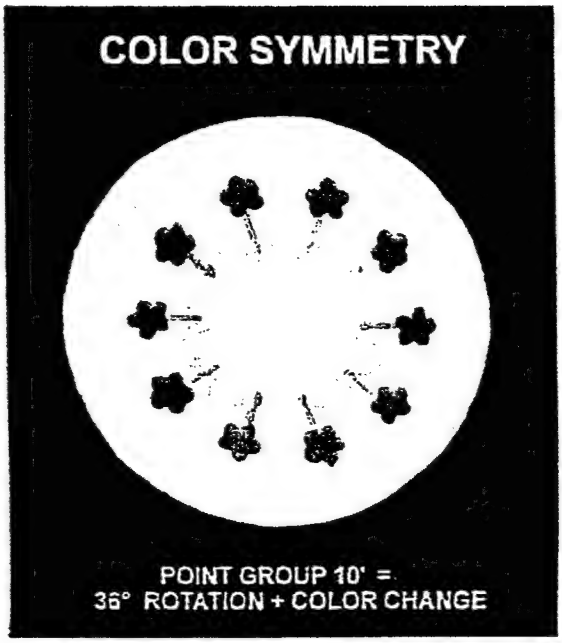


*FIGURE 2e - Color patterns.*

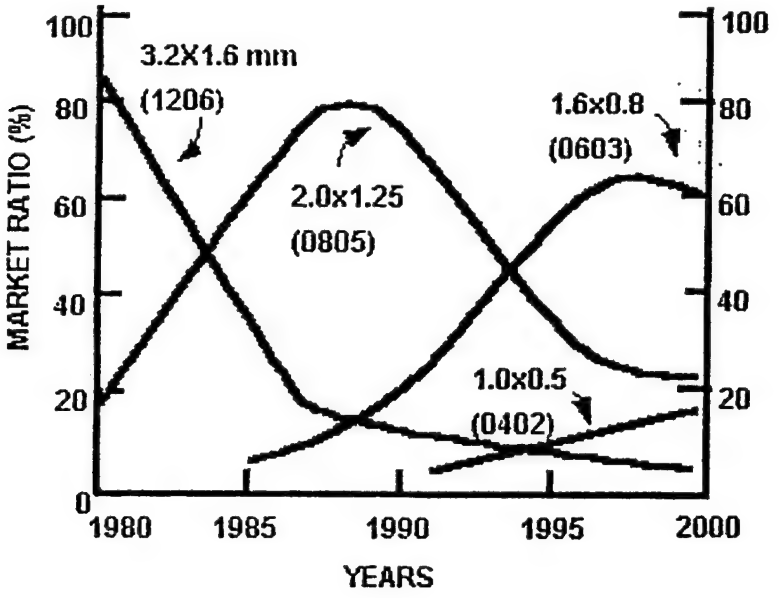


*FIGURE 3 - The sizes of ceramic capacitors have decreased steadily with time while the market continues to grow exponentially following Moore's Law.*

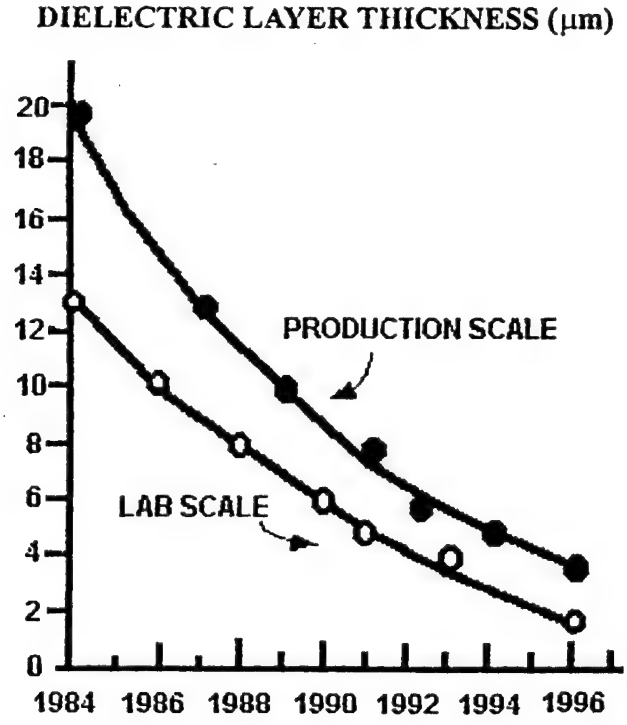


*FIGURE 4 - Layer thicknesses in multilayer capacitors are now nearing one micron with grain sizes around 0.2 μm.*

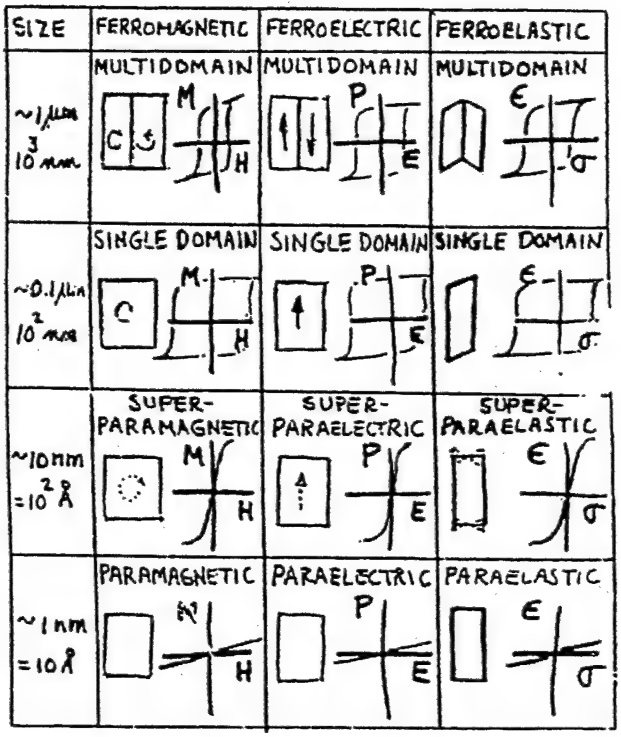


*FIGURE 5 - Profound changes in properties take place in ferroic ceramics when the grain sizes drop below the micron range.*

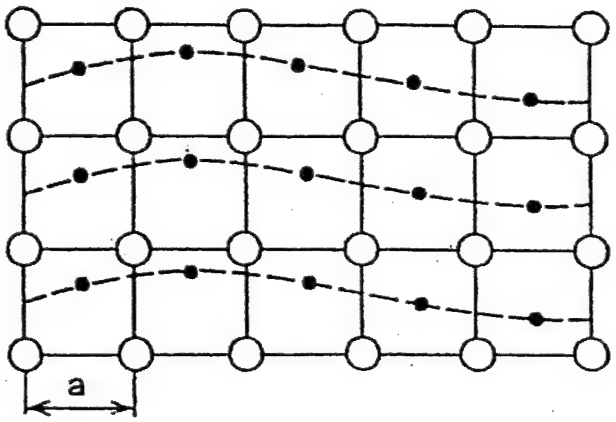


*FIGURE 6 - Formation of incommensurate phase as a result of the "freezing" of a displacement wave with a length incommensurate with the unit-cell parameter.*

*TABLE 1 - Nine types of ferroics in which domain walls can be moved by magnetic fields, electric fields, or mechanical stress. Each is controlled by a different term in the free energy function with an antisymmetry operator relating domain state orientations.*

| Type | Domain Difference | Antisymmetry Tensor |
|---|---|---|
| Primary Ferroics | | |
| Ferromagnetic | Magnetization | Axial First Rank |
| Ferroelectric | Polarization | Polar First Rank |
| Ferroelastic | Strain | Polar Second Rank |
| Secondary Ferroics | | |
| Ferrobielectric | Permittivity | Polar Second Rank |
| Ferrobimagnetic | Permeability | Polar Second Rank |
| Ferrobielastic | Elasticity | Polar Fourth Rank |
| Ferroelastoelectric | Piezoelectricity | Polar Third Rank |
| Ferromagnetoelectric | Magnetoelectricity | Axial Second Rank |
| Ferromagnetoelastic | Piezomagnetism | Axial Third Rank |

application.

Knowing the optimum symmetry groups, how does one go about creating these symmetries in a real material? Here one applies Curie's Principle of Symmetry Superposition and examines various composite ferroics (Newnham and Giniewicz, 2000). Symmetry patterns can be generated at many different size scales ranging from electron spin arrangements, crystal structures, defect structures, textured grains, tailored domain patterns, electrode geometries, connectivity patterns, and various morphologies using processing methods such as extrusion, tape-casting, and photolithography. Many of the more unusual point groups can be accessed when ferroic materials are prepared as fibers, films, tubes, disks, multilayers and hollow spheres. Using Curie's Principle of Symmetry Superposition, many unusual cross-coupled properties can be optimized by symmetry control. The new feature we are developing is a family of antisymmetry operators (polar vector reversal, polar second rank tensor reversal, axial second rank tensor reversal, etc.) which will augment our understanding of the symmetry of solids, and enable us to predict new families of functional materials for biomedical and industrial applications. Our goal is to control the acoustic and electromagnetic resonance phenomena in a wide range of electroceramic products.

## ANTISYMMETRIC CURIE GROUPS

In this section we describe a family of small electroceramic transducers, sensors, and actuators based on black-and-white Curie group symmetries (Fig. 7). One of the goals of this investigation is to control the acoustic vibration modes and radiation patterns by controlling the symmetries of the transducer's material, its external shape and poling pattern, together with the driving electrode geometry. Later we intend to extend these symmetry arguments to electromagnetic wave modes as in millimeter wave resonators and dielectric antennae.

We begin with an example to illustrate the basic idea. Consider a spherical shell made of a piezoelectric ceramic such as PZT with randomly oriented grains. When statistically averaged, randomly oriented grains in an unpoled ceramic conform to spherical symmetry ∞∞m1′ where ∞∞ represents an infinite number of infinite-fold rotation axes, m is an infinite number of mirror planes, and 1′ is the color reversal operator changing white to black, and vice versa.

In ferroelectric substances such as PZT we can use color to represent polar vector reversal. When electrically poled in a strong DC field near $T_c$, the altered domain structure changes the symmetry to ∞/m′m, the symmetry of an electric field. This is also the overall symmetry of an electric dipole with its positive and negatively-charged ends. The ∞-fold axis is parallel to the dipole.

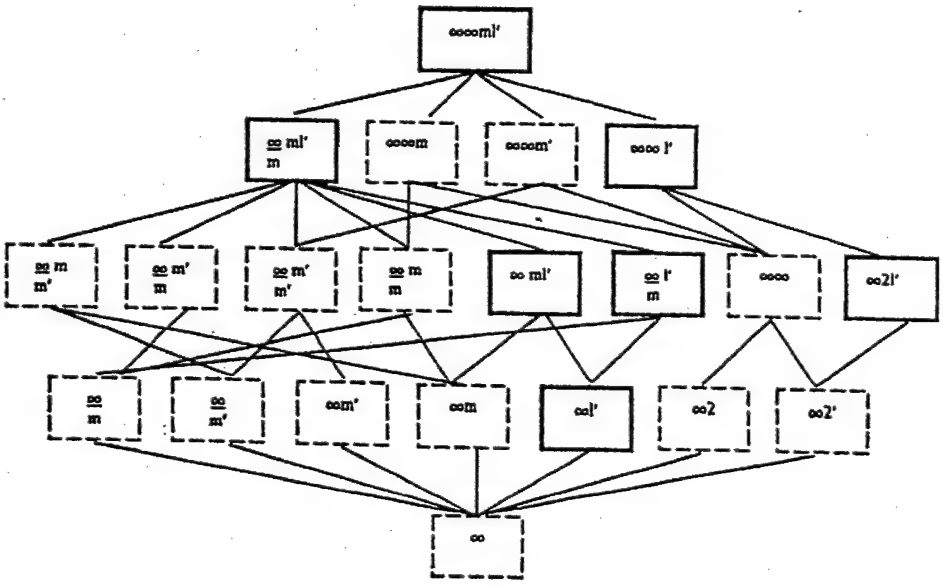


*FIGURE 7 - The seven Curie groups (solid boxes) and fourteen black and white Curie groups (dashed boxes). The interconnecting lines denote group-subgroup relationships.*

m' is a mirror plane accompanied by charge (color) reversal perpendicular to the ∞-fold axis. In the symbol ∞/m'm, m refers to the infinite number of mirror planes parallel to the ∞-fold dipole axis. This is the symmetry of the material, and that in turn determines the physical properties through Neumann's Law from crystal physics. That of course is why poled PZT is piezoelectric and pyroelectric.

But that is not the only symmetry that is important in transducer design. The vibration modes and radiation patterns depend on the symmetry of the transducer's shape, poling pattern, and driving electrodes as well. If we consider a spherical shell as an example, the shape conforms to spherical symmetry ∞∞m1', and if it is poled radially, the symmetry group changes to ∞∞m. This is a black- and- white symmetry group which exists in two physically-distinct states corresponding to a hollow sphere poled inside-out or outside-in. The principal piezoelectric and pyroelectric coefficients differ in sign for the two states which are related to one another by the symmetry element m¢, reflection accompanied by dipole reversal.

The symmetry of the radially-poled sphere (∞∞m) together with the symmetry of the material (∞/m'm) determines the vibration modes of the transducer. The material symmetry determines the non-zero piezoelectric coefficients: $d_{33}$, $d_{31} = d_{32}$, $d_{24} = d_{15}$. For a radially-poled sphere, the poling direction $X_3$ and the driving field $E_3$ are in the radial direction r, while $X_1$, and $X_2$ are orthogonal tangential directions designated by the symbol t. Therefore $d_{33} = d_{rr}$ and $d_{31} = d_{32} = d_{rt}$. When driven electrically, the radially-poled sphere vibrates in two fundamental modes: a high-frequency wall thickness mode governed by $d_{rr}$ and a low-frequency breathing mode controlled by $d_{rt}$. For a hollow sphere 2 mm in diameter with a wall thickness of about 0.1 mm, these resonances occur near 20 MHz and 600 kHz, respectively (Alkoy, 1999). As discussed later, a much more complex mode spectrum with ellipsoidal modes (symmetry group ∞/mm) is observed when the sphere is electroded at the N and S poles and poled tangentially.

Three additional types of symmetry control can also be illustrated with this example. The first involves re-electroding. The driving electrode pattern need not be the same as the poling electrode pattern. Poling is generally carried out at elevated temperatures under high voltage. After cooling and aging the poling pattern is relatively stable. The poling electrodes can then be removed and a new set of driving electrodes installed which create different vibration modes. This is indicated schematically in Fig. 8. In this way a radially poled sphere might be driven tangentially.

The second modification involves the use of a second transducer attached to the first transducer and driven in a different mode. It is relatively easy to build transducers in multilayer form with a common ground electrode and

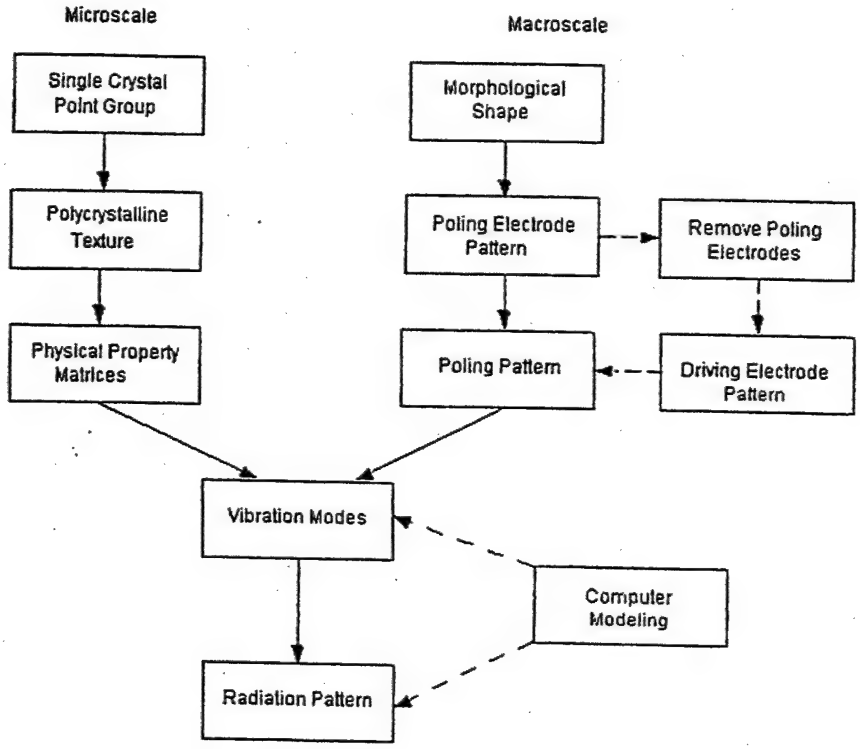


*FIGURE 8 - Outline of experimental approach.*

independently-driven external electrodes. This enables us to superimpose two vibration modes driven with different phases and amplitudes.

The practical aim of our program is to control the external radiation pattern by controlling the symmetry. If one transducer is driven in an omni-directional fundamental, and the second transducer in a dipole mode, the net result is a cardioid mode. In this way one can direct the radiation in the desired direction.

All of these patterns and their symmetries can be controlled independently by choosing the material and its processing. Our current objective in this research is to access the black-and-white symmetries in Fig.7 to generate interesting acoustic vibration modes using piezoelectric and magnetostrictive transducers.

## FERROIC SPHERES, HEMISPHERES, AND RINGS

Our initial aim is to study the vibration modes and radiation patterns from the fourteen black-and-white Curie groups ∞∞m, ∞∞m′, ∞∞, ∞/m′m, ∞/mm′, ∞/m′m′, ∞/mm, ∞/m, ∞/m′, ∞2, ∞2′, ∞m′, ∞m, and ∞. All fourteen symmetries can be accessed with ferroic hollow spheres or modified hollow

spheres shaped as rings or hemispheres. When polished down on one side, hollow spheres (symmetry group ∞∞m1′) become hollow hemispheres (symmetry group ∞m1′). When polished symmetrically on two opposite sides, hollow spheres become rings (symmetry group ∞/mm1′).

Following the processing steps laid out in the experimental procedure section, polycrystalline hollow spheres are prepared from strongly piezoelectric and magnetostrictive substances such as $PbZr_{1-x}Ti_xO_3$ (PZT) and $Tb_{1-x}Dy_xFe_2$ (Terfenol-D). After poling, magnetizing, and polishing all 14 of the black-and-white Curie groups can be generated according to the game plan shown in Table 2.

*TABLE 2 - Fourteen black-and-white symmetry groups to be obtained from processed hollow spheres. Initially we are concentrating on the piezoelectric elements, and then the magnetostrictive transducers. Combined elements are to be examined in the third stage using multilayer processing.*

| Antisymmetric Curie Group | Ferroic Morphology |
|---|---|
| ∞∞m | Radially-poled piezoelectric sphere |
| ∞∞m′ | Radially-magnetized magnetostrictive sphere |
| ∞∞∞ | Concentric radially-poled piezoelectric sphere and radially-magnetized magnetostrictive sphere |
| ∞/mm | Radially-poled piezoelectric ring |
| ∞/mm′ | Longitudinally-magnetized magnetostrictive ring |
| ∞/m′m | Longitudinally-poled piezoelectric ring |
| ∞/m′m′ | Radially-magnetized magnetostrictive ring |
| ∞/m | Concentric radially-poled piezoelectric and longitudinally-magnetized magnetostrictive rings |
| ∞/m′ | Concentric longitudinally-poled piezoelectric and radially-magnetized magnetostrictive rings |
| ∞2 | Concentric radially-poled piezoelectric and radially-magnetized magnetostrictive rings |
| ∞2′ | Concentric longitudinally-poled piezoelectric ring and longitudinally-magnetized magnetostrictive ring |
| ∞m | Radially-poled piezoelectric hemisphere |
| ∞m′ | Radially-magnetized magnetostrictive hemisphere |
| ∞ | Concentric radially-poled piezoelectric and radially-magnetized magnetostrictive hemisphere |

The next step is to determine the resonant vibration modes experimentally using impedance spectroscopy and to verify the measurements theoretically using the ATILA finite element code. Typical calculated spectra for a radially-poled piezoelectric hollow sphere and a tangentially poled hollow sphere are illustrated in Figures 9 and 10. For the radially-poled sphere, the low-frequency mode near 600 kHz is a breathing mode driven by piezoelectric coefficient $d_{31}$, and the high-frequency 20 MHz wall-thickness mode is governed by $d_{33}$. Miniature hydrophones and minipumps make use of the large hydrostatic piezoelectric coefficient $d_h$ of these transducers. Hollow sphere sensors and actuators have a stress amplification factor proportional to the sphere radius divided by the wall thickness, which is typically more than an order of magnitude in our transducers.

Similar amplification factors apply to the tangentially poled sphere in Fig. 10. This nicely illustrates how to control the vibration modes and their symmetry with the electrode pattern. In this case different size circular electrodes were applied to the top and bottom of the sphere, conforming to antisymmetry group ∞/m'm. When driven electrically, a series of ellipsoidal and egg-shaped vibrations were excited, as illustrated in Figure 10. The ATILA code is very helpful in identifying and visualizing the various modes of vibration of complex patterns and shapes.

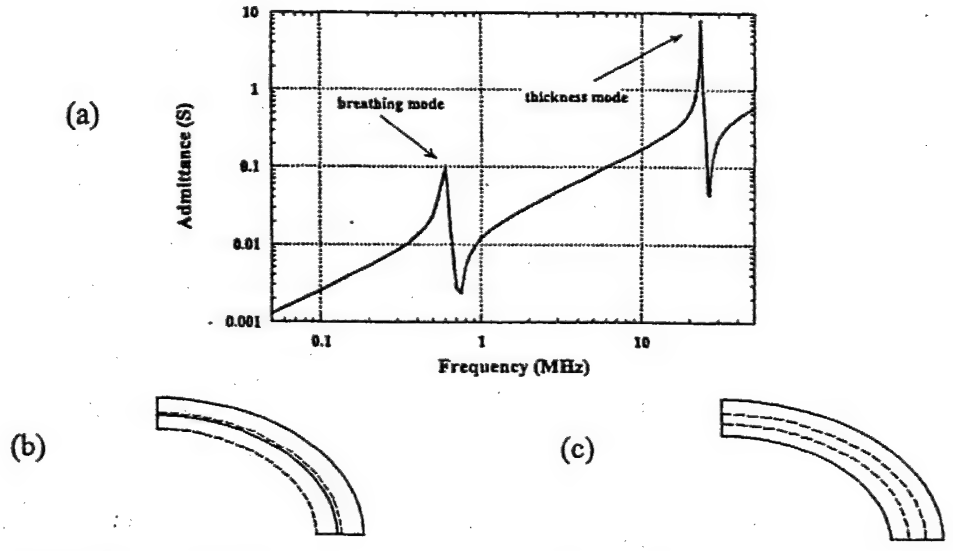


*FIGURE 9 - The (a) admittance spectrum of a hollow sphere electroded inside and outside and poled radially. The principal vibration modes are the (b) low frequency breathing mode and the (c) high frequency wall thickness mode. Both modes are spherically symmetric conforming to the shape and electrode pattern. The dashed lines correspond to the rest position and the solid line to the vibration motion. Scales are arbitrary. (Alkoy, 1999)*

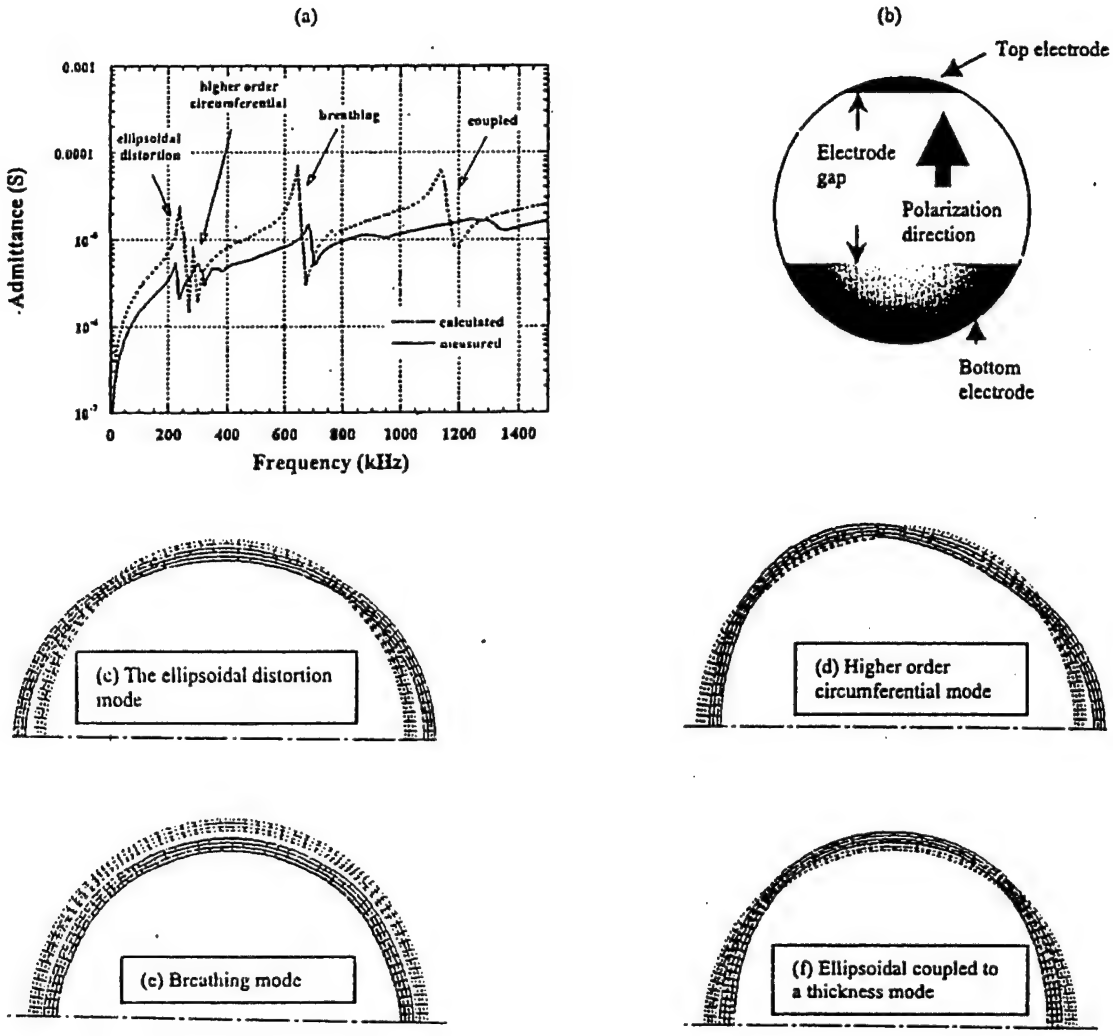


*FIGURE 10 - Comparison of the (a) calculated and measured admittance response of (b) a tangentially-poled hollow sphere with asymmetric electrodes. The displacement fields of four vibration modes, two of which are ellipsoidal in shape (∞/mm'), one is spherical (∞∞m'), and one egg-shaped (∞m'). This illustrates Neumann's Principle which says that the symmetry of a property must include the symmetry of the material and the way in which it is driven (Alkoy, 1999).*

## TRANSDUCER FABRICATION

The fabrication process is designed to produce spherical electroceramic devices with cofired inner electrodes. For commercial applications we need a process capable of producing large quantities of hollow sphere transducers in sizes ranging from a fraction of a millimeter to several millimeters. The process is illustrated schematically in Fig. 11.

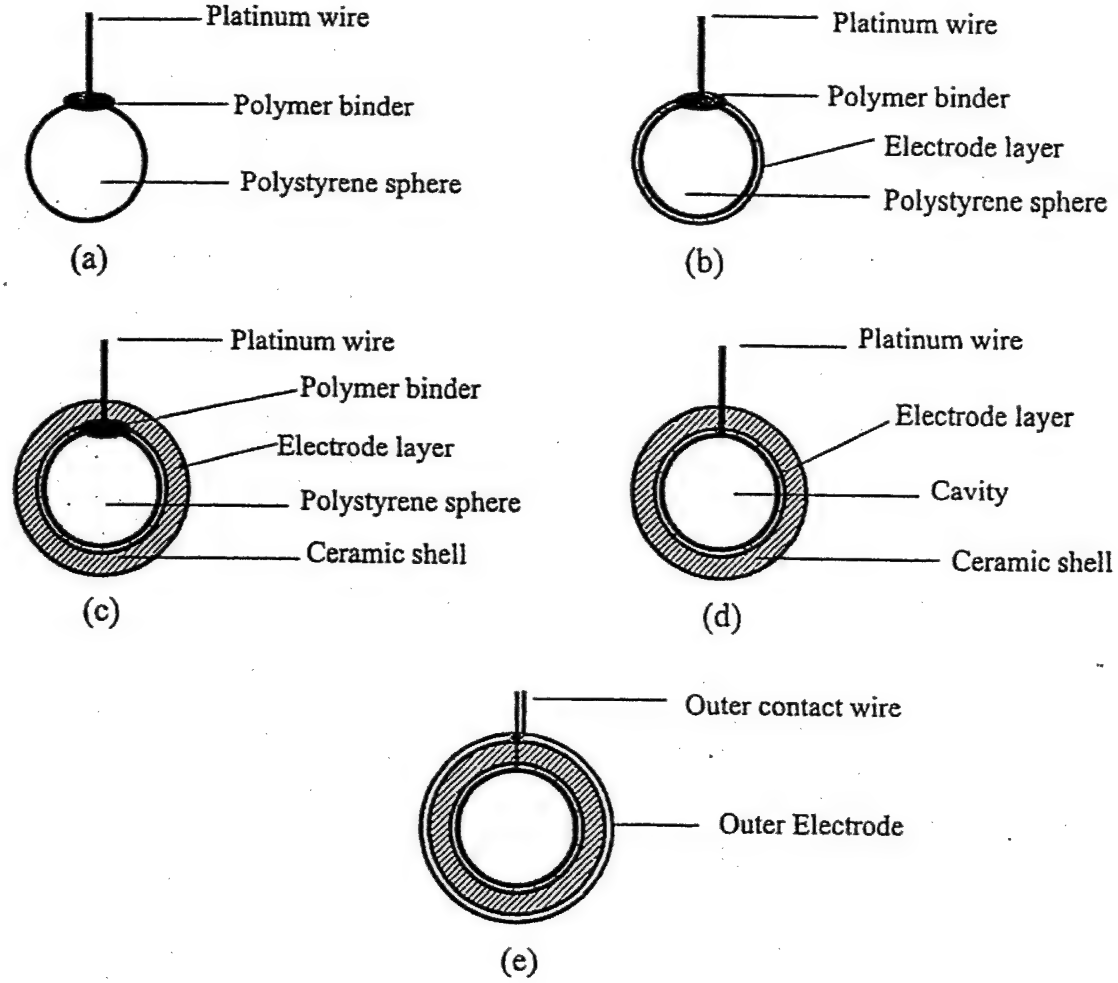


*FIGURE 11 - (a) A cross sectional view of the polystyrene spheres with platinum wires attached. A pyrolyzable binder (PVA, etc) is used to keep the wire in position, (b) illustrates the pre-wired polystyrene spheres coated with platinum contained slurry, (c) shows the pre-wired polystyrene spheres coated with a ceramic layer on top of a platinum layer, (d) shows the sintered ceramic hollow sphere with co-fired inner electrode and protruded platinum wire, (e) is a cross sectional view of illustrating the finished spherical transducer by electroding the outer surface of the hollow sphere whose inner surface is already electroded by co-firing.*

Thermally decomposable spheres made of polystyrene or hollow polystyrene spheres are used as a fugitive pattern. To achieve a ceramic layer with high green density, a sphere or hollow sphere with a porous structure is preferable. A thin metal wire, typically Pt or Ni, is first attached to the sphere and secured in position using a thermally decomposable binder such as PVA. The wire is used later to apply voltage to the inner electrode. An electrode layer is then coated on the outer surface of the polymer core by dipping it into

a slurry containing metal powders. The electrode is then dried and further serves as a mold for the ceramic slurry. A ceramic shell is then deposited on top of the dried electrode by dipping into a well dispersed ceramic slurry containing binder and dispersant. The ceramic slurry can be aqueous or non-aqueous. The ceramic layer thickness is controlled by immersion time, the solid loading of the ceramic slurry, and its viscosity. When a large wall thickness is desired, multiple coatings can be performed. When the sphere is removed from the slurry, excess slurry on the sphere can be removed by spinning the sphere. Spinning also improves the uniformity of the wall thickness. The porous polystyrene spheres and the electrode layer absorb water from the ceramic layer. The capillary suction allows a dense green body of ceramic shell to be formed, which is crucial in sintering a fully densified ceramic body.

After forming, the spheres are dried and taken through a polymer burnout process in the temperature range between 300 and 700 °C. A ceramic shell with an inner electrode is obtained after this process. Then the ceramic shell is cofired with its electrode. The sintering conditions vary according to the ceramic composition. In most cases, the ceramic and electrode materials are sintered in the temperature range between 1200 and 1400 °C. The immersion time and optimum sintering temperature must be adjusted experimentally to achieve the maximum sintering density of ceramic. For lead containing compositions, the ceramic shell needs to be fired in a closed container in a lead rich atmosphere to reduce lead loss from the ceramic body.

After sintering, the outer surface of the shell is coated with electrode metal through sputtering or dipping. A tiny lead wire is then attached to the outer electrode. The ceramic shell is poled in the case of piezoelectric materials by subjecting the ceramic shell to high electric field at elevated temperatures in the range between 100 and 200 °C. This completes the process of fabricating a hollow spherical transducer.

Multilayer hollow sphere transducers (Fig. 12) can be fabricated by a multiple dipping process to give a structure with alternating electrode and ferroic ceramic layers. After the first ceramic layer is deposited, it is dried and then coated with another layer of electrode material, followed by a coating of another layer of ceramic. Care must be taken to make certain the second electrode layer does not touch the platinum wire and a hole must be left in the second ceramic layer for electrical connection. The goal is to make multilayer hollow spheres with many thin layers similar to multilayer capacitors and multilayer actuators.

After polymer burnout and sintering, the electrodes are connected to electrical lead wires. Different connections are available depending on applications. For receive applications, the layers can be connected in series to improve the receive response. For projector applications, the layers can be

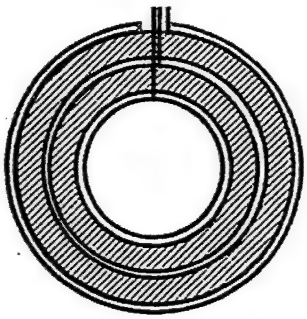

*FIGURE 12 - A multilayer hollow spherical transducer prepared using a multiple coating process.*

connected in parallel to increase the pressure output to transmit directional beams with the electrodes driven with different phases and amplitudes.

To access certain of the antisymmetric Curie group symmetries (Table 2) it is necessary to convert the hollow spheres into hemispheres or rings. This step is carried out by mounting the hollow sphere in a polymer matrix and polishing the sphere down on one side (for the hemisphere) or two sides (for the ring). The polymer matrix provides the mechanical strength required for the lapping operation.

Limited re-electroding can be accomplished after removing the outer electrodes used in poling the transducer. This enables us to apply driving fields in directions other than the poling field directions, and thereby generate different symmetries and different vibration modes.

## ACOUSTIC APPLICATIONS

Applications are not the main focus of this discussion but it is important to have practical goals in mind to justify the research. The increasing use of ultrasonic techniques in biomedical and underwater applications and the sophistication of these techniques has increased the need to characterize the acoustic fields using ultrasonic transducers. In the last forty years several different techniques and probe designs have been employed for this purpose, including rod-guided waves, thermoacoustic sensors, fiberoptic sensors utilizing acousto-optic interaction, and miniature acoustic probes made from ceramic and polymer-based piezoelectrics. Miniature ultrasonic probes have been used both for mapping the field of a hydrophone as well as the nonacoustic field of turbulent flow. There are, however, several important requirements for micro-probe sensors in these applications. In detecting underwater signals or biological pressure waves, omnidirectionality is highly advantageous. Accurate mapping of an acoustic field requires that: (i) the physical dimensions of the probe

should be smaller than the acoustical wavelength of interest, (ii) the resonance frequencies of the probe should be well above the frequency range of interest, (iii) adequate sensitivity with an acceptable signal-to-noise ratio and (iv) wide bandwidth.

Although volume expanders with spherical shape are thought to be the best way to achieve omnidirectionality, there are problems associated with fabricating hollow spheres with sizes in the millimeter range, as pointed out by previous researchers. There are a number of examples of transducers prepared from piezoelectric plates, but these transducers have a pronounced directivity even when the probe dimensions are smaller than a wavelength. Solutions proposed previously for the directivity problem include solid-core spherical probes and hollow cyclindrical probes.

In addition to the underwater applications, spherically shaped transducers are also desirable in medical ultrasound applications. Examples include a quasi-omnidirectional polymer-based transducer developed for ultrasonic guidance of intravascular catheters and a focused transducer for biomedical ultrasonic imaging, prepared from a spherical ceramic shell. Every year millions of medical procedures are performed in the United States using catheter systems a few millimeters in diameter. Typically, they are inserted through the skin into blood vessels or into various body cavities to deliver drugs or therapeutic devices.

At present catheters are guided with real-time X-ray imaging (fluoroscopy) despite the advantages of ultrasound imaging over X-ray imaging in terms of cost, safety and availability. Because the wavelengths used in medical ultrasonic imaging (0.2-0.5 mm) are several times smaller than the catheter, it acts as a reflector and the ultrasonic visibility of the catheter is highly direction dependent with regard to external ultrasonic beams. One solution to this problem is to mount an omnidirectional ultrasonic transducer on the catheter that can serve as an ultrasonic marker to help locate the catheter without the use of hazardous X-rays. The applications of these ultrasonic imaging catheters include guiding balloon angioplasties of the leg, guiding catheters inside the heart to ablate incorrectly functioning cardiac tissue, and guiding catheters within the uterus to inject fluid into the fallopian tubes to test for tubal blockage. Ceramic hollow sphere transducers have the required omnidirectionality and high sensitivity and can be electrically matched to the electronic systems.

It is our hope that the miniature hollow sphere transducers described in this paper will help satisfy the size, directionality and acoustic impedance matching requirements for biomedical and underwater applications. Later we hope to manufacture the transducers in large numbers by a simple inexpensive process, which makes it possible to mass-produce throw-away transducers. The basic understanding of vibration modes in small spherical transducers provided by this symmetry-guided approach will help immensely.

## REFERENCES

1. S. Alkoy, *Piezoelectric Hollow Sphere Transducers*, Penn State University Ph.D. Thesis in Materials Science and Engineering, p. 89 and p. 111 (1999).
2. R.R. Birss, *Symmetry and Magnetism*, North-Holland Publishing Co., Amsterdam (1964).
3. R.E. Newnham, *Domains in Minerals*, **Amer. Mineralogist**, Vol. 59, p. 906-918 (1974).
4. R.E. Newnham and L.E. Cross, *Symmetry of Secondary Ferroics*, **Mat. Res. Bull.**, Vol. 9, p. 927-934 and 1021-1032 (1974).
5. R.E. Newnham and J.R. Giniewicz, *Nonmechanical Properties of Composites*, **Comprehensive Materials**, Vol. 1, p. 431-463 (2000).
6. W. Voigt, *Lehrbuch der Kristallphysik*, B.G. Teubner, Leipzig (1928).

# APPENDIX 5

*Ferroelectrics*, 2001, Vol. 252, pp. 137-144
Reprints available directly from the publisher
Photocopying permitted by license only

© 2001 OPA (Overseas Publishers Association) N.V.
Published by license under the
Gordon and Breach Science Publishers imprint.
Printed in Malaysia

# The Structure of S-Walls in $m\bar{3}m \rightarrow mmm$ Ferroelastics

JIŘÍ ERHART[a], WENWU CAO[b] and JAN FOUSEK[a]

[a]*Department of Physics and International Center for Piezoelectric Research, Technical University of Liberec, Hálkova 6, CZ-461 17 Liberec 1, Czech Republic and* [b]*Materials Research Laboratory, The Pennsylvania State University, University Park, PA 16802, USA*

*(Received June 2, 2000)*

The S-walls (also called W′-walls) refer to those domain walls whose orientations do not coincide with crystallographic planes but rather change with temperature. A simple continuum model has been constructed to describe the S-wall structures that occur at a $m\bar{3}m \rightarrow mmm$ ferroelastic phase transition. The model describes local values of the elastic strain components and the temperature dependence of the S-wall orientation. Distortions of unit cells across an S-wall was obtained numerically.

*Keywords:* S-walls; W'-walls; Landau-Ginzburg model; crystal symmetry; ferroelastics; domain walls

## INTRODUCTION

The S-walls (also called W'-walls) occur in certain ferroic species [1,2,3] and generally do not coincide with crystallographic planes. The orientation of S-walls (SWs) in ferroelastics depends on the values of spontaneous strain, hence, will change with temperature.

Because the "strange" physical nature and the high application potential for these SW structures, there have been intense experimental studies on them and many interesting results have been obtained. For example, intersections between S-walls and W-walls in ferroelectric $KNbO_3$ [4], temperature induced SW switching in ferroelastic phases of

$NaNbO_3$ [5] and $AgNbO_3$ [6]. S-walls have also been observed in many other orthorhombic materials, such as $PbZrO_3$ [7], $PbHfO_3$ [8], $Pb(Zr_{1-x}Sn_x)O_3$ [9] and $Pb(Yb_{0.5}Nb_{0.5})O_3$ [10].

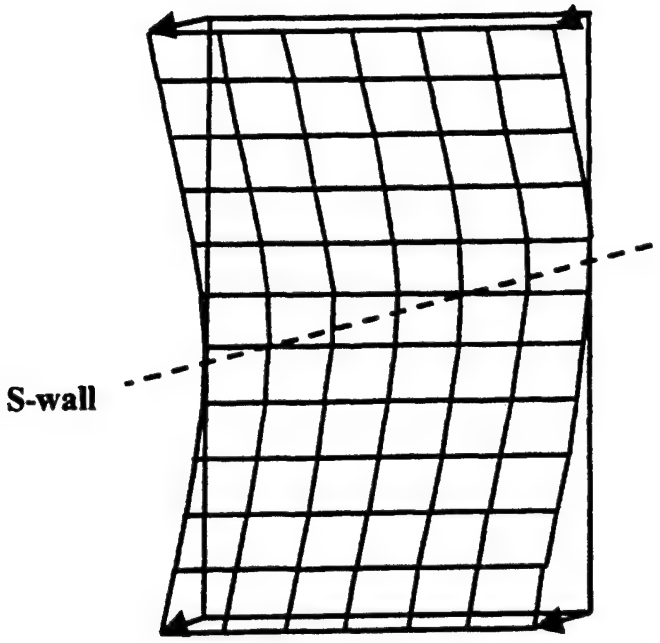


FIGURE 1. Distortion near the S-wall for *4/m→2/m* phase transition[11].

One earlier work on the SW structure was done for a *4/m→2/m* ferroelastic phase transition by using a two-dimensional continuum model [11]. More recently, high resolution transmission electron microscopy has been used to characterize the SWs in monoclinic $LaNbO_4$ (*4/m→2/m* ferroelastics) [12].

In this paper, we present a simple continuum model for the S-walls resulting from an $m\bar{3}m \rightarrow mmm$ phase transition, and also provide numerical solutions for the S-wall structure and strain variations near the SWs.

## THEORETICAL MODEL

The $m\bar{3}m \rightarrow mmm$ ferroelastic phase transition has a shear strain component as the order parameter; the other components of the elastic strain tensor serve as secondary order parameters.

We consider twin structure characterized by the following two spontaneous strains [3],

$$S^{(1)} = \begin{pmatrix} S_1 & S_6 & 0 \\ S_6 & S_2 & 0 \\ 0 & 0 & S_3 \end{pmatrix}, \quad S^{(2)} = \begin{pmatrix} S_3 & 0 & 0 \\ 0 & S_2 & -S_6 \\ 0 & -S_6 & S_1 \end{pmatrix} \tag{1a,b}$$

In order to match the elastic strain at the interface, the orientation of the domain wall plane will depend on the values of spontaneous strain according to the following relation

$$(S_1 - S_3)(x_1 - x_3) + 2S_6 x_2 = 0 \tag{2}$$

All strain components used here are expressed in the same cubic coordinate system of parent paraelastic phase.

Simplified free-energy density (invariant in $m\bar{3}m$) can be written as

$$\begin{aligned} F(\eta_{ij}, \eta_{ij,k}) = {} & \alpha_1(\eta_4^2 + \eta_5^2 + \eta_6^2) + (\eta_1^2 + \eta_2^2 + \eta_3^2) + \\ & \alpha_2\{\eta_1(\eta_5^2 + \eta_6^2 - 2\eta_4^2) + \eta_2(\eta_4^2 + \eta_6^2 - 2\eta_5^2) + \eta_3(\eta_4^2 + \eta_5^2 - 2\eta_6^2)\} \\ & \alpha_3(\eta_4^4 + \eta_5^4 + \eta_6^4) + g\{(\frac{\partial \eta_4}{\partial x_1})^2 + (\frac{\partial \eta_5}{\partial x_2})^2 + (\frac{\partial \eta_6}{\partial x_3})^2\}. \end{aligned} \tag{3}$$

The linear elastic strains, $\eta_{ij}$, are defined by the derivative of the elastic displacement $\boldsymbol{u}$

$$\eta_{ij} = \frac{1}{2}(u_{i,j} + u_{j,i}) \tag{4}$$

and expressed using the Voigt notation $\eta_1 = \eta_{11}$, $\eta_2 = \eta_{22}$, $\eta_3 = \eta_{33}$, $\eta_4 = 2\eta_{23}$, $\eta_5 = 2\eta_{13}$, $\eta_6 = 2\eta_{12}$. All the expansion coefficients in Equation (3) are assumed to be temperature independent except $\alpha_1 = \alpha_0 (T\text{-}T_0)$, with $\alpha_0 > 0$. In order to reduce the number of independent coefficients in the free energy expansion, we have normalized the free energy density by the coefficient of the second term.

SW problem is translationally invariant along the wall plane and hence all quantities characterizing the SW should depend on the dis-

tance from SW only. We choose a new coordinate system with one of the axes ($x'_1$) perpendicular to the SW, and the remaining two axes ($x'_2$, $x'_3$) parallel to the SW plane (Figure 2). Due to this choice the orientation of the coordinate system depends on the values of spontaneous strains, i.e. on temperature.

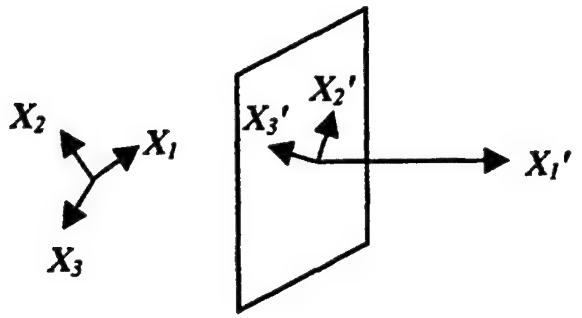


FIGURE 2. Relationship between the new and old coordinate systems.

The corresponding coordinate transformation can be chosen in a special form given by

$$\begin{pmatrix} x'_1 \\ x'_2 \\ x'_3 \end{pmatrix} = \begin{pmatrix} \frac{1}{\sqrt{2}}C & \frac{1}{\sqrt{2}} & -D \\ \sqrt{2}D & 0 & C \\ -\frac{1}{\sqrt{2}}C & \frac{1}{\sqrt{2}} & D \end{pmatrix} \begin{pmatrix} x_1 \\ x_2 \\ x_3 \end{pmatrix}, \tag{5}$$

$$C = \frac{S_1 - S_3}{\sqrt{(S_1 - S_3)^2 + 2S_6^2}}, \quad D = \frac{S_6}{\sqrt{(S_1 - S_3)^2 + 2S_6^2}} \tag{6a,b}$$

The components $\eta_{ij}$ of the elastic strain in the free-energy must be transformed to the new coordinate system (denoted by a prime, $\eta'_1, \eta'_2, \eta'_3$, etc.).

## S-WALL SOLUTIONS

The continuum SW solution can be derived from the Euler-Lagrange equations taking into account proper boundary conditions

$$\frac{\partial}{\partial x_k}\left[\frac{\partial F}{\partial \eta_{ij,k}}\right]-\frac{\partial F}{\partial \eta_{ij}}=0, \quad (i,j=1,2,3) \tag{7}$$

In materials without defects the following compatibility relations must also be satisfied [13]

$$\varepsilon_{ikl}\varepsilon_{jmn}\eta_{ln,km}=0, \quad (i,j,k,l,m,n=1,2,3) \tag{8}$$

where $\varepsilon_{ijk}$ is the Levi-Civita's tensor (permutation symbol). Equations (7) and (8) are given in invariant tensor form, independent of the choice of the coordinate system. In the rotated coordinate system the compatibility relations are reduced to

$$\eta'_{22,11}=0, \qquad \eta'_{33,11}=0, \qquad \eta'_{23,11}=0 \tag{9}$$

because all strains depend on $x'_1$ only due to the translational symmetry.

In non-homogeneous system, five components of the spontaneous strain in Equation (1) (transformed to the rotated coordinates) are equal in both domains, but the shear strain component $S'_6$ (order parameter) has opposite signs in the two domains. The boundary conditions for the elastic strains should match spontaneous strains of domain 1 as $x'_1 \to +\infty$ and domain 2 as $x'_1 \to -\infty$

$$\lim_{x'_1\to\pm\infty}\eta'_\alpha(x'_1)=S'^{(1)}_\alpha, \ \lim_{x'_1\to\pm\infty}\eta'_6(x'_1)=\pm S'^{(1)}_6, (\alpha=1,2,...,5) \tag{10a,b}$$

The compatibility relations Equation (9) can be integrated and the strain tensor components parallel to the SW ($\eta'_2, \eta'_3, \eta'_4$) must be constant due to the required boundary conditions Equation (10a). For convenience, we introduce the dimensionless strain components

$$y'_1=\frac{\eta'_1}{S'_1}, \quad y'_5=\frac{\eta'_5}{S'_5}, \quad y'_6=\frac{\eta'_6}{S'_6}.$$

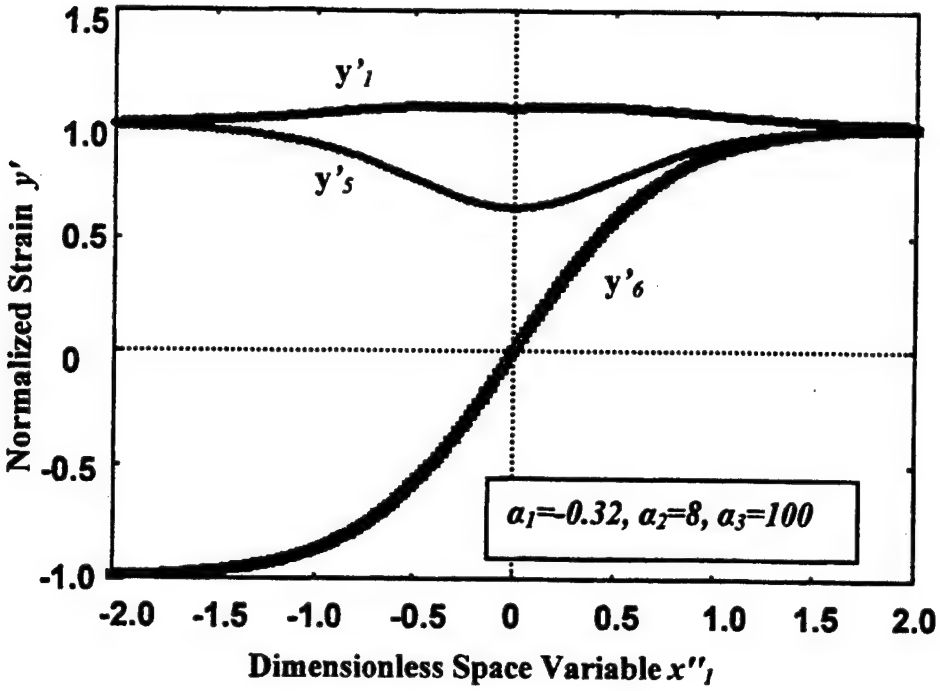


FIGURE 3. Normalized strain components across an S-wall at a specific temperature below $T_0$.

Finally, the SW problem reduces to solving the following three coupled differential equations (dimensionless coordinate $x_1^{\cdot}$ is defined by $x_1^{\cdot} = \frac{x_1}{\sqrt{g}}$)

$$\frac{d^2 y_\alpha^{\cdot}}{dx_1^{\cdot 2}} = R_\alpha(y_1^{\cdot}, y_5^{\cdot}, y_6^{\cdot}), \quad (\alpha = 1,5,6) \tag{11}$$

The functions $R_1$, $R_5$, $R_6$ are third-order polynomial functions in terms of the relative elastic strains $y'_1$, $y'_5$, and $y'_6$. The coefficient of each term is a complicated function of the coefficients $\alpha_1$, $\alpha_2$, and $\alpha_3$ and will change with temperature. Typical solution of a twin with an SW is given in Figure 3.

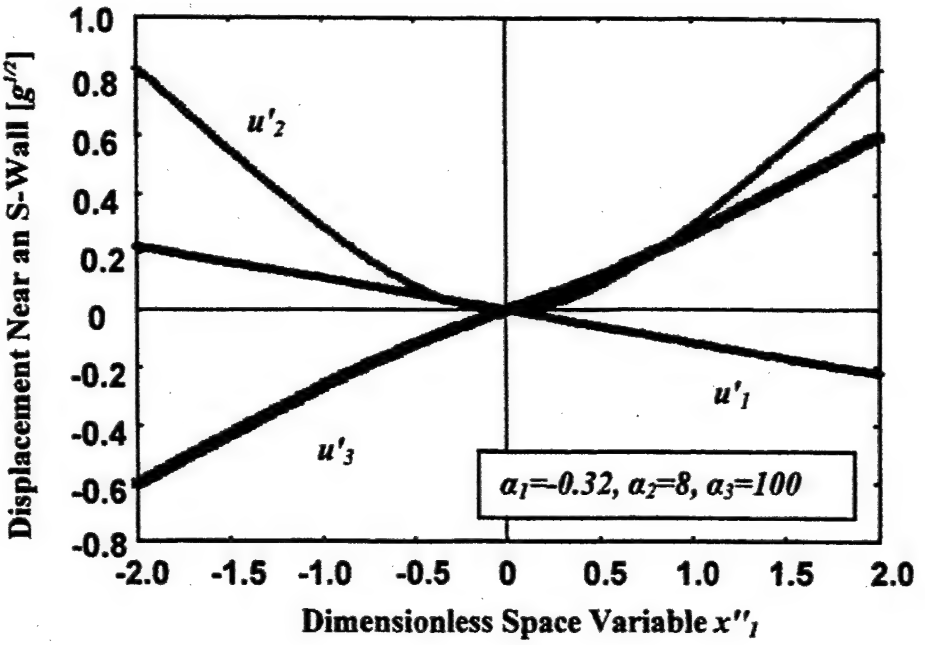


FIGURE 4. Displacement profile across an S-wall at a specific temperature below $T_0$.

The elastic displacements can be found by numerically integrating the corresponding strain components in rotated coordinates, i.e. Equation (4). Typical solutions of the elastic displacements are shown in Figure 4.

## SUMMARY

A simple three-dimensional continuum model has been developed for the ferroelastic S-wall structure produced by a $m\bar{3}m \rightarrow mmm$ ferroelastic phase transition. The elastic strains as well as displacements near an S-wall have been calculated using this model. In general, lattice deformation near the S-wall not only contains longitudinal strain but also includes nonzero shear strain components. Although the SW solution is only numerical, our three-dimensional model provides a unique theoretical tool to study SW structure in the systems produced through a $m\bar{3}m \rightarrow mmm$ ferroelastic phase transition.

## ACKNOWLEDGEMENTS

This work was supported by the NSF under grant number DNS 9704714 and the ONR under grant numbers N00014-98-1-0527 and N00014-96-1-1173. One of the authors (J.E.) is grateful for support from the Ministry of Education of the Czech Republic (J11/98:242200002) and from the Grant Agency of the Czech Republic (GAČR 202/00/1245).

## *References*

[1] J. Fousek, V. Janovec, J. Appl. Phys. **40**, 135 (1969).
[2] J. Fousek, Czech. J. Phys. B **21**, 955 (1971).
[3] J. Sapriel, Phys. Rev. B **12**, 11, 5128 (1975).
[4] E. Wiesendanger, Czech. J. Phys. B **23**, 91 (1973).
[5] S. Miga, J. Dec, M. Pawelczyk, J. Phys.: Condens. Matter **8**, 8413 (1996).
[6] S. Miga, J. Dec, J. Appl. Phys. **85**, 1756 (1999).
[7] L. E. Balyunis, V. Yu. Topolov, I. S. Bah, A. V. Turik, J.Phys.:Condens.Matter **5**, 1419 (1993).
[8] L. E. Balyunis, V.Yu.Topolov, A. V. Turik, O. E. Fesenko, Ferroelectrics **111**, 291 (1990).
[9] S. T. Bah, L. E. Balyunis, V. Yu.Topolov, O. E. Fesenko, Ferroelectrics **157**, 1 (1994).
[10] K. H. Park, W. K. Choo, J. Phys.: Condens. Matter **10**, 5995 (1998).
[11] Y. Ishibashi, J. Phys. Soc. Japan **47**, 1857 (1979).
[12] Li Jian, C.M.Wayman, J.Am.Ceram.Soc. **79**, 1642 (1996).
[13] E.A. Love, in *A Treatise on the Mathematical Theory of Elasticity*, Dover, New York (1944).

# APPENDIX 6

ELSEVIER

June 1999

Materials Letters 39 (1999) 287–291

MATERIALS LETTERS

www.elsevier.com/locate/matlet

# Possible piezoelectric composites based on the flexoelectric effect

J. Fousek [a,1], L.E. Cross [a,*], D.B. Litvin [b]

[a] *Materials Research Laboratory, The Pennsylvania State University, University Park, PA 16802, USA*
[b] *Department of Physics, The Pennsylvania State University, Berks Campus, Reading, PA 19610, USA*

Received 30 November 1998; accepted 2 December 1998

**Abstract**

Current piezoelectric composite materials contain two or more phases out of which at least one reveals piezoelectric properties in itself. We show that this is in fact not a necessary condition. The mechanism of the linear stress-polarization response averaged over a composite sample can be also based on flexoelectric properties of one or more constituents. Proper shaping of the composite constituents is required, such that the system as a whole acquires a symmetry allowing for nonzero piezoelectric coefficients even if none of the components is piezoelectric. Externally applied stress is transformed, due to proper geometry of the constituents with different elastic properties, into a strongly nonhomogeneous distribution of induced strain. Flexoelectric properties which are, by symmetry, allowed in all materials, transform the strain gradient into polarization. The proposed piezoelectric composite falls into the category of composites with product properties since it involves different assets of the phases (elastic, flexoelectric and dielectric) and the interaction between the phases, determining the inhomogeneous distribution of stress, is essential. © 1999 Elsevier Science B.V. All rights reserved.

*PACS:* 77.84 – s; 77.90 – k

*Keywords:* Piezoelectric materials: Composites; Flexoelectric effect

## 1. Introduction

Composites are multiple-phase solids which combine materials of different chemical composition and macroscopic properties with the aim to produce samples with the desired average response. Figures of merit of the final composite can be tuned by choosing component phases with the right properties and coupling them in an optimum manner. Newnham et al. [1] offered a classification of composites based on three criteria. The most important aspects are the macroscopic properties of the constituents, e.g., their response to electric, magnetic and elastic fields. This determines the final assets of the composite. The second, connectivity, indicates the way in which each phase connects to itself. It is essential for the magnitude and symmetry of the composite's response. The third is scale, which determines the response of the composite when wavelengths of propagating waves become comparable with the characteristic dimensions of any of the constituents.

Many composites have been considered in connection with their piezoelectric properties [1,2]. To discuss or model the piezoelectric response of a composite, it was generally assumed that at least one

* Corresponding author. Tel.: +1-814-865-1181; Fax: +1-814-863-7846

[1] On leave from the Department of Physics, University of Technology, CZ-46117 Liberec, Czech Republic.

00167-577X/99/$ - see front matter © 1999 Elsevier Science B.V. All rights reserved.
PII: S0167-577X(99)00020-8

of the components was piezoelectric. In this paper we reconsider this assumption.

## 2. Discussion

For a system to be piezoelectric, it has to fulfill certain symmetry criteria. If it has a crystalline structure, the material must, by symmetry, belong to one of 20 crystal classes. The remaining 12 classes do not show piezoelectric properties; these are the 11 centrosymmetric classes and the class 432 in which piezoelectricity is forbidden by the combined symmetry elements.

In Nye's widely used overview of the equilibrium properties of the 32 crystal classes [3], the properties of an isotropic medium are also included. The symmetry of an isotropic medium is primarily characterized by the presence of arbitrarily oriented symmetry axes of infinite order. Depending on whether its symmetry elements do or do not include arbitrarily oriented mirror planes, the isotropic medium represents one of the Curie symmetry groups (limiting groups), namely, $\infty$, $\infty/m$ or $\infty\infty$, respectively. In both these groups no nonzero piezoelectric coefficients are possible.

Table 1
Matrices of $d_{ijk}$ in Curie groups which are piezoelectric

$\infty$

$$\begin{vmatrix} 0 & 0 & 0 & d_{14} & d_{15} & 0 \\ 0 & 0 & 0 & d_{15} & -d_{14} & 0 \\ d_{31} & d_{31} & d_{33} & 0 & 0 & 0 \end{vmatrix}$$

$\infty 2$

$$\begin{vmatrix} 0 & 0 & 0 & d_{14} & 0 & 0 \\ 0 & 0 & 0 & 0 & -d_{14} & 0 \\ 0 & 0 & 0 & 0 & 0 & 0 \end{vmatrix}$$

$\infty m$

$$\begin{vmatrix} 0 & 0 & 0 & 0 & d_{15} & 0 \\ 0 & 0 & 0 & d_{15} & 0 & 0 \\ d_{31} & d_{31} & d_{33} & 0 & 0 & 0 \end{vmatrix}$$

In all groups the $\infty$ axis is taken as $x_3$; the axes $x_1$, $x_2$ are perpendicular to $x_3$ and to each other, otherwise their orientation is arbitrary.

Fig. 1. Characteristic forms representing symmetry of the Curie groups which allow for piezoelectricity [4].

In addition to these two groups, however, we may consider systems representing the remaining Curie groups, namely $\infty$, $\infty/m$, $\infty 2$, $\infty m$ and $\infty/mm$. Out of these, $\infty/m$ and $\infty/mm$ do not allow for the existence of nonzero components of a third-rank polar tensor $d_{ijk}$ of symmetry $V$ [$V^2$], i.e., of the piezoelectric tensor. In the remaining groups nonzero components are possible, as shown in Table 1. It is useful to illustrate symmetry properties of these point groups by characteristic forms [4]: these are shown in Fig. 1. We realize that systems revealing the symmetries $\infty$ or $\infty 2$ can exist in two forms, left- and right-handed.

Thus, for instance, a composite with connectivity 0–3, in which the phase '0' is represented by cone-shaped particles whose $\infty$-axes are parallel to each other but which are randomly distributed in the phase '3', has the symmetry $\infty m$. Next we can imagine that the cones are subject to helical deformations so that spiral-shaped particles result. This lowers the symmetry to $\infty$. The system can exist in two forms, right- or left-handed. The third piezoelectric Curie group can be visualized starting again with a composite of connectivity 0–3 in which the phase '0' is represented by cylinders: its symmetry is nonpiezoelectric $\infty/mm$. If now all cylinders are subject to a helical deformation, the symmetry is reduced to $\infty 2$, which again can exist in two forms differing in handedness. Fig. 2 shows such composites schematically. These particular models are based on the 0–3 connectivity but similar considerations can be made for other connectivities as well.

It thus appears easily possible to manufacture composites whose symmetry properties allow for the existence of piezoelectric tensor although they consist of components which by themselves need not be made of piezoelectric materials.

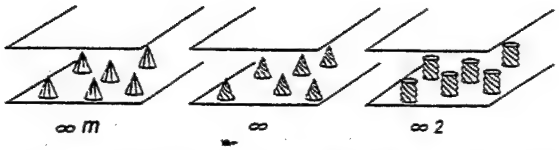


Fig. 2. Simple models of 0–3 composites allowing for piezoelectricity. There is an infinite number of shapes of the 0-constituent that could be tested for a maximum response of flexoelectric polarization.

A long time ago, Shubnikov et al. introduced the concept of *piezoelectric textures*; see Ref. [5] and the first chapter of Ref. [6]. This notion denotes systems composed of crystallites which show piezoelectric properties, some crystal axes of which are chaotically oriented in a given way, leading to specific averaging of properties characterizing the piezoelectric effect. In the subsequent parts of Ref. [6], two specific kinds of materials are discussed as examples. Plate-like samples containing crystallites of Rochelle salt separated by amorphous layers (chapter 2 by Konstantinova and Sil'vestrova) could indeed be considered a 0–3 composite. Polarized ceramic samples of barium titanate (chapter 3 by Zheludev), on the other hand, whose symmetry is $\infty m$, represent a piezoelectric texture by Shubnikov's definition but could only be included into the family of composites if the grain boundaries had an appreciable volume.

In both these cases basic components are piezoelectric by themselves (point symmetries 2 for Rochelle salt and $4mm$ for $BaTiO_3$). On the other hand, in the general symmetry approach this is not a specific requirement. As shown above, the possibility of a piezoelectric response in a 0–3 composite is assured, from the point of view of symmetry, already by shaping the particles of zero connectivity. We thus have to look for alternative mechanisms which would lead to formation of an average polarization proportional to an applied stress for a 0–3 composite made of nonpiezoelectric materials, with properly shaped particles.

For several decades, the effect of inducing polarization by imposing spatially nonuniform strain was repeatedly discussed in the literature. Originally discovered experimentally in centrosymmetric (and therefore nonpiezoelectric) liquid crystals, it was termed the flexoelectric effect and described by the equation

$$P_l = \mu_{ijkl}\frac{\partial \varepsilon_{ij}}{\partial x_k} \tag{1}$$

from which it is obvious that the tensor $\mu$ has the general symmetry $[V^2]\,V^2$, i.e., $\mu_{ijkl} = \mu_{jikl}$ is the only requirement imposed by symmetry. A tensor of this symmetry has nonzero components in all crystal classes. The first attempt to observe the flexoelectric effect in a solid crystal of point symmetry $4/m$, namely $CaWO_4$ was made by Zheludev et al. [7]. As shown by Tagantsev [8], the static effect includes a bulk and a surface contribution. The bulk part is due to the fact that the crystal lattice which has been nonhomogeneously deformed in accordance with the laws of the theory of elasticity is not in equilibrium from the point of view of displacements in the unit cell. The displacements that are necessary to reach true equilibrium give rise to a dipole moment of the cell, i.e., to polarization. In addition, the deformation of the surface of a finite sample, whose electrical neutrality in the original state was achieved by compensating free charges, leads to a surface contribution which can be expected to be of the same order of magnitude as the bulk part of the effect. The simplest estimates [8] for a common insulator indicate that both contributions to the value of $\mu$ are of the order of the ratio of the electron charge to the lattice constant.

We now have in mind a 0–3 composite made of nonpiezoelectric constituents, in which the 0-elements are shaped and oriented in such a way that the overall symmetry is one of the Curie groups $\infty$, $\infty m$ and $\infty 2$. As an example, consider a plate-like sample of composite of symmetry $\infty m$ in which the orientation of the 0-constituents is such that the $\infty$ axis is perpendicular to the major plane. Since the tensor $\mu_{ijkl}$ has nonzero components even for continuous groups $\infty\infty$ and $\infty\infty m$ [4], one can imagine that both the 0-component and 3-components are made of isotropic materials. Their shaping is such that when a load $\sigma_{33\mathrm{appl}}$ is applied, the spatial distribution of stress will be nonhomogeneous, leading to gradients of strain in both constituents. To be concrete, we can imagine that a plate-like sample of thickness $d$ is

divided into a regular system of cubes of linear size $d_0$, each cube containing one particle of the component with zero connectivity and only this component is assumed to have nonzero flexoelectric properties. The dipole moment of each 0-particle within one cube will be given by

$$p_{3\text{flex}} = \int_{(d_0^3)} \mu_{3ijk} \frac{\partial \varepsilon_{ij}(\mathbf{r})}{\partial x_k} \mathrm{d}\mathbf{r} \tag{2}$$

where the strain gradient will be determined by a factor $a_{ijk}$ which reflects the shape of the components 0 of the composite and depends on elastic compliances of both constituents:

$$\frac{\partial \varepsilon_{ij}(\mathbf{r})}{\partial x_k} = a_{ijk}(\mathbf{r})\,\sigma_{33\text{appl}}. \tag{3}$$

The induced charge density on the electrode of the plate will be

$$Q = \frac{p_{3\text{flex}}}{d_0^3} \tag{4}$$

so that the effective polarization of the sample $P_3 = Q$ will be given by

$$P_3 = d_{33\text{flex}}\,\sigma_{33\text{appl}}, \tag{5}$$

where

$$d_{33\text{flex}} = \frac{1}{d_0^3} \int_{(d_0^3)} a_{ijk}(\mathbf{r})\,\mu_{3ij3}\mathrm{d}\mathbf{r}. \tag{6}$$

A piezoelectric composite based on flexoelectricity will be useful if a reasonably high value of $d_{33\text{flex}}$ could be reached, e.g., 100 pC/N. It follows from the preceding formulae that the latter can be influenced by a proper tuning of several independent factors: selecting materials with high values of those components of $\mu_{ijkl}$ which are involved in a particular geometry of the constituents, choosing a high density of the constituents 0, but also by achieving large factors $a_{ijk}$ which depend on the shape of the 0-components and on the elastic tensors of both 0 and 3 constituents.

Newnham [2] classified properties of composite materials into three groups: sum properties (the composite property coefficient depends on the corresponding coefficients of its constituent phases), combination properties (the composite property coefficient depends on two or more corresponding coefficients of its constituent phases) and product properties. In the latter case the composite property coefficient involves different properties of the constituent phases with interactions between them. It appears that piezoelectric composites based on flexoelectricity fall into this last category and the effect might be referred to as a 'shape-controlled product property'; indeed the combined effect involves different properties of the constituent phases (elastic, flexoelectric and dielectric) and the interaction between the phases is essential; here it is the nonhomogeneous distribution of stress which depends primarily on the shapes of constituents and on their elastic tensors. The following sequence of phenomena describes the combined effect: homogeneous applied stress → inhomogeneous stress in the 0-constituents → polarization in the 0-constituents due to flexoelectric effect → nonhomogeneous distribution of polarization in the sample depending also on spatial distribution of permittivity → nonhomogeneous surface bound charge → averaged surface bound charge density defining effective polarization. Considering a stress $\sigma_{zz}$ applied perpendicularly to a plate-like composite sample, we have the sequence

$$\sigma_{zz,\text{appl}} \rightarrow \text{grad}\,\sigma_{ij,\text{sample}}(\mathbf{r}) \rightarrow P(\mathbf{r}) \rightarrow q(x,y)_{\text{surf}}$$

$$\rightarrow \bar{q}_{\text{surf}} \propto P_{z,\text{surf}} \propto \sigma_{zz,\text{appl}}.$$

At this stage very few data on the tensor $\mu_{ijkl}$ in solids seem to be available. A fairly strong flexoelectric response was reported for crystals of $Cd_2WO_4$ [7]. Marvan and Havránek [9] studied the flexoelectric effect in elastomers of isotropic symmetry. Samples in the form of truncated pyramids were deformed by axial pressure along the axis 3. Then for constant volume of the sample the only active coefficient is $\mu_{3333}$ which was estimated to be of the order $10^{-11}$ to $10^{-10}$ C/m. Experiments with 0–3 composites in which the 0-constituent or both components of the composite would be a polymer might be worthwhile.

We may also note that such composite samples might be interesting to investigate in which one of the constituents is piezoelectric; due to flexoelectricity, its induced dipole moment could be considerably enhanced by proper shaping to optimize the nonhomogeneous distribution of strain.

## Acknowledgements

J. Fousek: This work was supported in part through grants VS 96006 and 202/96/0722 of the Ministry of Education and of the Grant Agency of the Czech Republic, respectively. D.B. Litvin: This work was supported in part by the National Science Foundation through grant No. DMR-9722799.

## References

[1] R.E. Newnham, D.P. Skinner, L.E. Cross, Mater. Res. Bull. 13 (1978) 525.
[2] R.E. Newnham, Jpn. J. Appl. Phys. 25 (1986) 9, Suppl. 25-1.
[3] J.F. Nye, Physical Properties of Crystals, Clarendon Press, Oxford, 1993.
[4] Yu.I. Sirotin, M.P. Shaskolskaya, Fundamentals of Crystal Physics, Mir Publishers, Moscow, 1982.
[5] A.V. Shubnikov, Piezoelectric Textures (in Russian), Publishing House of the Academy of Sciences of USSR, Moscow–Leningrad, 1946.
[6] A.V. Shubnikov, I.S. Zheludev, V.P. Konstantinova, I.M. Sil'vestrova, Investigation of Piezoelectric Textures (in Russian), Publishing House of the Academy of Sciences of USSR, Moscow–Leningrad, 1955.
[7] I.S. Zheludev, Yu.S. Likhacheva, N.A. Lileeva, Sov. Phys. Crystallogr. 14 (1969) 425.
[8] A.K. Tagantsev, Sov. Phys. JETP 61 (1985) 1246.
[9] M. Marvan, A. Havránek, Progr. Colloid Polym. Sci. 78 (1988) 33.

# APPENDIX 7

# Observation of the flexoelectric effect in relaxor $Pb(Mg_{1/3}Nb_{2/3})O_3$ ceramics

Wenhui Ma and L. Eric Cross[a)]
*Materials Research Laboratory, Pennsylvania State University, University Park, Pennsylvania 16802*

(Received 31 October 2000; accepted for publication 22 January 2001)

The relationship between elastic strain gradient and electric polarization was investigated in the relaxor ferroelectric lead magnesium niobate ceramic. Experimental studies indicated that flexoelectric polarization is linearly proportional to the applied strain gradient, and the flexoelectric coefficient $\mu_{12}$ is calculated to be $4\times10^{-6}$ C/m, which is much higher than the early phenomenological estimations. © *2001 American Institute of Physics.* [DOI: 10.1063/1.1356444]

The piezoelectric effect is the linear relationship between electric polarization and applied elastic stress (direct effect) or between elastic strain and applied electric field (converse effect). Due to the symmetry requirements, the piezoelectric effect may only exist in 20 crystal point groups where center of symmetry is absent. More than three decades ago, phenomenological analysis[1] stated that electric polarization might be induced by inhomogeneous strain in the materials. Later the term flexoelectric was coined to describe such an effect in analogy to an effect discovered in the nonpiezoelectric liquid crystals,[2] and tensor property[3] and microscopic theory[4] were investigated theoretically for single crystals. The flexoelectric effect is defined by the following relation:

$$P_l = \mu_{ijkl}\frac{\partial \epsilon_{ij}}{\partial x_k}, \tag{1}$$

where $P_l$ is the $l$th component of flexoelectric polarization, $\mu_{ijkl}$ is the flexoelectric coefficient, $\epsilon_{ij}$ is the elastic strain, and $x_k$ is the position coordinate. Flexoelectricity is controlled by a fourth-rank tensor, and thus is a property of all insulating solids, but so far no flexoelectric coefficients have in fact been measured. In the late 1960s, attempts were made to investigate the electrical polarization in nonpiezoelectric $CaWO_4$ crystals during torsional deformation, which might be closely associated with the flexoelectric effect,[5] but the polarization had been attributed to the disappearance of the center of symmetry after torsion, rather than the effect of the strain gradient. In the late 1980s, a tiny flexoelectric effect was observed in an isotropic elastomer with a static flexoelectric coefficient of the order of magnitude of $10^{-11}$–$10^{-10}$ C/m.[6]

Recently, an idea was developed for designing 0–3 piezoelectric composites based on the flexoelectric effect where none of the components are piezoelectric.[7] If the flexoelectric coefficients are large enough for practical applications a range of properly engineered flexoelectric composite structures could provide completely new piezoelectric capability. Recent studies[8,9] have indicated that the relaxor ferroelectric perovskites like $Pb(Mg_{1/3}Nb_{2/3})O_3$ (PMN) are exceedingly sensitive to elastic stress in the region of temperature between the dielectric permittivity maximum $T_m$ and the freezing temperature $T_f$ from the Vogel–Fulcher relationship. In this letter, we report the investigation of flexoelectric effect in relaxor PMN ceramics.

The flexoelectric measurements were carried out at room temperature by using an experimental setup shown schematically in Fig. 1. The PMN ceramic bars (76.3 mm length, 12.7 mm width, and 2.5 mm thickness) were provided by the TRS company of State College, Pennsylvania. A very thin layer of sputtered gold was used as electrode, the bottom surface of the sample is fully covered with gold while on the top a series of 3 mm diameter electrodes were prepared. Strain gradient was generated in the samples along the thickness direction by a loudspeaker. A MicroStrain DVRT transducer was used to measure the displacement at several positions along the sample bar. The loudspeaker was driven by an HP467A power amplifier with a 1 Hz sinusoidal signal from an SR830 DSP lock-in amplifier. The generated current was monitored by the lock-in amplifier. The generated polarization may be calculated using the following equation:

$$P_3 = \frac{i}{2\pi f A}, \tag{2}$$

where $i$ is the alternating current, $A$ is the electrode area, and $f$ is the driving frequency of the loudspeaker.

The macroscopic symmetry of PMN between $T_m$ and $T_f$ is cubic $m3m$, while the unpoled ceramics are regarded as isotropic. Thus, the flexoelectric tensor matrices may be written as

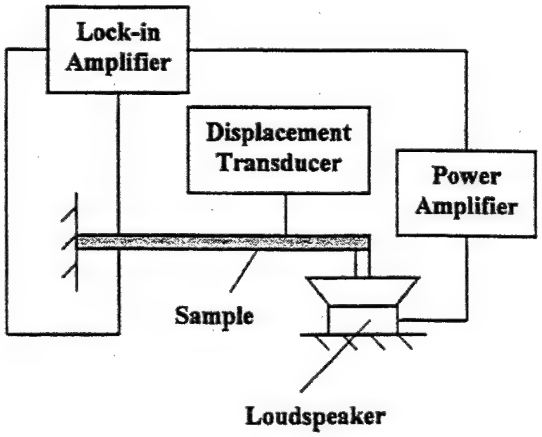


FIG. 1. Experimental setup for the measurement of the flexoelectric effect.

a)Electronic mail: lec3@psu.edu

 © 2001 American Institute of Physics
Downloaded 02 May 2001 to 146.186.113.144. Redistribution subject to AIP license or copyright, see http://ojps.aip.org/aplo/aplcr.jsp

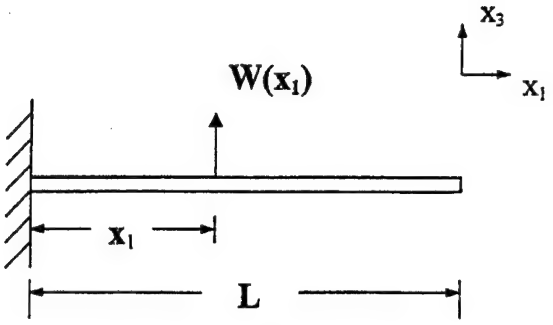


FIG. 2. Schematic diagram of a cantilevered beam and the axial arrangement.

$$\begin{pmatrix} \mu_{11} & \mu_{12} & \mu_{12} & 0 & 0 & 0 \\ \mu_{12} & \mu_{11} & \mu_{12} & 0 & 0 & 0 \\ \mu_{12} & \mu_{12} & \mu_{11} & 0 & 0 & 0 \\ 0 & 0 & 0 & \mu_{44} & 0 & 0 \\ 0 & 0 & 0 & 0 & \mu_{44} & 0 \\ 0 & 0 & 0 & 0 & 0 & \mu_{44} \end{pmatrix}.$$

For the present situation in Fig. 1, only the transverse effect exists, so the flexoelectric equation may be simplified as

$$P_3 = \mu_{12} \frac{\partial \epsilon_{11}}{\partial x_3}. \tag{3}$$

The strain in the PMN ceramic bar was calculated by assuming the natural vibration of a cantilevered beam shown in Fig. 2. The mode shape[10] can be written as

$$W_r(x_1) = A_r[(\sin \beta_r L - \sinh \beta_r L)(\sin \beta_r x_1 - \sinh \beta_r x_1) + (\cos \beta_r L + \cosh \beta_r L) \times (\cos \beta_r x_1 - \cosh \beta_r x_1)], \tag{4}$$

where $A_r = C_1/(\sin \beta_r L - \sinh \beta_r L)$, $r = 1,2,\ldots$.

Here we only consider the fundamental mode ($r=1$), therefore we have $\beta_1 L = 1.875$. $C_1$ can be determined from the boundary condition, i.e., the measured vertical displacement of the PMN bar.

The gradient of transverse strain along the thickness direction can be written as[11]

$$\frac{\partial \epsilon_{11}}{\partial x_3} = \frac{\partial^2 W(x_1)}{\partial x_1^2}. \tag{5}$$

Figure 3 showed the experimental results of the strain gradient induced polarization at two positions of the PMN bar, one is near the clamped end ($x_1/L = 0.18$) where the strain gradient is supposed to be higher, while the other is near the free end ($x_1/L = 0.67$). It is seen that the flexoelectric polarization is proportional to the strain gradient. The slopes of the polarization versus strain gradient curve obtained at two positions are very close. At the same driving voltage, the clamped end generated higher polarization than the free end. Based on the experimental results, $\mu_{12}$ was calculated to be about $4 \times 10^{-6}$ C/m.

The temperature dependence of dielectric permittivity and tangent loss at various frequencies ranging from 1 kHz to 1 MHz have been investigated and the dielectric peak temperatures are well below room temperature. At room temperature, the materials should be cubic and the unpoled ceramics are isotropic and should not exhibit any piezoelectric effect in principle. Furthermore, for the current measurement configuration, the upper and lower parts of the sample endure strain of opposite sign. So even if there is any remnant piezoelectric effect, the net effect in the whole sample should be zero because the piezoelectric polarization generated in the upper and lower halves would cancel.

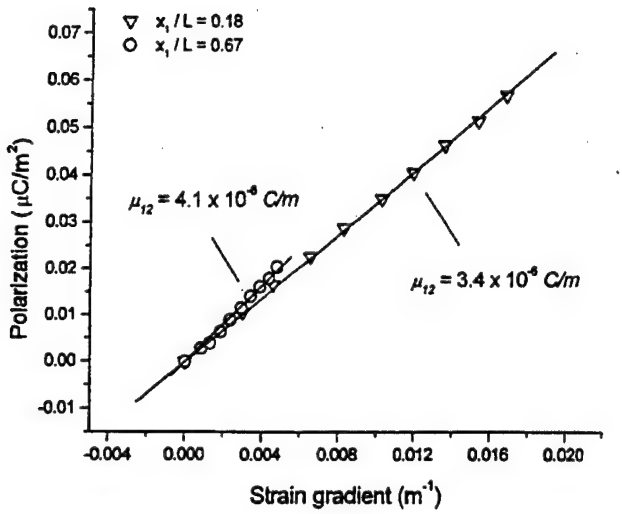


FIG. 3. The relationship between flexoelectric polarization and strain gradient in the relaxor $Pb(Mg_{1/3}Nb_{2/3})O_3$ ceramics.

Former theoretical analysis estimated the flexoelectric coefficient to be of the order of magnitude of $e/a$,[1,3,4] where $e$ is the absolute value of electron charge and $a$ is the lattice parameter. Generally, $e/a$ is around $10^{-10}$ C/m for almost all materials, which is very small. The current experimental results on the relaxor PMN ceramics are much higher than the phenomenological estimations and are very encouraging. Such high flexoelectric effect observed in the relaxor PMN ceramics may be associated with the high dielectric constant (around 13 000 at 1 kHz and room temperature), so the charge separation becomes much easier than those in the low permittivity materials.

In summary, a flexoelectric effect has been investigated in the relaxor ferroelectric PMN ceramic, the measured flexoelectric coefficient is about four orders of magnitude higher than the earlier theoretical estimation.

[1] Sh. M. Kogan, Sov. Phys. Solid State 5. 2069 (1964).
[2] R. B. Meyer, Phys. Rev. Lett. 22, 918 (1969).
[3] V. L. Indenbom, E. B. Loginov, and M. A. Osipov, Sov. Phys. Crystallogr. 26, 656 (1981).
[4] A. K. Tagantsev, Sov. Phys. JETP 61, 1246 (1985).
[5] I. S. Zheludev, Yu. S. Likhacheva, and N. A. Lileeva, Sov. Phys. Crystallogr. 14, 425 (1969).
[6] M. Marvan and A. Havránek, Prog. Colloid Polym. Sci. 78, 33 (1988).
[7] J. Fousek, L. E. Cross, and D. B. Litvin, Mater. Lett. 39, 287 (1999).
[8] L. Eric Cross, Ferroelectrics 76, 241 (1987).
[9] D. Viehland, Ph.D. dissertation, The Pennsylvania State University, 1991.
[10] L. Meirovitch, *Principles and Techniques of Vibrations* (Prentice Hall, Upper Saddle River, NJ, 1997).
[11] R. L. Bisplinghoff, J. W. Mar, and T. H. H. Pian, *Statics of Deformable Solids* (Addison-Wesley, Reading, MA, 1965).

Downloaded 02 May 2001 to 146.186.113.144. Redistribution subject to AIP license or copyright, see http://ojps.aip.org/aplo/aplcr.jsp

# Observation of the flexoelectric effect in relaxor $Pb(Mg_{1/3}Nb_{2/3})O_3$ ceramics

Wenhui Ma and L. Eric Cross[a)]
*Materials Research Laboratory, Pennsylvania State University, University Park, Pennsylvania 16802*

(Received 31 October 2000; accepted for publication 22 January 2001)

The relationship between elastic strain gradient and electric polarization was investigated in the relaxor ferroelectric lead magnesium niobate ceramic. Experimental studies indicated that flexoelectric polarization is linearly proportional to the applied strain gradient, and the flexoelectric coefficient $\mu_{12}$ is calculated to be $4\times10^{-6}$ C/m, which is much higher than the early phenomenological estimations. © *2001 American Institute of Physics.* [DOI: 10.1063/1.1356444]

The piezoelectric effect is the linear relationship between electric polarization and applied elastic stress (direct effect) or between elastic strain and applied electric field (converse effect). Due to the symmetry requirements, the piezoelectric effect may only exist in 20 crystal point groups where center of symmetry is absent. More than three decades ago, phenomenological analysis[1] stated that electric polarization might be induced by inhomogeneous strain in the materials. Later the term flexoelectric was coined to describe such an effect in analogy to an effect discovered in the nonpiezoelectric liquid crystals,[2] and tensor property[3] and microscopic theory[4] were investigated theoretically for single crystals. The flexoelectric effect is defined by the following relation:

$$P_l=\mu_{ijkl}\frac{\partial\epsilon_{ij}}{\partial x_k}, \tag{1}$$

where $P_l$ is the $l$th component of flexoelectric polarization, $\mu_{ijkl}$ is the flexoelectric coefficient, $\epsilon_{ij}$ is the elastic strain, and $x_k$ is the position coordinate. Flexoelectricity is controlled by a fourth-rank tensor, and thus is a property of all insulating solids, but so far no flexoelectric coefficients have in fact been measured. In the late 1960s, attempts were made to investigate the electrical polarization in nonpiezoelectric $CaWO_4$ crystals during torsional deformation, which might be closely associated with the flexoelectric effect,[5] but the polarization had been attributed to the disappearance of the center of symmetry after torsion, rather than the effect of the strain gradient. In the late 1980s, a tiny flexoelectric effect was observed in an isotropic elastomer with a static flexoelectric coefficient of the order of magnitude of $10^{-11}$–$10^{-10}$ C/m.[6]

Recently, an idea was developed for designing 0–3 piezoelectric composites based on the flexoelectric effect where none of the components are piezoelectric.[7] If the flexoelectric coefficients are large enough for practical applications a range of properly engineered flexoelectric composite structures could provide completely new piezoelectric capability. Recent studies[8,9] have indicated that the relaxor ferroelectric perovskites like $Pb(Mg_{1/3}Nb_{2/3})O_3$ (PMN) are exceedingly sensitive to elastic stress in the region of temperature between the dielectric permittivity maximum $T_m$ and the freezing temperature $T_f$ from the Vogel–Fulcher relationship. In this letter, we report the investigation of flexoelectric effect in relaxor PMN ceramics.

The flexoelectric measurements were carried out at room temperature by using an experimental setup shown schematically in Fig. 1. The PMN ceramic bars (76.3 mm length, 12.7 mm width, and 2.5 mm thickness) were provided by the TRS company of State College, Pennsylvania. A very thin layer of sputtered gold was used as electrode, the bottom surface of the sample is fully covered with gold while on the top a series of 3 mm diameter electrodes were prepared. Strain gradient was generated in the samples along the thickness direction by a loudspeaker. A MicroStrain DVRT transducer was used to measure the displacement at several positions along the sample bar. The loudspeaker was driven by an HP467A power amplifier with a 1 Hz sinusoidal signal from an SR830 DSP lock-in amplifier. The generated current was monitored by the lock-in amplifier. The generated polarization may be calculated using the following equation:

$$P_3=\frac{i}{2\pi fA}, \tag{2}$$

where $i$ is the alternating current, $A$ is the electrode area, and $f$ is the driving frequency of the loudspeaker.

The macroscopic symmetry of PMN between $T_m$ and $T_f$ is cubic $m3m$, while the unpoled ceramics are regarded as isotropic. Thus, the flexoelectric tensor matrices may be written as

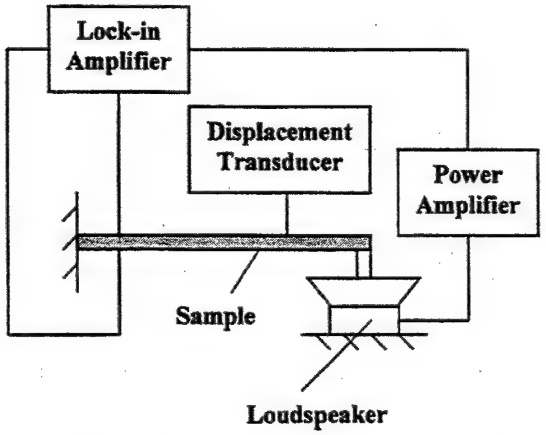


FIG. 1. Experimental setup for the measurement of the flexoelectric effect.

a)Electronic mail: lec3@psu.edu

 © 2001 American Institute of Physics
Downloaded 02 May 2001 to 146.186.113.144. Redistribution subject to AIP license or copyright, see http://ojps.aip.org/aplo/aplcr.jsp

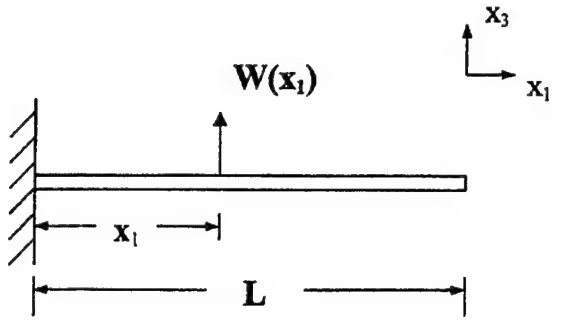


FIG. 2. Schematic diagram of a cantilevered beam and the axial arrangement.

$$\begin{pmatrix} \mu_{11} & \mu_{12} & \mu_{12} & 0 & 0 & 0 \\ \mu_{12} & \mu_{11} & \mu_{12} & 0 & 0 & 0 \\ \mu_{12} & \mu_{12} & \mu_{11} & 0 & 0 & 0 \\ 0 & 0 & 0 & \mu_{44} & 0 & 0 \\ 0 & 0 & 0 & 0 & \mu_{44} & 0 \\ 0 & 0 & 0 & 0 & 0 & \mu_{44} \end{pmatrix}.$$

For the present situation in Fig. 1, only the transverse effect exists, so the flexoelectric equation may be simplified as

$$P_3 = \mu_{12} \frac{\partial \epsilon_{11}}{\partial x_3}. \tag{3}$$

The strain in the PMN ceramic bar was calculated by assuming the natural vibration of a cantilevered beam shown in Fig. 2. The mode shape[10] can be written as

$$W_r(x_1) = A_r[(\sin \beta_r L - \sinh \beta_r L)(\sin \beta_r x_1 - \sinh \beta_r x_1) + (\cos \beta_r L + \cosh \beta_r L) \times (\cos \beta_r x_1 - \cosh \beta_r x_1)], \tag{4}$$

where $A_r = C_1/(\sin \beta_r L - \sinh \beta_r L)$, $r = 1,2,\ldots$.

Here we only consider the fundamental mode ($r=1$), therefore we have $\beta_1 L = 1.875$. $C_1$ can be determined from the boundary condition, i.e., the measured vertical displacement of the PMN bar.

The gradient of transverse strain along the thickness direction can be written as[11]

$$\frac{\partial \epsilon_{11}}{\partial x_3} = \frac{\partial^2 W(x_1)}{\partial x_1^2}. \tag{5}$$

Figure 3 showed the experimental results of the strain gradient induced polarization at two positions of the PMN bar, one is near the clamped end ($x_1/L = 0.18$) where the strain gradient is supposed to be higher, while the other is near the free end ($x_1/L = 0.67$). It is seen that the flexoelectric polarization is proportional to the strain gradient. The slopes of the polarization versus strain gradient curve obtained at two positions are very close. At the same driving voltage, the clamped end generated higher polarization than the free end. Based on the experimental results, $\mu_{12}$ was calculated to be about $4 \times 10^{-6}$ C/m.

The temperature dependence of dielectric permittivity and tangent loss at various frequencies ranging from 1 kHz to 1 MHz have been investigated and the dielectric peak temperatures are well below room temperature. At room temperature, the materials should be cubic and the unpoled ceramics are isotropic and should not exhibit any piezoelectric effect in principle. Furthermore, for the current measurement configuration, the upper and lower parts of the sample endure strain of opposite sign. So even if there is any remnant piezoelectric effect, the net effect in the whole sample should be zero because the piezoelectric polarization generated in the upper and lower halves would cancel.

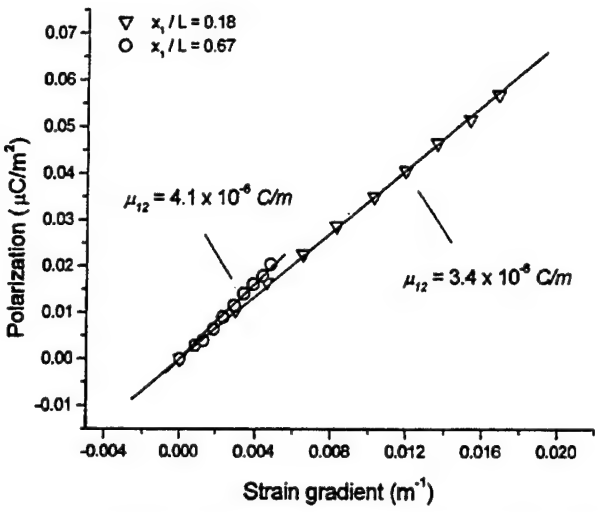


FIG. 3. The relationship between flexoelectric polarization and strain gradient in the relaxor $Pb(Mg_{1/3}Nb_{2/3})O_3$ ceramics.

Former theoretical analysis estimated the flexoelectric coefficient to be of the order of magnitude of $e/a$,[1,3,4] where $e$ is the absolute value of electron charge and $a$ is the lattice parameter. Generally, $e/a$ is around $10^{-10}$ C/m for almost all materials, which is very small. The current experimental results on the relaxor PMN ceramics are much higher than the phenomenological estimations and are very encouraging. Such high flexoelectric effect observed in the relaxor PMN ceramics may be associated with the high dielectric constant (around 13 000 at 1 kHz and room temperature), so the charge separation becomes much easier than those in the low permittivity materials.

In summary, a flexoelectric effect has been investigated in the relaxor ferroelectric PMN ceramic, the measured flexoelectric coefficient is about four orders of magnitude higher than the earlier theoretical estimation.

[1] Sh. M. Kogan, Sov. Phys. Solid State 5, 2069 (1964).
[2] R. B. Meyer, Phys. Rev. Lett. 22, 918 (1969).
[3] V. L. Indenbom, E. B. Loginov, and M. A. Osipov, Sov. Phys. Crystallogr. 26, 656 (1981).
[4] A. K. Tagantsev, Sov. Phys. JETP 61, 1246 (1985).
[5] I. S. Zheludev, Yu. S. Likhacheva, and N. A. Lileeva, Sov. Phys. Crystallogr. 14, 425 (1969).
[6] M. Marvan and A. Havránek, Prog. Colloid Polym. Sci. 78, 33 (1988).
[7] J. Fousek, L. E. Cross, and D. B. Litvin, Mater. Lett. 39, 287 (1999).
[8] L. Eric Cross, Ferroelectrics 76, 241 (1987).
[9] D. Viehland, Ph.D. dissertation, The Pennsylvania State University, 1991.
[10] L. Meirovitch, *Principles and Techniques of Vibrations* (Prentice Hall, Upper Saddle River, NJ, 1997).
[11] R. L. Bisplinghoff, J. W. Mar, and T. H. H. Pian, *Statics of Deformable Solids* (Addison-Wesley, Reading, MA, 1965).

Downloaded 02 May 2001 to 146.186.113.144. Redistribution subject to AIP license or copyright, see http://ojps.aip.org/aplo/aplcr.jsp

# APPENDIX 8

# Large flexoelectric polarization in ceramic lead magnesium niobate

Wenhui Ma and L. Eric Cross[a)]
*Materials Research Laboratory, Pennsylvania State University, University Park, Pennsylvania 16802*

(Received 6 August 2001; accepted for publication 4 October 2001)

Flexoelectric coefficient $\mu_{12}$ is greatly enhanced in the relaxor ferroelectric lead magnesium niobate ceramic. Phenomenological analysis suggests the high dielectric permittivity is inadequate to explain the great enhancement. Temperature dependent measurement reveals a close relation between the flexoelectric polarization and the preexisting polar microregions in this relaxor ferroelectrics. It is proposed that the strain gradient might change the Gibbs free energy of the relaxor system and easily reorient the already existing polar microregions, leading to the greatly enhanced flexoelectric effect. © *2001 American Institute of Physics.* [DOI: 10.1063/1.1426690]

Flexoelectricity describes the generation of electric polarization in an insulating solid by an elastic strain gradient. Phenomenological treatment of the flexoelectric effect was first made by Kogan,[1] who proposed that piezoelectric polarization in an inhomogeneously deformed medium should be a function not only of deformation but also of the spatial derivatives of the deformation at the same point. For a centrosymmetric crystal subjected to inhomogeneous deformation, only the strain gradient contributes to the polarization, so the flexoelectric effect can be investigated independently. The flexoelectric coefficient $\mu_{ijkl}$ is a fourth-rank polar tensor, so that for a cubic crystal the nonzero components are $\mu_{1111}$, $\mu_{1122}$, and $\mu_{1212}$, or in matrix notation $\mu_{11}$, $\mu_{12}$, and $\mu_{44}$. For homogeneous solids, all earlier investigators agree that the effect is very small in simple low permittivity dielectrics, and the $\mu_{ijkl}$ flexoelectric coefficients are of the order of $10^{-10}$–$10^{-11}$ C/m.[2–4] In a previous article, we announced our measurement of the flexoelectric effect in lead magnesium niobate (PMN) ceramic, where the $\mu_{12}$ coefficient is greatly enhanced, about $4\times10^{-6}$ C/m at room temperature.[5] In this letter, we report the temperature dependent measurement of the flexoelectric polarization in PMN.

Temperature dependent flexoelectric measurement was performed by using an experimental setup schematically shown in Fig. 1. The measurement configuration, sample dimension, and electrode geometry are the same as those used previously.[5] As shown in Fig. 1, one end of the sample was fixed to form a cantilevered beam. Temperature is uniform all over the sample bar. A loudspeaker was used to drive the beam at a frequency of 1 Hz, so a natural vibration was generated at the fundamental mode. By measuring the mode shape, we can calculate the strain all over the sample bar. Because the top and bottom surfaces are subjected to strain of opposite sign, there is a strain gradient along the thickness direction. Our former measurements[5] show that the flexoelectric polarization is proportional to the applied strain gradient and the $\mu_{12}$ coefficients obtained from measurements at different positions along the beam are close.

Figure 2 shows the experimental result of flexoelectric polarization as a function of temperature obtained in the PMN ceramic. There is a maximum around the dielectric maximum temperature, $T_m$. Above $T_m$, the flexoelectric polarization decreases rapidly with increasing temperature. As shown in Fig. 2, an exponential decay function fits the experimental data well. By extrapolation, it is found that the flexoelectric polarization becomes close to zero around $T_d$, the so-called Burns temperature.[6] At this temperature, the polar microregions disappear and the relaxor reverts to classical Curie–Weiss behavior. Our result indicates that there is a close relation between the flexoelectric polarization and the already existing polar microregions in PMN, suggesting that the preexisting polar microregions might play a dominant role in the polarization mechanism.

In order to understand the origin of the greatly enhanced $\mu_{12}$ coefficients in relaxor PMN, let us make a simple analysis of the contributors to the flexoelectric effect. In the mid 1980's, Tagantsev developed the theory for flexoelectric effect in single crystals.[2,3] In a crystal whose bulk symmetry does not allow the piezoelectric interaction the appearance of a polarization proportional to a strain gradient can be comprised of four components: a bulk static flexoelectric effect; a bulk dynamic flexoelectric effect; a surface flexoelectric effect, and a surface piezoelectric effect. As shown in the discussion by Tagantsev, for a simple homogeneous ionic solid of cubic centric symmetry based on the rigid ion model, all four components of the flexoelectric response are of the or-

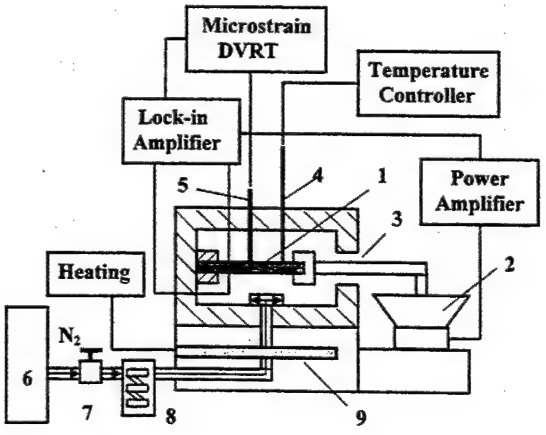


FIG. 1. Experimental setup for the temperature dependent flexoelectric measurement: (1) PMN bar, (2) loudspeaker, (3) driving arm, (4) thermocouple, (5) microstrain transducer core, (6) high purity nitrogen, (7) gas flow meter, (8) copper coils immersed in liquid nitrogen, (9) heating elements.

a)Electronic mail: lec3@psu.edu

0003-6951/2001/79(26)/4420/3/$18.00



© 2001 American Institute of Physics

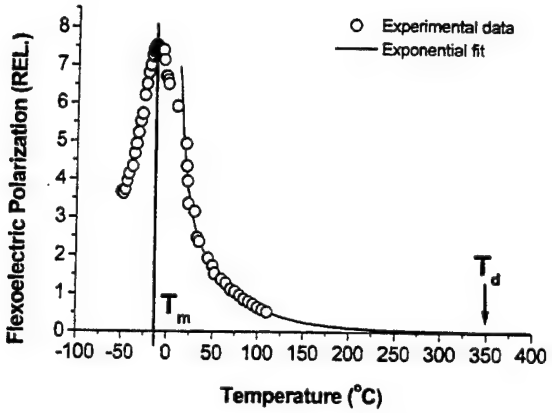


FIG. 2. Flexoelectric polarization as a function of temperature in the PMN ceramic.

der of $10^{-10}$ C/m, although the magnitude of surface piezoelectric effect depends markedly on the nature of the surface. For a soft-mode ferroelectric dielectric above $T_c$ in the cubic phase the flexoelectric behavior is much simplified, both static and dynamic bulk coefficients become larger in proportion to the enhanced dielectric susceptibility, and the surface flexoelectric coefficient becomes unimportant as it does not scale with the susceptibility. The surface piezoelectric effect might also be enlarged in proportion to the dielectric susceptibility, but again depends on details of the surface characteristics. For the current measurement configuration, the piezoelectric polarization from the upper and lower halves neutralize, so there should be no net effect even in the low temperature ferroelectric phase. We have also performed the flexoelectric measurements with the sample bar turned over, i.e., with the upper and lower surfaces interchanged, the results obtained for the two opposite orientations are found to be in-phase, evidencing the absence of a piezoelectric effect due to unbalanced inhomogeneous surface layers.

Figure 3 displays the dielectric response of the PMN ceramic sample. As shown in the dielectric spectrum, the dielectric maximum temperature increases with frequency, which is typical for a relaxor ferroelectric dielectric. Permittivity of PMN at room temperature is of the order of 15 000, while the dielectric permittivity for a simple ionic solid on the point charge model is about 5, so an enhancement of $3\times10^3$ can be expected from the high dielectric permittivity. However, the flexoelectric coefficient $\mu_{12}$ of PMN is of the

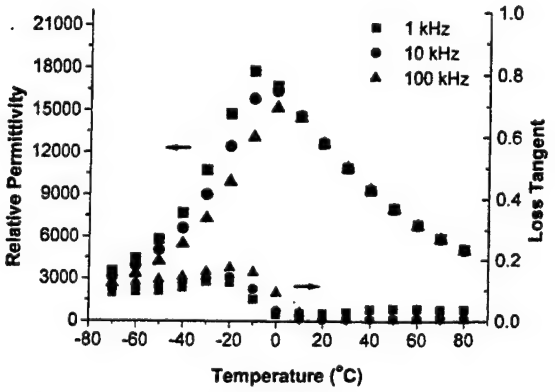


FIG. 3. Dielectric permittivity and loss tangent vs temperature for the PMN ceramic.

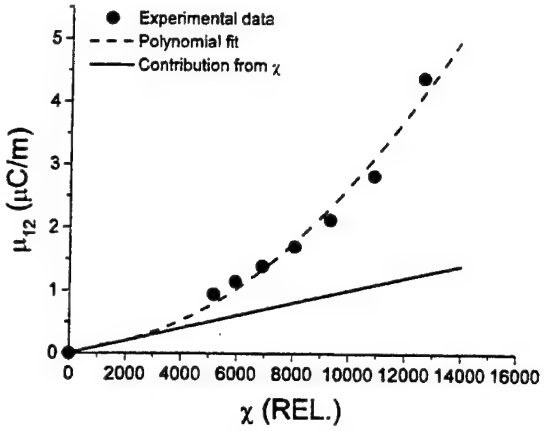


FIG. 4. Flexoelectric coefficient $\mu_{12}$ vs dielectric susceptibility $\chi$ in the PMN ceramic, where the solid circles are the experimental data, the dashed curve is the polynomial fit, and the solid line is the estimated $\mu_{12}$ values by phenomenological analysis.

order of $5\times10^{-6}$ C/m, some $5\times10^4$ times larger than that of the simple ionic solid. It is clear that the high dielectric permittivity is inadequate to explain the observed larger $\mu_{12}$ value. Figure 4 shows the curve of measured $\mu_{12}$ coefficient versus dielectric susceptibility $\chi$, and the solid line is from the phenomenological analysis [$\mu_{ijkl}\sim\chi(e/a)$, where $e$ is the elementary charge and $a$ is the dimension of lattice cell]. It is found that there is discrepancy between the experimentally observed $\mu_{12}$ values and the linear estimations, which increases with the increase of dielectric susceptibility or decrease of temperature below $T_d$. It may be noted that similar deviations from linear extrapolation of high temperature

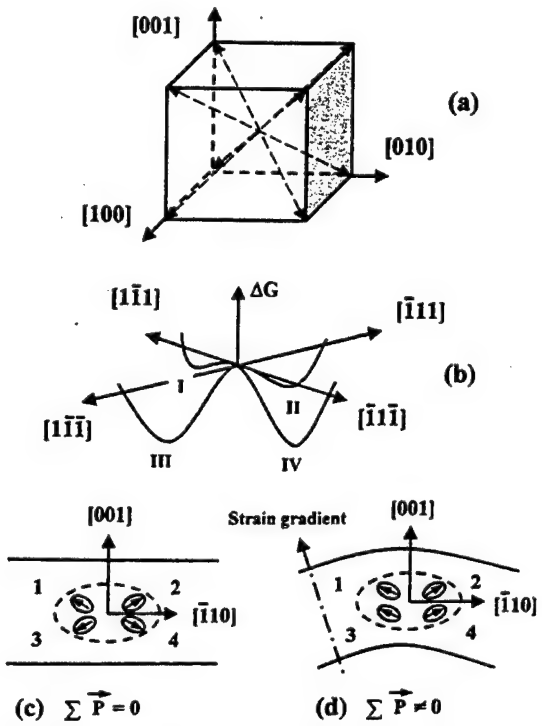


FIG. 5. Schematic illustrations of (a) eight equivalent ⟨111⟩ polarization orientations in a cubic lattice cell, (b) Gibbs free energy $\Delta G$ vs polarization for four of the eight equivalent ⟨111⟩ orientations in a rhombohedral ferroelectric phase, and cross sections of the PMN bar showing the arrangement of orientation of the nanopolar regions in a [001]-oriented grain (defined by the dotted ellipse) (c) before and (d) after being subject to an elastic strain gradient.

properties have been found during the temperature-dependent measurements of optic index of refraction[6] and thermal expansion[7] in PMN, which were unanimously attributed to the appearance of localized polarization.

Relaxor ferroelectrics are inhomogeneous media containing micropolar regions even at temperatures well above $T_m$, and the existence of nanoscale $B$-site order has been directly confirmed by the TEM investigations.[8] The dielectric behavior in relaxor ferroelectrics can be understood by the combination of the compositional heterogeneity model[9] and superparaelectric model.[7] Above $T_d$, PMN is cubic both globally and locally without any polar regions. Figure 5(a) shows a lattice cell of cubic paraelectric phase of perovskite structure displaying eight equivalent $\langle 111 \rangle$ orientations. With temperature going down below $T_d$, localized polarization appears. According to the superparaelectric model, it is expected that the nanopolar regions are dynamically disordered in the thermal field and the chance of appearance of a polar vector along any of the eight $\langle 111 \rangle$ directions is equivalent. Figure 5(b) shows the Gibbs free energy for four of the eight $\langle 111 \rangle$ polarizations for a low temperature ferroelectric phase, it is clear that all energy minima are of the same depth in the infinite perfect crystal. However, in the relaxor ferroelectrics, due to composition fluctuation it is expected that the local symmetry will be lower than the global symmetry so that the eight $\langle 111 \rangle$ polarization orientations are now inequivalent in the local polar microregions. Under zero strain condition, a possible arrangement for the orientations of the nanosized domains in a [001]-oriented grain in the PMN bar is schematically shown in Fig. 5(c), the sum of all those polar vectors is zero. In Fig. 5(d), the sample bar is subject to an elastic strain gradient whose direction is defined as pointing from contraction to expansion and is parallel to the normal direction of sample surface. When the PMN bar is bent, some polarization orientations become free energy unfavorable and it is suggested that the inhomogeneously deformed nanosized polar regions reorient themselves towards the direction of strain gradient by polarization rotation between adjoining $\langle 111 \rangle$ directions, e.g., from $[1\bar{1}\bar{1}]$ to $[1\bar{1}1]$, so as to reach the Gibbs free energy minima and there will be net polarization in the strain gradient direction.

In summary, flexoelectric coefficient $\mu_{12}$ has been measured as a function of temperature and the results suggest that the observed large flexoelectric polarization might be caused by reorientation of the preexisting polar clusters in the relaxor ferroelectrics by the elastic strain gradient.

This work was supported by the Office of Naval Research, Contract No. N00014-99-1-1011. We thank M. Marvan from Charles University, Czech Republic for his suggestion of the importance of preexisting polar microregions in the PMN ceramics.

[1] Sh. M. Kogan, Sov. Phys. Solid State **5**, 2069 (1964).
[2] A. K. Tagantsev, Sov. Phys. JETP **61**, 1246 (1985).
[3] A. K. Tagantsev, Phys. Rev. B **34**, 5883 (1986).
[4] M. Marvan and A. Havránek, Progr. Colloid. Polym. Sci. **78**, 33 (1988).
[5] W. Ma and L. E. Cross, Appl. Phys. Lett. **78**, 2920 (2001).
[6] G. Burns and F. H. Dacol, Solid State Commun. **48**, 853 (1983).
[7] L. E. Cross, Ferroelectrics **76**, 241 (1987).
[8] C. A. Randall and A. S. Bhalla, Jpn. J. Appl. Phys., Part 1 **29**, 327 (1990).
[9] G. A. Smolensky, J. Phys. Soc. Jpn. **28**, 26 (1970).

# APPENDIX 9

# Flexoelectric polarization of barium strontium titanate in the paraelectric state

Wenhui Ma and L. Eric Cross[a)]
*Materials Research Laboratory, Pennsylvania State University, University Park, Pennsylvania 16802*

(Received 9 May 2002; accepted 10 September 2002)

The strain-gradient-induced polarization (flexoelectric effect) was investigated in $Ba_{0.67}Sr_{0.33}TiO_3$ (BST) ceramic at temperatures above the 21 °C Curie point. At 23 °C the flexoelectric coefficient $\mu_{12}$ was more than one order of magnitude greater than the highest value measured in lead magnesium niobate ceramic. Over the temperature range of linear Curie–Weiss behavior, the coefficient $\mu_{12}$ was roughly proportional to the dielectric permittivity; however, the constant of proportionality was higher than predicted for simple ionic solids. The unexpected behavior in the BST ceramic suggests the need for a broader database of flexoelectric coefficients. © *2002 American Institute of Physics.* [DOI: 10.1063/1.1518559]

Recently we investigated the flexoelectric polarization in lead magnesium niobate (PMN) ceramic,[1,2] a material which is often regarded as the prototype for a broad family of relaxor ferroelectrics.[3] The high values measured, and particularly the observed temperature dependence of the flexoelectric coefficient $\mu_{12}$ suggested that the polarization was associated with a reorientation of micropolar regions which are known to occur in the temperature region above the weak field dielectric maximum, but below a so-called Burns temperature $T_D$ which is just the temperature range where the high $\mu_{12}$ values are observed. Alternatively the high response may be a consequence of the very high dielectric permittivity in the relaxor where the relative permittivity $\varepsilon_r$ reaches up to 13 000 (measured at 1 kHz) at room temperature. Tagantsev[4] suggested that the $\mu_{ij}$ may in fact be proportional to the dielectric susceptibility $\chi_{ij}$ following a relation of the form

$$\mu_{ij} = \gamma \chi_{ij} \frac{e}{a}, \tag{1}$$

where $\gamma$ is a constant of value close to unity, $e$ is the electron charge, and $a$ the lattice parameters.

To test the possible role of micropolar regions it was desirable to measure the response of a "normal" paraelectric cubic perovskite with comparable or higher dielectric permittivity but no lower frequency dielectric dispersion in the temperature region above $T_c$. Barium strontium titanate solid solutions have perovskite structure, very high non-dispersive dielectric permittivity, and Curie temperature $T_c$ which can be positioned just below room temperature by appropriate choice of composition. It must be cautioned however that this is an exceedingly difficult system to synthesize as a homogeneous solid solution. We were fortunate to be able to use a composition fabricated by Texas Instruments (TI), using a complex wet chemical route to the very demanding specification for their long wavelength infrared dielectric bolometric imager. In that system local homogeneity is essential to maintain the weak first order transition at $T_c$ which keeps $\varepsilon_r$ at high value under dc bias fields, and global uniformity is necessary to avoid fixed pattern noise in the detector pixel array.

The BST ceramic sample used in this study was cut from a boule supplied by TI and was in the form of a bar 68 mm long, 12.7 mm wide, and 1.8 mm thick. As for the earlier measurements on PMN ceramics[2] 3 mm diameter thin sputtered gold electrodes were spaced along the bar. Dielectric measurements were carried out in a delta design temperature chamber to check local and global uniformity. Typical data for permittivity and loss as a function of temperature and frequency are given in Fig. 1 and the corresponding reciprocal permittivity (dielectric stiffness) in Fig. 2. The high quality of the sample which has a Curie point at 21 °C is attested by the very high sharp permittivity peak at $T_c$, the low dielectric loss and the complete absence of dielectric dispersion over the frequency range from 100 Hz to 100 kHz in the paraelectric range. Polarization measurements confirm that the Curie transition is weakly first order. It is important to note the small upturn in dielectric loss below 35 °C (Fig. 1) which correlates closely with the departure from Curie–Weiss behavior. We suspect that even in these TI prepared

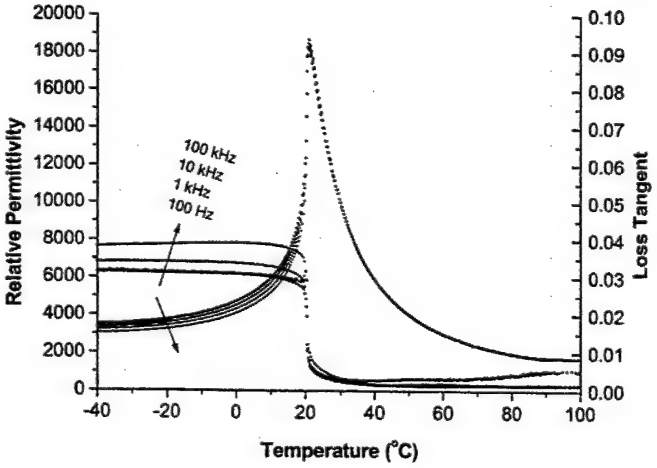


FIG. 1. Dielectric permittivity and loss in $Ba_{0.67}Sr_{0.33}TiO_3$ ceramic as a function of temperature, measured at frequencies of 100 Hz, 1 kHz, 10 kHz, and 100 kHz at a field level of 5 V/cm.

a)Electronic mail: lec3@psu.edu

 © 2002 American Institute of Physics

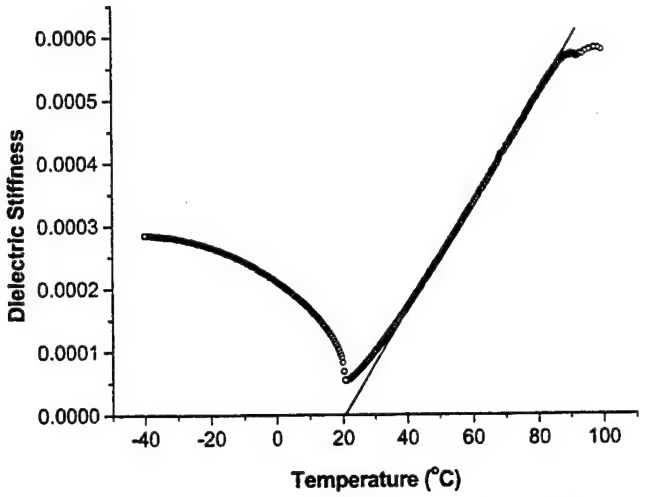


FIG. 2. Curie–Weiss plot of reciprocal dielectric permittivity (stiffness) as a function of temperature in $Ba_{0.67}Sr_{0.33}TiO_3$.

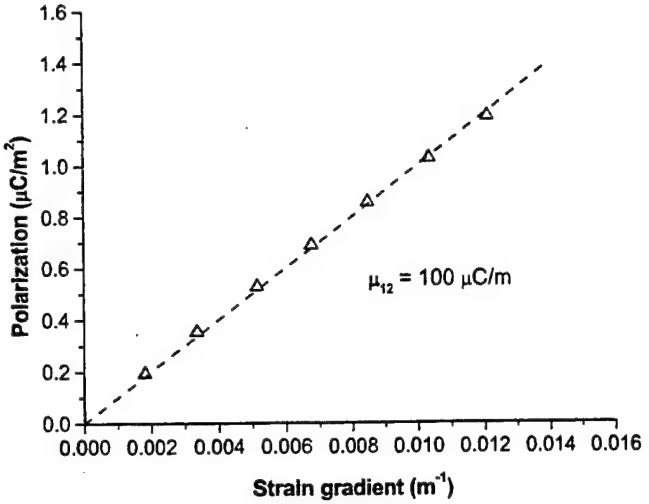


FIG. 4. Flexoelectric polarization as a function of applied strain gradient measured at a flexure frequency of 1 Hz.

samples there is a weak persistance of macroferroelectric regions above $T_c$ reducing permittivity from the expected Curie–Weiss behavior and enhancing dielectric loss.

The system used for flexoelectric measurements is identical to that used in earlier studies of PMN and is reproduced here in schematic form in Fig. 3. The ceramic bar sample is rigidly clamped at one end and driven into transverse vibration at the "free" end by a small moving coil loudspeaker. Current generated from the small gold electrode is measured by a lock-in amplifier, phase locked to the loudspeaker driving frequency of 1 Hz. A Microstrain DVRT (differential variable reluctance transducer) is used to measure the ac strain as a function of position along the bar. For the outer 1/3 of the bar length the measured vertical displacement curve correlates closely with the curve calculated for the first fundamental mode of a freely vibrating cantilevered bar.[1] Close to the clamped end, the measured amplitude is slightly larger, probably indicating that our best clamping is not sufficiently rigid for the stiff BST ceramic. The free bar model, with the measured amplitudes was used to calculate the strain gradient at the positions of the electrodes.

Experimental results for the flexoelectric polarization as a function of the transverse strain gradient are presented in Fig. 4. The measurements were made near the clamped end of the bar ($x/L=0.25$) at a temperature of 23 °C where this BST solid solution is in the paraelectric phase. As expected the polarization is linearly proportional to the elastic strain gradient, but the slope of the line gives a magnitude of $\mu_{12}$ of 100 $\mu$C/m. This magnitude of $\mu_{12}$ was a major surprise as the value is not less, but in fact some 20 times larger than the highest value ($\mu_{12}\sim 4$ $\mu$C/m) measured in the PMN ceramic.

For the BST ceramic measurements of $\mu_{12}$ as a function of temperature above $T_c$ are shown in Fig. 5. The break in the curve near 35 °C correlates well with the departure from Curie–Weiss behavior. The plot of $\mu_{12}$ versus relative dielectric permittivity (closely equivalent to susceptibility $\chi$ in these high $K$ ceramics) is shown in Fig. 6 compared with the expectation from Eq. (1) with $\gamma=1$. There is a quasilinear range between $\varepsilon_r=2500$ and $\varepsilon_r=11\,000$ but the measured slope gives $\gamma=9.3$. The change above $\varepsilon_r\sim 11\,000$ is not unexpected as the departure from Curie–Weiss law and the enhanced loss signal the onset of an additional polarization

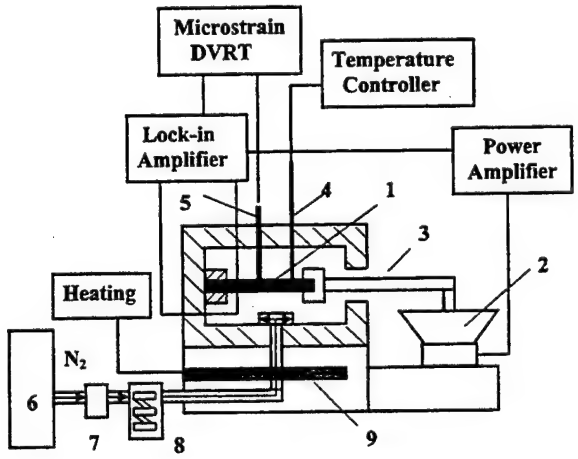


FIG. 3. Experimental setup for the temperature dependent flexoelectric measurement: (1) BST bar, (2) loudspeaker, (3) driving arm, (4) thermocouple, (5) microstrain transducer core, (6) high purity nitrogen, (7) gas flow meter, (8) copper coils immersed in liquid nitrogen, (9) heating elements.

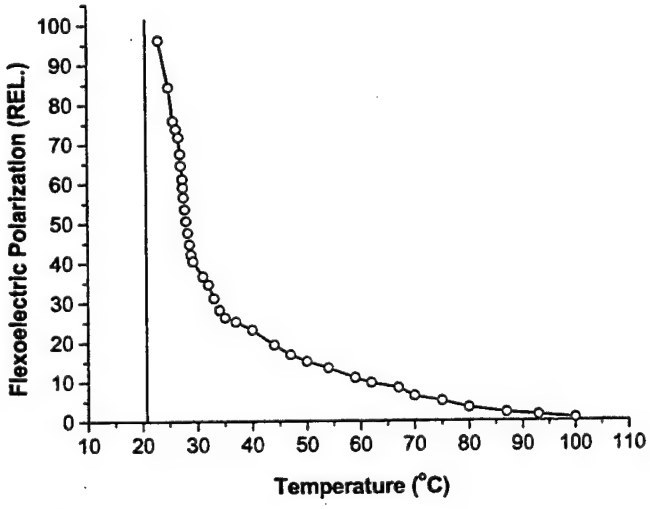


FIG. 5. Flexoelectric coefficient derived from plots such as those in Fig. 4 as a function of temperature above the Curie point $T_c$.

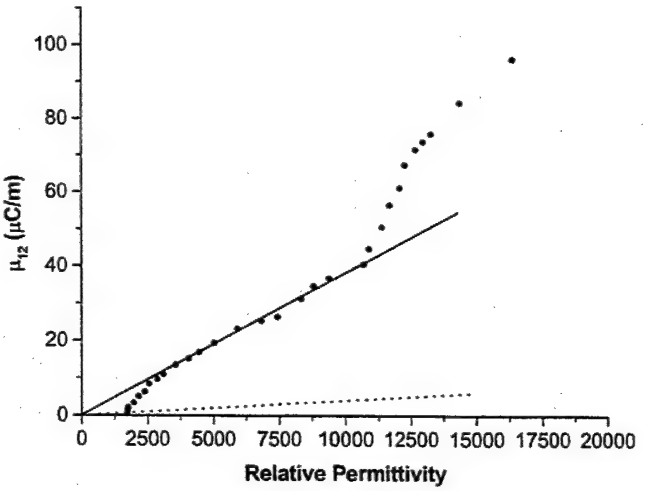


FIG. 6. Flexoelectric coefficient $\mu_{12}$ vs dielectric permittivity. Solid dots: measured values on BST; dotted straight line: expectation from Eq. (1) with $\gamma=1$; and solid line is plotted to highlight the quasilinear range between $\varepsilon_r=2500$ and $\varepsilon_r=11\,000$.

mechanism, perhaps due to the survival of some ferroelectric domains above the general $T_c$. The dropoff of response below $\varepsilon_r=2500$ is unexpected and not associated with the inadequate sensitivity since PMN response levels below 4 $\mu$C/m were measured on the same system.

It may be argued that working close to $T_c$ in the paraelectric phase stresses engendered by the transverse drive may be sufficient to raise $T_c$ and induce ferroelectricity. In these studies however the drive levels are very low so that the maximum strain at the surface is of order of $1.1\times10^{-6}$. Assuming values of elastic compliance and electrostriction constants similar to $BaTiO_3$,[5] the associated stress would move the Curie point ~0.03 °C. With equal but opposite stresses at the two surfaces this would produce an undetectable broadening of the response. That $SrTiO_3$ based ceramics may potentially have polar grain boundaries is likely as demonstrated by Petzelt[6] for pure $SrTiO_3$ ceramic. In the volume of the ceramic one may expect the $\infty\infty m$ Curie group symmetry of the randomly axed structure to average the piezoeffect to zero. For the surface however, the symmetry is lower and residual piezoelectricity is possible. In the flexure experiment, the two major surfaces are subjected to equal and opposite tractions, so the effect should largely balance out. However the two surfaces may not be exactly equivalent, leaving a small response. To test for this possibility we measured the phase of the flexoelectric signal with the sample inverted. Thus if the signal was piezoelectric, the phase should change by 180°. No change of phase was measured, thus precluding the surface effect.

Although the stable narrow polar grain boundary phase will not by symmetry affect the elasto–dielectric responses, as Petzelt[6] suggests, close to $T_c$ the surface polarity may induce macropolar domains in some grains. Such domains would now contribute a new dielectric contribution to response, strongly coupled to the elastic behavior and could be the origin of the departure from Curie–Weiss law and the enhanced flexoelectric response observed in BST samples close to $T_c$.

There is extensive literature on flexoelectricity[7–11] mostly focused upon low permittivity simple ionic solids and soft elastomer systems. Tagantsev[4] appears to have been one of the first to highlight the importance of the dielectric susceptibility in enhancing both surface and volume contributions, and raising the magnitude above the accepted level of $e/a$ which gives a low $\mu_{ij}$ value of $10^{-10}$–$10^{-11}$ C/m. The enhancement due to dielectric susceptibility is of cardinal importance for the high permittivity incipient ferroelectrics of interest here. Long experience with electrostriction in perovskites has shown a remarkable consistency in the magnitudes of the $Q_{ijkl}$ constants. It may be noted however, that in spite of excellent potential in transducers, the relaxor ferroelectrics like PMN have unusually low $Q_{ijkl}$ values, particularly at temperatures close to $T_m$, the temperature of the dielectric maximum.[12] Should we expect similar consistency in the normalized flexoelectric constant $\mu_{ij}/\chi$ and will the relaxors again appear anomalous. Unfortunately there is currently almost no database of flexoelectric constants from which to judge.

Recent measurements on the Frequency Agile Materials for Electronics (FAME) DARPA program[13] suggest that lead strontium titanate (PST) solid solutions can be fabricated with Curie points close to ambient, classic Curie–Weiss behavior, no dispersion and very low dielectric loss, testifying to the absence of relaxor effects. Large samples are difficult to procure but will be measured. Similarly, flexoelectric measurements on a nonlead based relaxor ferroelectric such as barium zirconium titanate could also give important additional information.

This work has been supported by the Office of Naval Research (ONR) under Grant No. N00014-99-1-1011. The authors would also like to thank Dr. Ahmed Amin of NUWC for making the excellent BST solid solution ceramic samples available for these measurements.

[1] W. Ma and L. E. Cross, Appl. Phys. Lett. **78**, 2920 (2001).
[2] W. Ma and L. E. Cross, Appl. Phys. Lett. **79**, 4420 (2001).
[3] L. E. Cross, Ferroelectrics **76**, 241 (1987).
[4] A. K. Tagantsev, Sov. Phys. JETP **61**, 1246 (1985).
[5] F. Jona and G. Shirane, *Ferroelectric Crystals* (Pergamon, New York, 1962).
[6] J. Petzelt *et al.*, Phys. Rev. B **64**, 184111 (2001).
[7] V. S. Mashkevich and K. B. Tolpygo, Sov. Phys. JETP **5**, 435 (1957).
[8] S. M. Kogan, Sov. Phys. Solid State **5**, 2069 (1964).
[9] V. L. Indenbom, E. B. Loginov, and M. A. Osipov, Sov. Phys. Crystallogr. **26**, 656 (1981).
[10] M. Marvan and A. Havránek, Prog. Colloid Polym. Sci. **78**, 33 (1988).
[11] M. Schulz and M. Marvan, Colloid Polym. Sci. **269**, 553 (1991).
[12] Q. M. Zhang and J. Zhao, Appl. Phys. Lett. **71**, 1649 (1997).
[13] Y. Somiya, A. S. Bhalla, and L. E. Cross, J. Inorg. Mater. **3**, 709 (2001).

# APPENDIX 10

# Strain-gradient-induced electric polarization in lead zirconate titanate ceramics

Wenhui Ma [a)]

*Max-Planck-Institute of Microstructure Physics, Weinberg 2, D-06120 Halle, Germany*

L. Eric Cross

*Materials Research Laboratory, The Pennsylvania State University, University Park Pennsylvania 16802, USA*

## Abstract

Strain-gradient-induced polarization or flexoelectricity was investigated in unpoled soft lead zirconate titanate (PZT) ceramic where the texture symmetry $\infty\infty m$ forbids macro-piezoelectricity. Even under high strain gradient (1 $m^{-1}$) the induced polarization is small (1.6 $\mu C/m^2$) at 20 °C. Higher strain gradients induce ferroelastic poling and an additional extrinsic contribution to the flexoelectric coefficient $\mu_{12}$ raising the value from 0.5 to 2.0 μC/m. Cooling through the Curie Point ($T_c$) under maximum stress (80 MPa) where the peak permittivity (~20,000) could raise $\mu_{12}$ to 20 μC/m, the equivalent electric field is still only ~1 kV/m, inadequate to achieve significant ferroelectric poling. The situation may be different in thin PZT films where much larger strain gradients can occur.

[a)] E-mail: mawenhui@mpi-halle.de

The well-known elasto-electric coupling effects include piezoelectric effect, electrostrictive effect, and Maxwell stress effect. Piezoelectric ceramics [1] and more recently single crystals [2] have demonstrated the capability for broad applications in sensor, actuator and transducer devices. In soft polymers, it is shown recently that Maxwell stress effect (attractive forces between opposite charges on the electrodes) can generate ultrahigh strain responses and exhibit great potential for a variety of electromechanical device applications [3]. All the above-mentioned physical effects, however, generally assume the situations of uniform stress or strain. In nature, there is elasto-electric coupling caused by inhomogeneous deformation where stress or strain gradient associated polarization effects (flexoelectric effects) need to be considered. Overall, mechanical stress or strain can generate electric polarization in a deformable dielectric material through the following two mechanisms,

$$P_i = d_{ijk}\sigma_{jk} + \mu_{ijkl}\frac{\partial \varepsilon_{jk}}{\partial x_l}. \qquad (1)$$

In Eq. (1) and thereafter Einstein summation convention is assumed ($i, j, k, l = 1, 2, 3$). The first term on the right-hand side refers to the well-known direct piezoelectric effect, where $\sigma_{jk}$ is the stress uniformly distributed across the sample and $d_{ijk}$ is the piezoelectric coefficient, a third-rank polar tensor. The second term on the right-hand side refers to the strain gradient ($\frac{\partial \varepsilon_{jk}}{\partial x_l}$) induced polarization and $\mu_{ijkl}$ is the flexoelectric coefficient, a fourth-rank polar tensor. In centrosymmetric materials, $d_{ijk} \equiv 0$, so the piezoelectric term in Eq. (1) can be eliminated, therefore,

$$P_i = \mu_{ijkl}\frac{\partial \varepsilon_{jk}}{\partial x_l} \qquad (2)$$

where $P_i$ is the electric polarization induced solely by strain gradient.

When reviewing the history of flexoelectric investigations, it is noted that while the concept was originally formed in early 1960s [4, 5], not until 1981 was such effect in crystalline solids given the name "flexoelectric" [6]. Based upon an ionic model [7], Tagantsev analyzed the flexoelectric effect and suggested possible larger effects in ferroelectrics. In soft polymers Marvan et al. [8] observed flexoelectric coefficients of the order of $10^{-11}$ to $10^{-10}$ C/m. Up to now very little attention has been paid to test the magnitude of flexoelectric coefficients and the mechanism remains unclear. Recently we measured the flexoelectric coefficients ($\mu_{12}$) in lead magnesium niobate (PMN) [9, 10] (a well-known relaxor ferroelectric material) and barium strontium titanate (BST) [11] (a normal ferroelectric material). Both materials were tested in the phase region with macroscopic cubic symmetry, moreover the samples were measured in the form of a cantilevered beam so that any remnant piezoelectric contributions from the top and bottom halves of the beam would cancel. In this letter, we investigate the flexoelectric effect in a well-known PZT piezoelectric ceramic in the ferroelectric phase by using a four-point bend fixture to generate a uniform strain gradient.

In this work several interesting questions were explored: (i) Using a four point bending fixture is it possible to induce and measure a quasi-static flexoelectric polarization generated by $\mu_{12}$; (ii) Is the flexoelectric polarization enhanced or inhibited by the onset of ferroelastic domain wall motion which will be evidenced by change of the flexural stiffness and the development of remnant curvature in the sample; (iii) Is it possible in soft PZT to reach levels of flexoelectric induced field sufficient to pole the ceramic into a piezoelectric form.

The samples used were unpoled PZT-5H ceramics (doped with La and Sn) fabricated by TRS ceramics company, State College, Pennsylvania. Dielectric measurements performed using an HP4284A LCR meter show a weak field permittivity of 2,200 at 20 °C and a strong but rounded dielectric maximum ($\varepsilon_3 \approx 20{,}000$) without little dispersion over the frequency range of 1 kHz to 1MHz [Fig.1(a)], suggesting a diffuse phase transition without strong relaxor character. Polarization hysteresis loops measured using a modified Sawyer-Tower circuit show remnant polarization of 35 $\mu C/cm^2$ and coercive field of 7 kV/cm [Fig.1(b)] with no discernable bias. Young's modulus was measured to be 70 GPa by a dynamic resonance method.

A uniform strain gradient was generated using a 4-point bend fixture schematically illustrated in Fig.2(a). Samples for measurement had dimensions 60 mm long, 7 mm wide and 3 mm thick. Surfaces were carefully polished and the samples were annealed at 700°C to relieve surface stresses. Sputtered gold electrodes with dimensions 10 x 7 $mm^2$ were applied to upper and lower surfaces in the center of the beam. No residual piezoelectricity could be detected by Berlincourt $d_{33}$ meter, and the impedance trajectory from 1 kHz to 1MHz was free from evidence of piezoelectric resonance. The bend test was carried out according to the ASTM C-1161-94 by using an Instron machine Model 4202 with a 10 kN load cell. Outer and inner spans of the fixture are 40 mm and 20 mm respectively. The generated electric charge was detected by a Keithley 6517 electrometer that can resolve 10 fC and will measure up to 2.1 μC. Before measurement the electrometer was carefully calibrated for voltage burden and input offset current.

The stress distribution along the sample length direction ($x_1$) is shown in Fig.2(b). Within the inner span the stress $\sigma_{11}(x_1)$ is uniform along the length, while along the

thickness direction ($x_3$) the stress $\sigma_{11}(x_3)$ varies and there is a stress or strain gradient as shown by Fig. 2(c), which can generate electric polarization through the flexoelectric effect. Because the bar length is much greater than the bar thickness, we omit the shear stress and strain and only consider the principal stress and strain. Therefore, for simplification here only one suffix was used for describing the stress and strain tensors. The absolute value of surface stress was calculated using the following equation

$$\sigma_1(x_3)\big|_{x_3=\pm\frac{d}{2}} = \frac{3FL}{4wd^2} \qquad (3)$$

where $F$ is the load, $w$ the width, $d$ the thickness, and $L$ the outer span of the bend fixture.

The strain gradient in the thickness direction is given by

$$\frac{\partial \varepsilon_1(x_3)}{\partial x_3} = \frac{12st}{L^2} \qquad (4)$$

where $s$ is the crosshead speed and $t$ the time gone by.

Figure 3 presents data on the surface stress vs. strain curves for tests carried out at 1 mm/min and 0.2 mm/min crosshead speed. As shown in Fig.3(a), the flexure strength is measured to be 85 MPa. The softening of the samples at certain stress/speed levels (e.g., around 30 MPa for 1 mm/min crosshead speed) we believe corresponds to the onset of ferroelastic domain motion. As expected in PZT the sample becomes softer at lower loading rates due to the relaxational nature of ferroelastic domain switching. That ferroelastic switching has occurred at the higher loading levels is evident by a static remnant curvature in the sample after testing (Fig.4).

For an unpoled PZT ferroelectric ceramic at the morphotropic phase boundary, although individual grains may have lower symmetry (tetragonal or rombohedral) which permit piezoelectricity, in the volume of the ceramic one may expect a macroscopic

symmetry of $\infty\infty m$, so the non-zero components for the flexoelectric coefficient $\mu_{ijkl}$ should be $\mu_{1111}$, $\mu_{1122}$, and $\mu_{1212}$, or in matrix notation $\mu_{11}$, $\mu_{12}$ and $\mu_{44}$. Since in the current investigation any remnant piezoelectric effects from the top and bottom halves are well balanced and there is only strain gradient in the thickness or $x_3$ direction, so the generated electric polarization can be composed of only flexoelectric polarization as shown below,

$$P_3 = \frac{2}{d}\int_{\frac{d}{2}}^{\frac{d}{2}} d_{31}\sigma_1(x_3)dx_3 + \mu_{12}\frac{\partial\varepsilon_1(x_3)}{\partial x_3} = \mu_{12}\frac{\partial\varepsilon_1(x_3)}{\partial x_3} \qquad (5)$$

Flexoelectric polarization vs. strain gradient is displayed in Fig.5. It is clear that the behavior is not linear, showing a low-gradient and high-gradient linear behavior but of different slope. The changeover occurs at the gradient ~ 0.3 $m^{-1}$ corresponding to the onset of ferroelastic switching. At very small strain level, the sample is only subjected to elastic deformation, so the measured electric polarization response represents the intrinsic flexoelectric effect. The low-gradient slope corresponds to a flexoelectric coefficient $\mu_{12}$ $\approx$ 0.5 μC/m, and the high-gradient slope takes $\mu_{12} \approx$ 2.0 μC/m showing that ferroelastic domain wall motion aids the response.

The measured flexoelectric polarization is very small compared to the remnant polarization, only 1.6 μC/$m^2$ at a strain gradient of 1 $m^{-1}$. By using a relative permittivity value of $\varepsilon_r$ =2,200 (at 1 kHz), we figure out that a strain gradient of 1 $m^{-1}$ is equivalent to an electric field of 100 V/m, which is obviously too small compared to the coercive field. On a simple point charge model, flexoelectric coefficients $\mu_{ij}$ has the magnitude $e/a$ where $e$ is the electron charge and $a$ the dimension of the unit cell [5]. Thus in high-permittivity ferroelectrics we may expect from elementary theory of flexoelectricity [7] that $\mu_{ij}$ be proportional to dielectric susceptibility $\chi_{ij}$ following a relation [11]:

$$\mu_{ij} = \gamma \chi_{ij} \frac{e}{a} \qquad (6)$$

where $\gamma$ is a constant of value close to unity. For the PZT unpoled ceramic at low gradient levels the normalized flexoelectric coefficients $\mu_{12}/\chi_{22}$ at 20 °C is 0.23 nC/m giving $\gamma \approx 0.57$. In lead magnesium niobate (PMN) from our earlier study [9, 10], $\mu_{12}/\chi_{22}$ is 0.26 nC/m giving $\gamma \approx 0.65$, both in reasonable accord with the elementary theory. For $Ba_{0.67}Sr_{0.33}TiO_3$ (BST) ceramic at 25°C however $\mu_{12}/\chi_{22} \approx 3.72$ nC/m yielding a value $\gamma = 9.3$ [11] much higher than those in the lead-based systems.

It may be noted that in earlier investigations of the thermo-polarization effects Strukov et. al. [13] found exceedingly high values for the normalized thermopolarization coefficient ($b_{ij}^0$) in triglycine sulfate (TGS) which they attributed to the order-disorder nature of the ferroelectric phase change in this compound. We note that in $Ba_xSr_{1-x}TiO_3$ [13], there is strong evidence of a local order-disorder component between polarization vectors in the unit cell. It will be interesting to measure $\mu_{12}$ in potassium niobate tantate (KTN), where again order-disorder has been identified [14], to see if the coefficients are again anomalously large.

In conclusion, the PZT ceramic does exhibit modest flexoelectricity and ferroelastic domain wall motion enhances the response, but it is not possible in our samples using stress levels up to the full fracture strength to induce ferroelectric poling, although ferroelastic poling was patently obvious.

In the PZT thin films epitaxially grown on lattice-mismatched substrates the strain gradient between surfaces and strain-relieving dislocations can be exceedingly large and the flexoelectric effects could be of major importance in these systems.

**References**


[1] B. Jaffe, W. Cook, and H. Jaffe, *Piezoelectric Ceramics* (Academic Press, New York, 1971).

[2] S. Park, T. R. Shrout, *J. Appl. Phys.* **82**, 1804 (1997).

[3] R. Pelrine, R. Kornbluh, Q. Pei, J. Joseph, *Science* **287**, 836 (2000).

[4] V. S. Mashkevich, and K. B. Tolpygo, *Soviet Physics* JETP **5**, 435 (1957).

[5] Sh. M. Kogan, *Soviet Physics-Solid State* **5**, 2069 (1964).

[6] V. L. Indenbom, E. B. Loginov, and M. A. Osipov, *Sov. Phys.-Crystallogr.* **26**, 656 (1981).

[7] A. K. Tagantsev, *Sov. Phys. JETP* **61**, 1246 (1985).

[8] M. Marvan, A. Havránek, *Progr. Colloid Polym. Sci.* **78**, 33 (1988).

[9] Wenhui Ma, L. Eric Cross, *Appl. Phys. Lett.* **78**, 2920 (2001).

[10] Wenhui Ma, L. Eric. Cross, *Appl. Phys. Lett.* **79**, 4420 (2001).

[11] Wenhui Ma, L. Eric Cross, *Appl. Phys. Lett.* **81**, 3440 (2002).

[12] B.H. Strukov, A.V. Dautyan, E.L. Sorkin, K.A. Minaeva, *Bulletin of the Academy of Sciences of the USSR*: Physical Series **49**, 276 (1985).

[13] O. Tikhomirov, H. Jiang, J. Levy, *Appl. Phys. Lett.* 77, 2048 (2000).

[14] G. A. Samara, L. A. Boatner, *Phys. Rev.* **B61**, 3889 (2000).

**Figure Captions**

Fig.1 (a) Weak field dielectric permittivity (E ~ 10 V/cm) as a function of frequency and temperature in the soft PZT-5H sample measured; (b) dielectric hysteresis (P vs. E) in the soft PZT-5H composition.

Fig.2 Schematic illustration of strain gradient induced quasi-static polarization measurement, (a) typical 4-point bending fixture; (b) stress distribution; (c) schematic of strain gradient and the induced polarization along the thickness of the sample.

Fig.3 Surface stress as a function of strain measured at two different crosshead speeds on PZT-5H bar, (a) 1 mm/min cross head speed (the arrow indicates the level of stress at which the sample broke); (b) 0.2 mm/min crosshead speed.

Fig.4 Obvious static curvature induced in the PZT-5H sample by ferroelastic domain wall motion at the higher stress levels.

Fig.5 Polarization versus strain gradient for an unpoled PZT-5H sample induced during a 4-point bend test carried out at a crosshead speed of 0.2 mm/min.

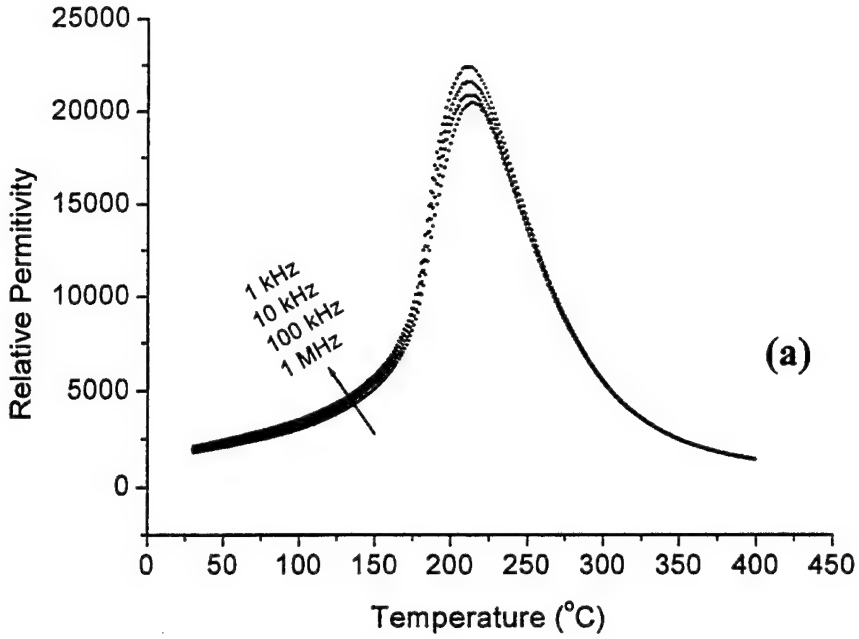
25000
20000
15000
10000
5000
0
Relative Permitivity
1 kHz
10 kHz
100 kHz
1 MHz
(a)
0
50
100
150
200
250
300
350
400
450
Temperature (°C)

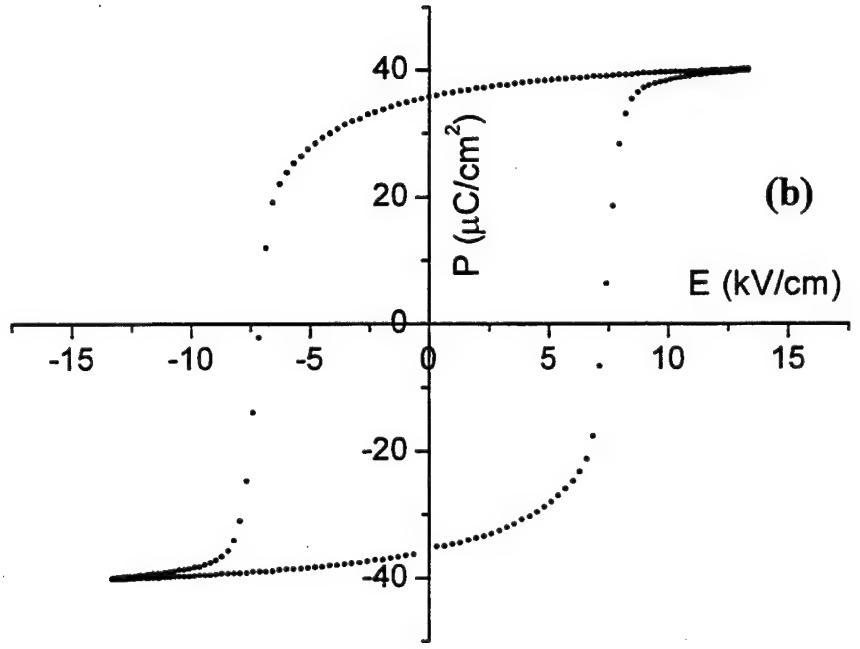
40
20
0
-20
-40
P (μC/cm²)
(b)
E (kV/cm)
-15
-10
-5
0
5
10
15

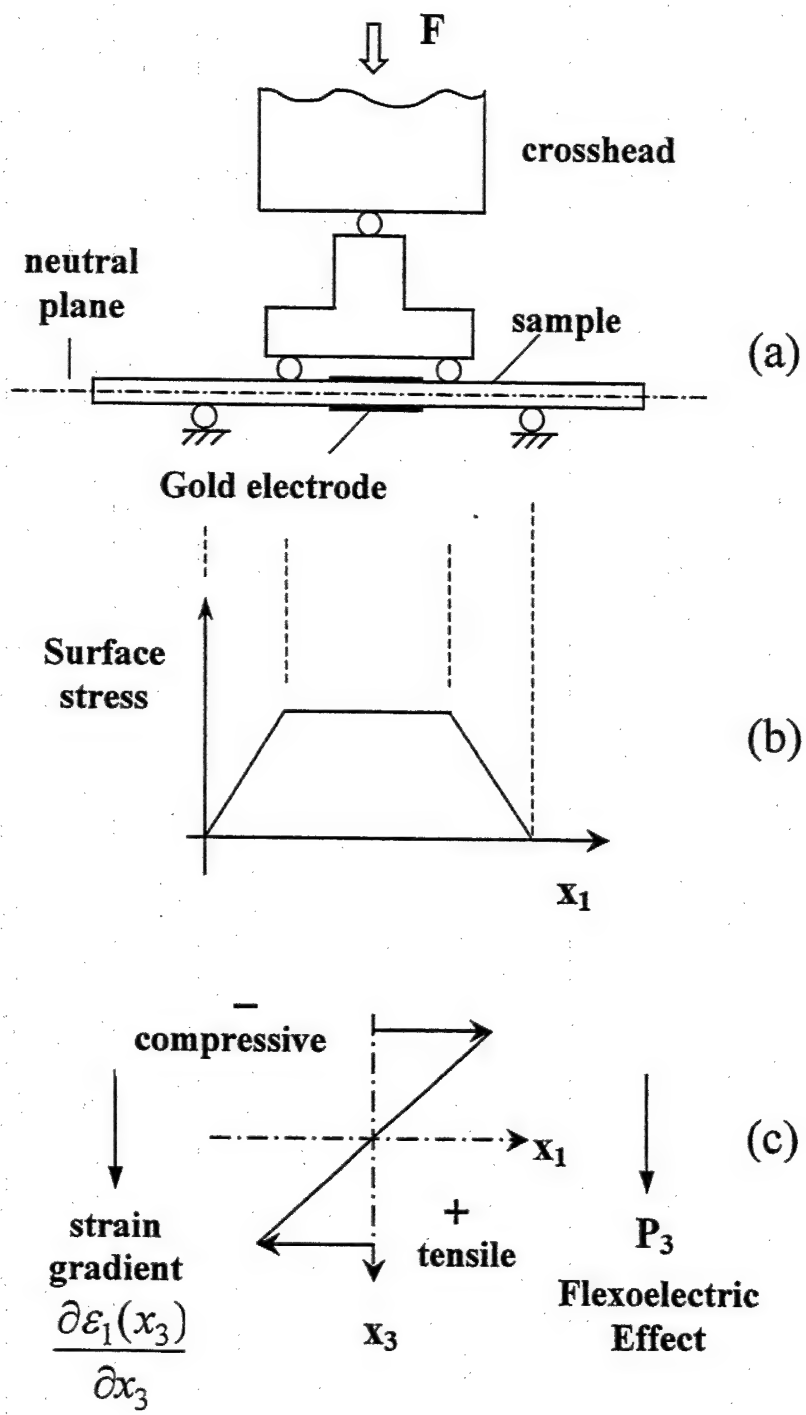
F
crosshead
neutral plane
sample
(a)
Gold electrode
Surface stress
(b)
x1
compressive
x1
(c)
strain gradient
$\frac{\partial \varepsilon_1(x_3)}{\partial x_3}$
+
tensile
x3
P3
Flexoelectric Effect

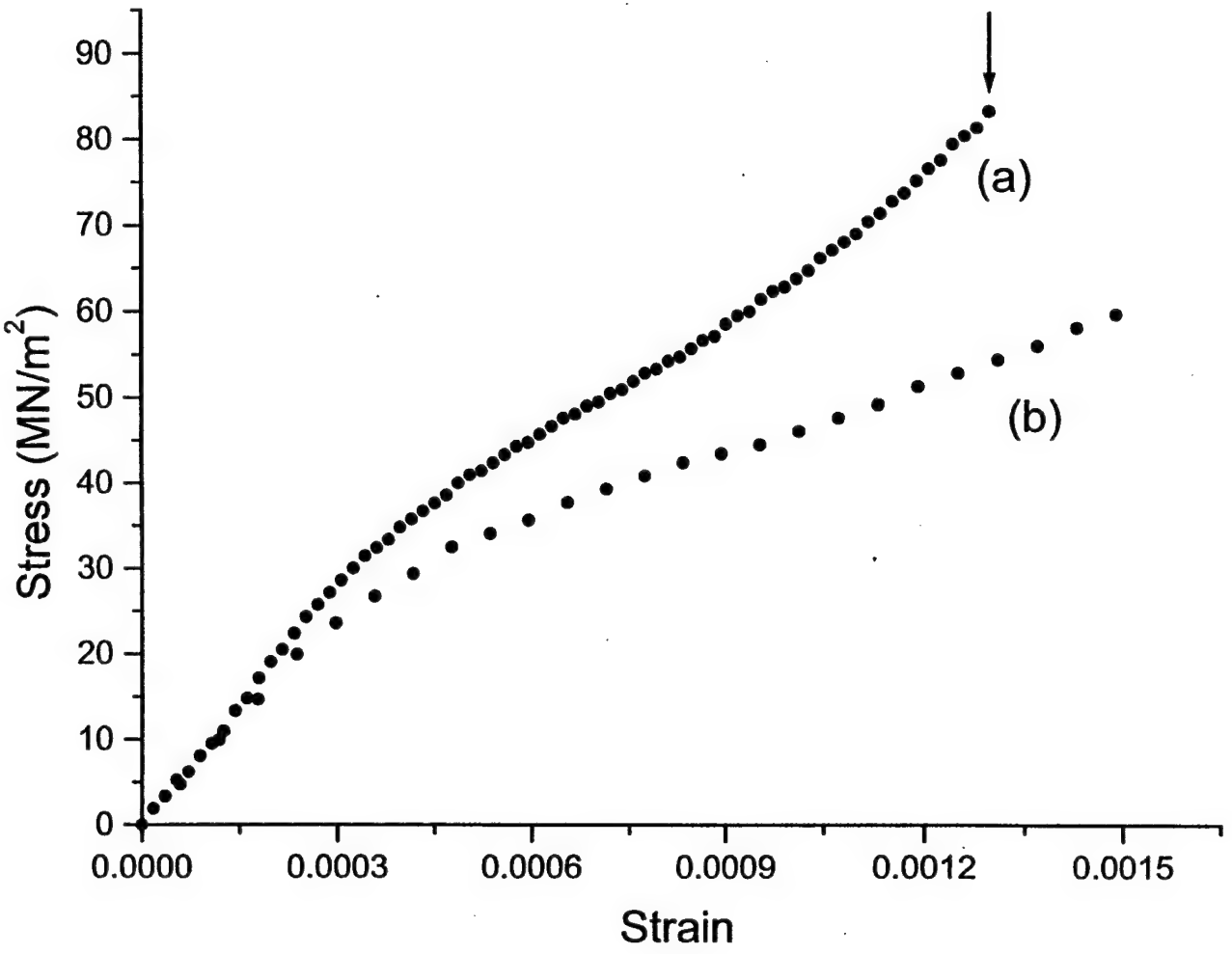
Stress (MN/m$^2$)
90
80
70
60
50
40
30
20
10
0
0.0000
0.0003
0.0006
0.0009
0.0012
0.0015
Strain
(a)
(b)

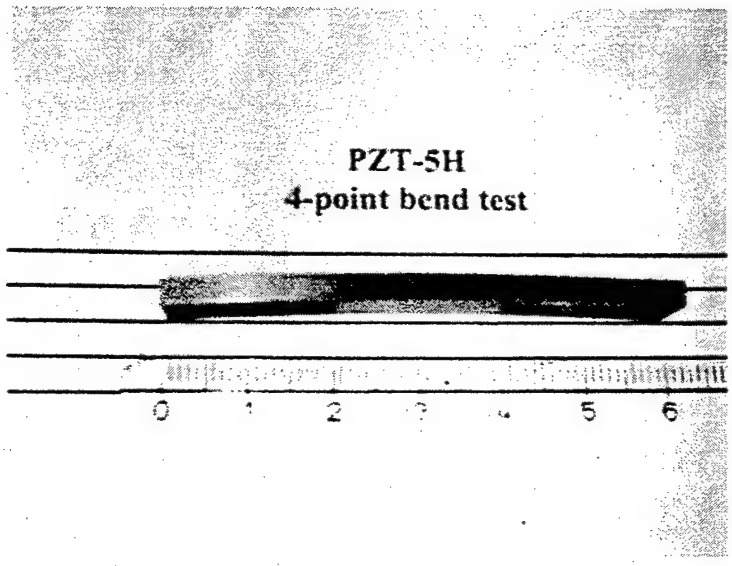
PZT-5H
4-point bend test
0
1
2
5
6

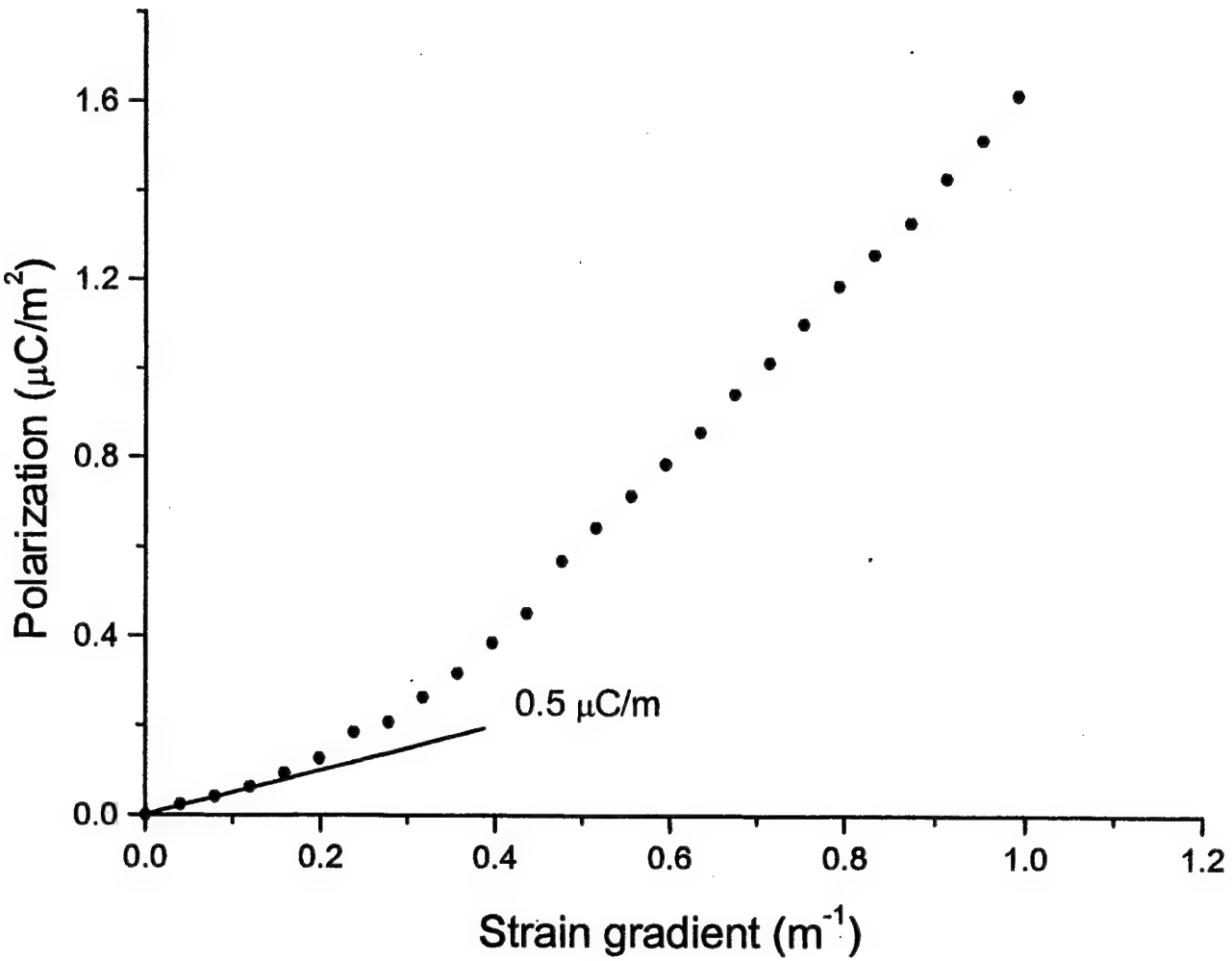
Polarization (μC/m²)
1.6
1.2
0.8
0.4
0.0
0.5 μC/m
0.0
0.2
0.4
0.6
0.8
1.0
1.2
Strain gradient (m⁻¹)

**List of the changes on Ms. #L02-3586**

1. The discussion of physical nature for the experimental result is added, please see the 1st and 2nd paragraphs in Page 7. It appears that the lead-based systems (PMN, PZT) are in reasonable accord with the elementary theory, while in BST the coefficients are exceedingly large. The order-disorder components are supposed to be related to this phenomenon, but future efforts are needed to clarify it.

2. Ref. 11 was completed, ref. 12 was changed, and refs. 13 and 14 were added.

3. Dielectric measurements and ferroelectric hysteresis loop were added and listed as Fig.1(a) and Fig.1(b), respectively.

   A picture showing the remnant curvature after 4-point bend test was added and listed as Fig.4.

4. Eqs 4, 5 and 9 in the old manuscript were removed in order to make the paper more concise.

5. In the abstract, the last paragraph in Page 3, and the last paragraph in Page 7, the significance of the investigations on flexoelectric effect were further elaborated and it is suggested that in thin films the effect can be of major importance.

# APPENDIX 11

*Ferroelectrics*, 2001, Vol. 252, pp. 129-136
Reprints available directly from the publisher
Photocopying permitted by license only

© 2001 OPA (Overseas Publishers Association) N.V.
Published by license under the
Gordon and Breach Science Publishers imprint.
Printed in Malaysia

# Microscopic Origin of the Two-Sublattice Model for Antiferroelectric State

R.A. HATT and W. CAO

*Materials Research Laboratory, The Pennsylvania State University, University Park, Pennsylvania 16802, USA*

*(Received June 2, 2000)*

The macroscopic model proposed by Kittel for antiferroelectrics assumes two interpenetrating sublattices with antiparallel polarizations. Although the model can explain many properties, it does not provide microscopic lattice displacement patterns associated with these sublattices since the order parameter in the model is a volume-averaged quantity. We propose a model based on microscopic positioning of symmetry elements and use an order parameter field directly associated with the local dipoles, which can provide a more transparent definition for the sublattices used in the Kittel model. We also include nonlocal gradient interactions to model multidomain structures and domain walls in ferroelectrics.

*Keywords:* antiferroelectric; Landau theory of phase transitions; sublattice model; microscopic symmetry

## INTRODUCTION

The antiferroelectric (AFE) state was modeled by Kittel based on the Landau theory and use two interpenetrating sublattices with equal but opposite polarizations.[1] This model can successful describe the double hysteresis loops[2] observed in antiferroelectrics, but contains no mechanism to describe the spatial relationship between the two

sublattices. In other words, there is no mechanism to guarantee the two sublattices to exist alternately in space to form the antiferroelectric state.

We propose a microscopic model for the AFE state, which not only provides the origin of the Kittel sublattices, but also gives the fixed spatial relationship between them. This model is based on microscopic symmetry and group theoretical methods. By adding the gradient energy associated with the AFE state, it can also be used to describe inhomogeneous structures, i.e., orientation twins and antiphase configurations.

In describing this model, we will use ammonium dihydrogen phosphate, or ADP, as a prototype. The method itself is quite general, and can be applied to any other antiferroelectric species.

## MICROSCOPIC SYMMETRY

The high-temperature paraelectric phase[3-6] of ADP is tetragonal, with space group $I\bar{4}2d$. At $T_C \approx -125°C$, a transition to an orthorhombic AFE phase[4-7] with space group $P2_12_12_1$ occurs, with a doubling of the primitive unit cell.

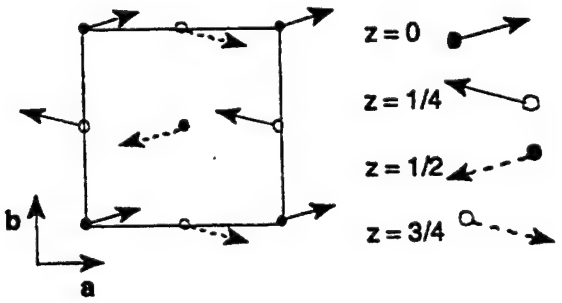


**Figure 1** Dipole moments within the AFE unit cell.

The transition is driven by an M-point soft mode corresponding to the $M_3M_4$ physically irreducible representation.[8] The antiferroelectric state consists of four individual molecular dipole moments, parallel to the ***a-b*** plane, within the unit cell of the AFE phase as shown in Fig. 1. The transition can be described by a two-component order parameter

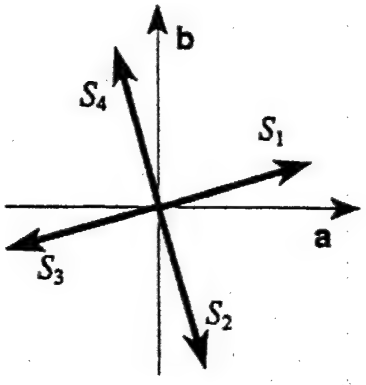


**Figure 2** Directions of (000) dipole moment in the four AFE domains.

that corresponds to the components of the molecular dipole at the (000) position. There are four energetically equivalent orientations for this dipole, as shown in Figure 2, and so there are four distinct domains in the AFE phase, with the two-component order parameters as listed in Table I. For convenience, we assume $p_a > p_b$ in the low temperature orthorhombic structure with space group $P2_12_12_1$.

TABLE I. Values of the order parameter for the four different domain states.

| Domain | Order Parameter |
|---|---|
| $S_1$ | $(p_a, p_b)$ |
| $S_2$ | $(p_b, -p_a)$ |
| $S_3$ | $(-p_a, -p_b)$ |
| $S_4$ | $(-p_b, p_a)$ |

Since the space groups of the two phases and the irreducible representation are known, the symmetry allowed distortions, based on the positions of the microscopic symmetry elements, can be calculated. This is done using the ISOTROPY computer program[9], and the results for the Wyckoff *a*-sites are shown in Table II. Using the distortions in this table, the dipole arrangement can be reproduced for any single domain state given in Table I (similar to the arrangement shown in Fig. 1 for $S_1$). The relationship between these allowed

distortions and the positions of the microscopic symmetry operations is illustrated for domain $S_1$ in Fig. 3

TABLE II. Group-theoretically allowed distortions at Wyckoff *a*-sites in domain $S_1$.

| Position | Distortions |
|---|---|
| $(0,0,0)$ | $p_a\,(1,0,0) + p_b\,(0,-1,0)$ |
| $(\frac{1}{2},\frac{1}{2},\frac{1}{2})$ | $p_a\,(-1,0,0) + p_b\,(0,1,0)$ |
| $(0,\frac{1}{2},\frac{1}{4})$ | $p_a\,(-1,0,0) + p_b\,(0,-1,0)$ |
| $(\frac{1}{2},1,\frac{3}{4})$ | $p_a\,(1,0,0) + p_b\,(0,1,0)$ |

## RELATIONSHIP TO THE KITTEL SUBLATTICES

Our model has focused on the microscopic structure of the AFE state. In order to understand the macroscopic behavior (in particular, the double hysteresis loops observed when the antiferroelectric material is placed in an external electric field), we must make a connection

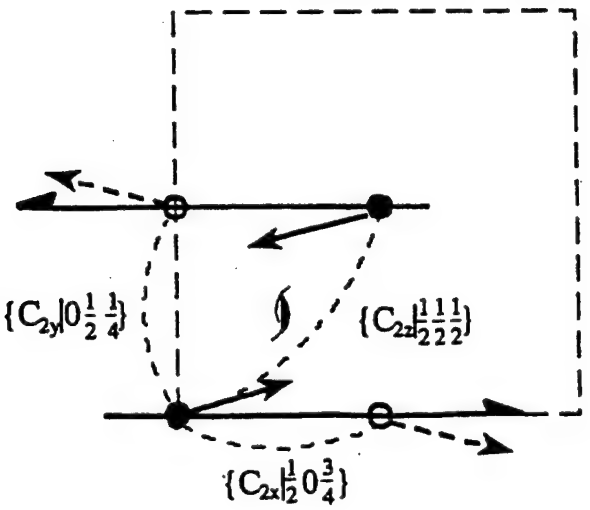


**Fig. 3** Actions of symmetry elements generate dipole arrangement

between our microscopic model and the Kittel macroscopic model. Since polarization is an average of molecular dipole moments over a given volume, the sublattice polarizations $P_1$ and $P_2$ in the one-dimensional Kittel model can be defined, in terms of the molecular dipole moments, as

$$P_1 = \frac{1}{V} \sum_{\substack{i \\ (p_{ai}>0)}} p_{ai}, \qquad P_2 = \frac{1}{V} \sum_{\substack{i \\ (p_{ai}<0)}} p_{ai}. \tag{1a,b}$$

In other words, in the AFE state those dipole moments with a positive component in the $a$-direction form one sublattice with polarization $P_1$, and those dipole moments with a negative component in the $a$-direction form the other sublattice with polarization $P_2$, as shown in Fig. 4.

On a unit cell level, we can further define the sublattices in terms of symmetry operations. Referring to the positioning of symmetry operations in Fig. 3, define $p_+$ and $p_-$ as

$$\begin{aligned} p_+ &= p + \{C_{2x} \mid \tfrac{1}{2}0\tfrac{3}{4}\}p \\ p_- &= \{C_{2z} \mid \tfrac{1}{2}\tfrac{1}{2}\tfrac{1}{2}\}p + \{C_{2y} \mid 0\tfrac{1}{2}\tfrac{1}{4}\}p \end{aligned} \tag{2a,b}$$

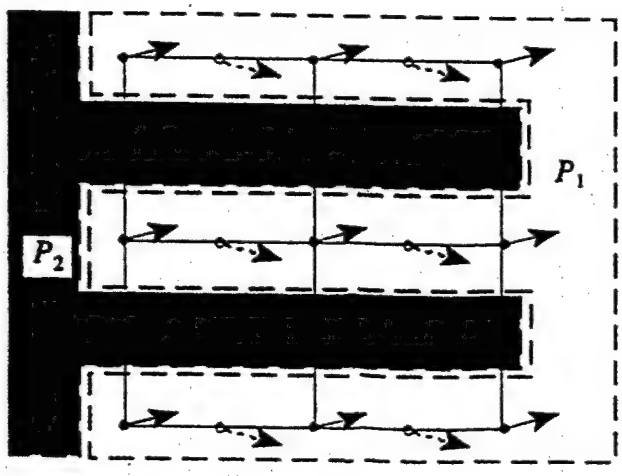


**Figure 4** Defining the macroscopic Kittel sublattices in terms of the microscopic dipole moments.

These two quantities, when volume averaged over all unit cells, naturally recreate the Kittel sublattices on the microscopic scale.

Our microscopic theory presented here not only can derive the macroscopic Kittel model, but also can account for the spatial relationships among dipoles of adjacent cells. More importantly, it also gives the dipole tilt, which occurs in the ADP system, leading to the observed unit cell doubling associated with the antiferroelectric phase transition.

## FREE ENERGY DENSITY

The free energy originally incorporated in the Kittel model included only local terms:

$$F = \alpha_1 ( P_1^2 + P_2^2 ) + \alpha_2 P_1 P_2 + \alpha_3 ( P_1^4 + P_2^4 ) \tag{3}$$

In our model, however, knowledge of the irreducible representation involved in the transition allows non-local terms to be added in the form of gradient invariants. For the ADP case being considered, this free energy density can be written as

$$\begin{aligned} F = {} & A(p_1^2 + p_2^2) + B_1(p_1^2 + p_2^2)^2 + B_2(p_1^4 + p_2^4) \\ & + B_3(p_1^3 p_2 - p_1 p_2^3) + C_1(p_1^2 + p_2^2)^3 + C_2(p_1^4 p_2^2 + p_1^2 p_2^4) \\ & + C_3(p_1^5 p_2 - p_1 p_2^5) + D_1\left[\left(\frac{\partial p_1}{\partial x}\right)^2 + \left(\frac{\partial p_2}{\partial y}\right)^2\right] \\ & + D_2\left(\frac{\partial p_1}{\partial x}\frac{\partial p_2}{\partial x} - \frac{\partial p_1}{\partial y}\frac{\partial p_2}{\partial y}\right) + D_3\left[\left(\frac{\partial p_1}{\partial y}\right)^2 + \left(\frac{\partial p_2}{\partial x}\right)^2\right] \end{aligned} \tag{4}$$

where $p_1$ and $p_2$ refer to the two components of the order parameter, i.e., the *a*- and *b*- components of the (000) molecular dipole moment. All coefficients are temperature independent except $A = A_0(T - T_0)$. With the addition of the order parameter gradient terms, this free energy can be used to describe the change in order parameter across a

domain wall in an inhomogeneous structure. For example, the change in order parameter across the domain wall in an orientation twin formed by domains $S_1$ and $S_2$ can be calculated by normalizing the order parameter using the following change of variables:

$$p_1 = p_a^{(0)} f_1 + p_b^{(0)} f_2 = p_a^{(0)} (f_1 + \kappa f_2) \tag{5a}$$

$$p_2 = p_b^{(0)} f_1 - p_a^{(0)} f_2 = p_a^{(0)} (\kappa f_1 - f_2) . \tag{5b}$$

This leads to a coupled set of differential equations upon energy minimization,

$$f_{1,x''x''} = -\tau f_1 - f_1^3 + f_1^5 + b' f_1 f_2^2 + c' (2 f_1^3 f_2^2 + f_1 f_2^4) \tag{6a}$$

$$f_{2,x''x''} = -\tau f_2 - f_2^3 + f_2^5 + b' f_1^2 f_2 + c' (f_1^4 f_2 + 2 f_1^2 f_2^3) , \tag{6b}$$

with the boundary condition

$$f_1 = \begin{cases} \sqrt{\frac{1}{2} + \sqrt{\frac{1}{4} + \tau}} , & x'' \to -\infty \\ 0 , & x'' \to +\infty \end{cases} , \quad f_2 = \begin{cases} 0 , & x'' \to -\infty \\ \sqrt{\frac{1}{2} + \sqrt{\frac{1}{4} + \tau}} , & x'' \to +\infty \end{cases} \tag{7}$$

where $\tau$ describes the temperature dependence. These equations can be solved numerically, and solutions for three temperatures are shown in Fig. 5. Further details of this process are reported elsewhere.[10-11]

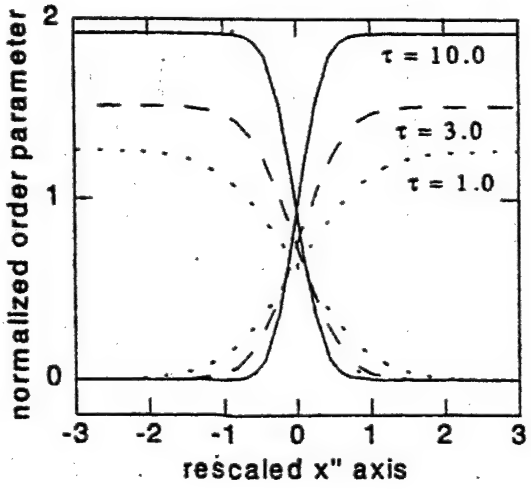


**Fig. 5** Calculated profiles for a representative orientation twin for three different temperatures.

## CONCLUSION

We proposed a Landau-Ginzburg type model for the antiferroelectric state based on microscopic symmetry and group theory. The order parameter corresponds to the local dipole moment within the unit cell, instead of the macroscopically averaged polarization conventionally used. Our model can rigorously derive the sublattices of the model proposed by Kittel and address the dipole tilt and cell doubling in the antiferroelectric transition. The so derived sublattices are intrinsically linked, which resolved the confusion encountered in the Kittle model.

The model is also extended to include order parameter gradient terms. These nonlocal interaction terms allow inhomogeneous structures, such as, orientation twins and antiphase walls, to be modeled.

### *Acknowledgements*

This research was sponsored by the Office of Naval Research.

### *References*

[1] C. Kittel, Phys. Rev., **82**, 729 (1951).
[2] L.E. Cross, J. Phys. Soc. Japan, **23**, 77 (1967).
[3] H. Meister, et. al., Phys. Rev., **184**, 550 (1969).
[4] H. Konwent and J. Lorenc, Phys. Stat. Sol. B, **88**, 747 (1978).
[5] L. Tenzer, B.C. Frazer, R. Pepinsky, Acta Cryst., **11**, 505 (1958).
[6] R.O. Keeling, Jr. and R. Pepinsky, Z. Kristallogr., **106**, 236 (1955).
[7] R. Blinc, J. Slak, and I. Zupancĉik, J. Chem. Phys., **61**, 988 (1974).
[8] S.C. Miller and W.F. Love, *Tables of Irreducible Representations of Space Groups and Co-Representations of Magnetic Space Groups* (Pruett, Boulder, 1967).
[9] H.T. Stokes and D.M. Hatch, *Isotropy Subgroups of the 230 Crystallographic Space Groups,* (World Scientific, Singapore, 1988). Internet and DOS (PC) versions of this software are available at *http://www.physics.byu.edu/~stokesh/isotropy.html.*
[10] R.A. Hatt and W. Cao, *Phys. Rev. B,* in press (July, 2000).
[11] R.A. Hatt and W. Cao, *J. Appl. Phys.,* to be published.

# APPENDIX 12

# Landau-Ginzburg model for antiferroelectric phase transitions based on microscopic symmetry

Richard A. Hatt
*Materials Research Laboratory, The Pennsylvania State University, University Park, Pennsylvania 16802*

Wenwu Cao
*Materials Research Laboratory and Department of Mathematics, The Pennsylvania State University, University Park, Pennsylvania 16802*

(Received 15 February 2000)

The only Landau-type model for antiferroelectric phase transitions was proposed by Kittel, in which two interpenetrating sublattices with opposite polarizations of equal amplitude were assumed. The theory, however, did not include any mechanism to specify the relative spatial positions of the two sublattices, and therefore could not address the cell doubling during antiferroelectric phase transitions. We propose a Landau-Ginzburg-type model based on microscopic symmetry and group theory, which can, without having to assume sublattices, account for all aspects of antiferroelectric states, including local dipole orientation and cell doubling. The average of these dipoles naturally leads to the Kittel model. The inclusion of gradient terms in the free energy allows the modeling of multidomain structures and domain walls in antiferroelectric states.

## INTRODUCTION

Kittel[1] proposed a macroscopic Landau-type model for the antiferroelectric (AFE) state by introducing two interpenetrating sublattices with opposite polarizations. His model describes a second-order transition from the paraelectric state to the antiferroelectric state, by truncating the free energy at the fourth order:

$$F=\alpha_1(P_1^2+P_2^2)+\alpha_2P_1P_2+\alpha_{11}(P_1^4+P_2^4), \qquad (1)$$

where $P_1$ and $P_2$ are the polarizations of the sublattices. If $\alpha_2>0$, the transition will favor $P_1$ and $P_2$ being antiparallel, making the low-temperature phase antiferroelectric. On the other hand, if $\alpha_2<0$, the transition will favor $P_1$ and $P_2$ being parallel, and the transition will lead to a ferroelectric state.[1–2]

This model has the intrinsic limitation that it contains only local interactions. In other words, there is no mechanism to fix the spatial relationship between the two sublattice polarizations within the crystal. This local model creates uncertainty in the antiferroelectric state. For example, the sublattice polarizations $P_1$ and $P_2$ are assumed at the same location in space (or can be anywhere in space), which leads to the cancellation of $P_1$ and $P_2$. Such a situation does not fully describe the antiferroelectric state in which adjacent primitive cells acquire opposite dipole moments and the local polarization at any space point is actually nonzero. Using group-theoretical techniques, we propose a continuum model for the antiferroelectric state built upon microscopic symmetry. The symmetry allowed distortions associated with the soft mode are given in our model, which accounts for the formation of antiparallel dipoles in adjacent cells. The free energy has also been expanded to include gradient terms of the order parameter so that multidomain structures, such as orientation twins and antiphase walls, can be modeled using the same formulation. Specifically, in this paper we will use ammonium dihydrogen phosphate $(NH_4)H_2(PO_4)$ (commonly referred to as ADP) as a prototype system to illustrate the procedure and the characteristics of the antiferroelectric phase transition.

## ANTIFERROELECTRIC PHASE TRANSITION

The high-temperature phase of ADP is tetragonal with space group $I\bar{4}2d$.[3–6] Following the notation of the *International Tables for Crystallography*,[7] the conventional (nonprimitive) unit cell contains four formula units. Two of the formula units are in the primitive cell while the other two are related by the centering translation $(\frac{1}{2}\frac{1}{2}\frac{1}{2})$. At $T_C\approx -125\,^{\circ}\mathrm{C}$, the material undergoes an antiferroelectric transition to an orthorhombic phase with space group $P2_12_12_1$.[6,8] The transition is driven by a zone-boundary $M$-point soft mode and results in ionic displacements that create one dipole moment in each formula unit (four dipoles per AFE unit cell) as shown in Fig. 1. These dipole moments form a net antiferroelectric polarization along the [100] or [010] of the parent phase. This means that the fourfold rotational inversion axis of the parent paraelectric phase is lost during the transition, which leads to two rotationally related, energetically equivalent orientation domain states in the low-temperature phase. Moreover, the transition causes a primitive-cell doubling (equivalently, the centering point in the conventional parent cell is lost), leading to two additional

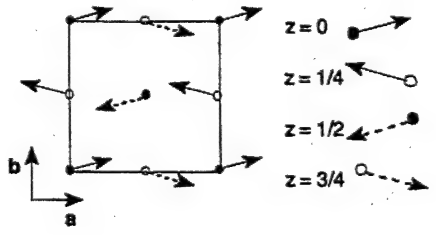


FIG. 1. Dipoles formed in the antiferroelectric phase of ADP in a conventional cell. The lattice displacement pattern can be generated from group theory.

 ©2000 The American Physical Society

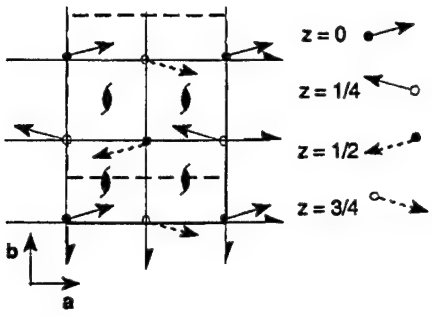


FIG. 2. Microscopic positions of the symmetry elements, creating the antiferroelectric polarization. The AFE unit cell is shown by the dashed line, with origin at $(0, \frac{1}{4}, \frac{3}{8})$. The screw axes parallel to **a** are at $z=\frac{3}{8}$, and the screw axes parallel to **b** are at $z=\frac{1}{4}$.

antiphase states that are translationally related to the two orientation states. Overall, there are four possible domains in the AFE state of ADP.

## GROUP THEORETICAL DESCRIPTION OF THE TRANSITION

Once the structures and space groups of the high- and low-temperature phases have been determined, the microscopic positions of the symmetry elements are fixed (we will use the settings of Ref. 7), as shown in Fig. 2. Specifically, we note that the three mutually perpendicular twofold screw axes in the AFE phase do not allow a net dipole moment for the unit cell of the low-temperature phase, although they do allow antiferrolectric polarizations.

The $M$-point soft mode driving the transition in ADP may be described by the physically irreducible $M_3M_4$ representation,[4] which is simply the direct sum $M_3 \oplus M_3^*$ (here we use the labeling of Miller and Love[9]). This representation carries a two-component order parameter (OP), $(p_1,p_2)$, whose values are listed in Table I. Physically, the OP corresponds to the molecular dipole moments within the **a**-**b** plane; $p_1$ represents the component along the **a** direction, and $p_2$ represents the component along the **b** direction. This OP is a continuum field, which is equal to the dipole moment at the sites of each formula unit.

Knowing the irreducible representation allows the lattice distortions that arise in the transition to be calculated using the ISOTROPY[10] software package. For simplicity we will restrict our discussion to distortions arising at Wyckoff **a** sites only, which are listed in Table II. These distortions can be used to construct the dipole arrangement within the low-temperature unit cell. As an example, consider the distortions that arise in domain $S_1$, for which the OP is $(p_1,p_2) = (p_a,p_b)$. If $p_a > p_b$, the distortions result in the configuration shown in Fig. 1, which agree well with the observed dipolar distribution by Blinc *et al.*[8]

TABLE I. Values of the order parameter for different domain states.

| Domain | Order parameter |
|---|---|
| $S_1$ | $(p_a,p_b)$ |
| $S_2$ | $(p_b,-p_a)$ |
| $S_3$ | $(-p_a,-p_b)$ |
| $S_4$ | $(-p_b,p_a)$ |

TABLE II. Group theoretically allowed distortions at Wyckoff **a** sites in domain $S_1$.

| Position | Distortions | Relationship to (0,0,0) site |
|---|---|---|
| (0,0,0) | $p_a(1,0,0)+p_b(0,-1,0)$ | $\{E\|000\}$ |
| $(\frac{1}{2},\frac{1}{2},\frac{1}{2})$ | $p_a(-1,0,0)+p_b(0,1,0)$ | $\{C_{2z}\|\frac{1}{2}\frac{1}{2}\frac{1}{2}\}$ |
| $(0,\frac{1}{2},\frac{1}{4})$ | $p_a(-1,0,0)+p_b(0,-1,0)$ | $\{C_{2y}\|\frac{1}{2}\,\overline{1}\,\frac{3}{4}\}$ |
| $(\frac{1}{2},1,\frac{3}{4})$ | $p_a(1,0,0)+p_b(0,1,0)$ | $\{C_{2x}\|\frac{1}{2}\,1\,\frac{3}{4}\}$ |

Figure 1 was constructed based only on the microscopic positioning of the symmetry elements and the allowed distortions from group theoretical considerations, as in Fig. 2. For example, a dipole moment at position (0, 0, 0) necessarily means, by action of the screw axis parallel to the $z$ axis, an oppositely directed dipole moment at the parent cell centering point of $(\frac{1}{2}\frac{1}{2}\frac{1}{2})$. The screw axis parallel to the $x$ axis further implies, from these two dipoles, that the other two antialigned dipoles within the AFE unit cell must be present. Hence, there is no need for defining sublattices and no need to explain why such sublattices would adopt exactly equal magnitudes but opposite orientation. More importantly, the spatial relationship between the two sublattices naturally comes out of our model. If a single dipole moment is formed within a parent formula unit, one can generate its counterparts by symmetry requirements to form the antiferroelectric polarization of the whole unit cell of the low-temperature phase. Also, since the dipole moment at the centering point $(\frac{1}{2}\frac{1}{2}\frac{1}{2})$ is opposite to the dipole moment at (0,0,0), the doubling of the unit cell size is naturally explained.

## HYSTERESIS AND THE RELATION TO THE SUBLATTICES PROPOSED BY KITTEL

A well-known characteristic of antiferroelectrics is the double hysteresis loop, as shown in Fig. 3. In the one-dimensional antiferroelectric model proposed by Kittel, there is no net polarization. However, if an external electric field is applied, the sublattice polarization parallel to the field grows and the other sublattice polarization opposite to the field shrinks, resulting in a net polarization. When the field strength becomes sufficiently large, the polarization in the direction opposite to the field abruptly switches orientation to become parallel to the field, resulting in a ferroelectric state. Because of symmetry constraints, a double hysteresis

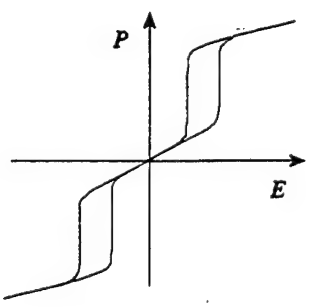


FIG. 3. Double hysteresis loop, a characteristic of the antiferroelectric state.

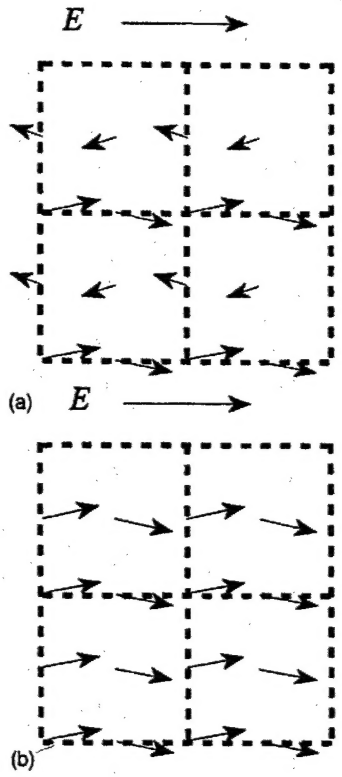


FIG. 4. Molecular dipole moments in the presence of an external electric field, (a) before switching and (b) after switching.

will be produced during such a switching process.[2]

In our model, we describe the hysteresis in terms of the dipole moments associated with each of the four formula units in an AFE unit cell. Consider an external electric field applied to domain $S_1$, parallel to the **+a** direction. This field will interact with the dipoles, causing $p_a>0$ to increase in magnitude and $p_a<0$ to decrease in magnitude, as shown in Fig. 4(a). Note that $p_b$ is not affected in our model. At sufficiently large field strength, the dipoles with $p_a$ antiparallel to the external field will flip so that $p_a$ becomes parallel to **+a**, as shown in Fig. 4(b). This results in a state in which the dipole components are parallel along the **a** direction and antiparallel along the **b** direction. It is a ferroelectric state with the polarization along **a**, but with a cell size twice that of the Kittel model.

In order to make the connection between our microscopic model and the Kittel macroscopic model, we use the definition of the polarization, which is an average of molecular dipole moments over a given volume $P=(1/V)\Sigma p_i$. The sublattice polarizations $P_1$ and $P_2$ in the Kittel one-dimensional model can then be defined, in terms of the molecular dipole moments in our model, as

$$P_1=\frac{1}{V}\sum_{(p_a>0)} p_{ai}, \quad P_2=\frac{1}{V}\sum_{(p_a<0)} p_{ai}. \tag{2}$$

In other words, in the AFE state the formula units containing a positive dipole-moment component in the **a** direction form one sublattice with polarization $P_1$, and the formula units containing a negative dipole-moment component in the **a** direction form the other sublattice with polarization $P_2$. The difference between the microscopic theory presented here and macroscopic continuum theory of Kittel is that the latter cannot provide the spatial relationships among dipoles of adjacent cells, and cannot account for the dipole tilt which occurs in the ADP system.

TABLE III. Invariants for the antiferroelectric transition driven by a soft mode corresponding to the $M_3M_4$ irreducible representation.

| | |
|---|---|
| $\phi^{(2)}=p_1^2+p_2^2$ | $\delta_1=\left(\frac{\partial p_1}{\partial x}\right)^2+\left(\frac{\partial p_2}{\partial y}\right)^2$ |
| $\phi_1^{(4)}=(p_1^2+p_2^2)^2$ | $\delta_2=\frac{\partial p_1}{\partial x}\frac{\partial p_2}{\partial x}-\frac{\partial p_1}{\partial y}\frac{\partial p_2}{\partial y}$ |
| $\phi_2^{(4)}=p_1^4+p_2^4$ | $\delta_3=\left(\frac{\partial p_1}{\partial y}\right)^2+\left(\frac{\partial p_2}{\partial x}\right)^2$ |
| $\phi_3^{(4)}=p_1^3p_2-p_1p_2^3$ | |

## LANDAU-GINZBURG FREE ENERGY BASED ON MICROSCOPIC SYMMETRY

Adding OP gradient terms to the free energy, i.e., using the Landau-Ginzburg-type free energy, will allow us to describe inhomogeneous structures, such as orientational twins and antiphase walls. The invariant polynomials of the OP and its derivatives can also be obtained using the ISOTROPY program. In this paper, we have truncated the free energy at the fourth power of the OP to limit our discussions to a second-order transition. We also assume that the OP field varies slowly in space so that only the first derivatives of the OP are included in the free energy. We write

$$F=A\varphi^{(2)}+B_i\varphi_i^{(4)}+D_i\delta_i \quad (i=1,2,3), \tag{3}$$

where the invariant polynomials $\varphi^{(2)}$, $\varphi_i^{(4)}$, and $\delta_i$ are given in Table III. The coefficients $A=A_0(T-T_c)$, $B_i$, and $D_i$ are constants.

For single domain states, all derivatives of the OP must vanish; i.e., $\delta_i=0$. Considering the single domain state $S_1$, the two component OP is $(p_a,p_b)$ with both $p_a$ and $p_b$ nonzero. Since the symmetry of the low-temperature phase is known, the ionic displacements and dipole moments in each unit cell can be determined experimentally from neutron scattering. In other words, the ratio of the amplitudes $\kappa=p_a/p_b$ can be measured in the antiferroelectric state

$$p_b=\kappa p_a. \tag{4}$$

Because all derivatives of the OP vanished in the single domain state, energy minimization of Eq. (3) leads to

$$\left.\frac{\partial F}{\partial p_1}\right|_{p=(p_a,\kappa p_a)}=2Ap_a+[4B_1(l+\kappa^2)+4B_2+B_3(3\kappa-\kappa^3)]p_a^3=0, \tag{5a}$$

$$\left.\frac{\partial F}{\partial p_2}\right|_{p=(p_a,\kappa p_a)} = 2A\kappa p_a + \left[4B_1(1+\kappa^2)+4B_2\kappa^2 + B_3\left(\frac{1}{\kappa}-3\kappa\right)\right]\kappa p_a^3 = 0. \quad (5b)$$

In order for Eqs. (5a) and (5b) to give the same solution for $p_a$, the sum involving the $B_2$ and $B_3$ terms must be equal,

$$4B_2+B_3(3\kappa-\kappa^3)=4B_2\kappa^2+B_3\left(\frac{1}{\kappa}-3\kappa\right), \quad (6)$$

which can be written as a fourth-degree polynomial equation in $\kappa$:

$$\kappa^4+b\kappa^3-6\kappa^2-b\kappa+1=0 \quad (7)$$

with $b=4B_2/B_3$. This equation has four roots,

$$\left(\kappa_1,-\frac{1}{\kappa_1},\kappa_2,-\frac{1}{\kappa_2}\right), \quad (8)$$

where

$$\kappa_1=-\frac{b}{4}-\frac{1}{4}\sqrt{16+b^2}+\frac{1}{2\sqrt{2}}(16+b^2)^{1/4}\sqrt{b+\sqrt{16+b^2}}, \quad (9a)$$

$$\kappa_2=-\frac{b}{4}+\frac{1}{4}\sqrt{16+b^2}+\frac{1}{2\sqrt{2}}(16+b^2)^{1/4}\sqrt{-b+\sqrt{16+b^2}}. \quad (9b)$$

One of the above solutions, Eq. (9a), will be less than 1 and greater than 0 (i.e., $0<\kappa<1$), which is the solution we seek since it corresponds to the OP in domain $S_1$, with $p_a>p_b$ (see Fig. 1). Because Eq. (7) does not contain any temperature-dependent terms, the solution $\kappa$ will be temperature independent.

Once $\kappa$ is determined, Eq. 5(a) allows the value of $p_a$ to be determined as a function of the expansion coefficients in Eq. (3):

$$p_a^2=\frac{-2A}{4B_1(1+\kappa^2)+4B_2+B_3(3\kappa-\kappa^3)}. \quad (10)$$

We note that the expansion coefficient $A$ is temperature dependent, $A=A_0(T-T_c)$, so that the amplitude of the order parameter satisfies the universal relation for a second order phase transition, i.e.,

$$p_b \propto p_a \propto \sqrt{T_c-T}.$$

## ORDER-PARAMETER PROFILES FOR TWINS AND ANTIPHASE STRUCTURES

The Landau-Ginzburg free energy, Eq. (3), allows us to describe inhomogeneous structures. We will study both orientation twins and antiphase structures in the AFE phase, each composed of two different domains separated by a domain wall. Since there are four possible domains in the AFE state, there will be $4\times4=16$ possible pairings of domains from which we can construct orientation twins or antiphase walls. However, using the idea of equivalence in group theory, the pairing set can be much reduced. We find three classes of two-domain structures to be considered, as listed in Table IV along with the type of structure represented (the trivial degenerate structure that has the same domain on both sides of the wall is actually a single domain structure): two orientation twins, and one antiphase structure.

TABLE IV. Equivalence classes of two-domain (twins and antiphase) structures.

| Domain pair | Type | Relation to $S_1$ |
|---|---|---|
| $(S_1,S_2)$ | orientation twin | $\{\sigma_{bd}\|0\frac{1}{2}\frac{1}{4}\}$ |
| $(S_1,S_4)$ | orientation twin | $\{\sigma_{bd}\|\frac{1}{2}\,1\,\frac{3}{4}\}$ |
| $(S_1,S_3)$ | antiphase structure | $\{E\|\frac{1}{2}\frac{1}{2}\frac{1}{2}\}$ |

We will first consider the orientation twin formed by domains $S_1$ and $S_2$. The domain wall orientation for such a twin can be determined by strain matching,[11,12] noting that this transition belongs to the Aizu[13] species $\bar{4}2mF222$. The strain allowed domain walls are the planes $x=\pm y$ (see Fig. 5). Since properties of the crystal will change only along the direction normal to this wall, we will rotate to a new coordinate system so that $x'$ is normal to the wall. The OP components (and any other properties of the twin) then will be functions of $x'$ only. This means that the derivatives in the gradient part of the free energy, Eq. (3), can be rewritten as

$$\frac{\partial p}{\partial x}\to\pm\frac{1}{\sqrt{2}}\frac{\partial p}{\partial x'}, \quad \frac{\partial p}{\partial y}\to\pm\frac{1}{\sqrt{2}}\frac{\partial p}{\partial x'}. \quad (11)$$

For such a twin structure, the OP varies across the wall from its value in $S_1$ to its value in $S_2$,

$$p_1=\begin{cases}p_a, & x'\to-\infty\\ p_b, & x'\to+\infty\end{cases}, \quad p_2=\begin{cases}p_b, & x'\to-\infty\\ -p_a, & x'\to+\infty\end{cases}. \quad (12)$$

In order to match the boundary conditions in Eq. (12), it is convenient to change the dependent variables

$$p_1=p_af_1+p_bf_2,$$
$$p_2=p_bf_1-p_af_2. \quad (13)$$

Here, the functions $f_1$ and $f_2$ are normalized order-parameter components and have simpler boundary conditions

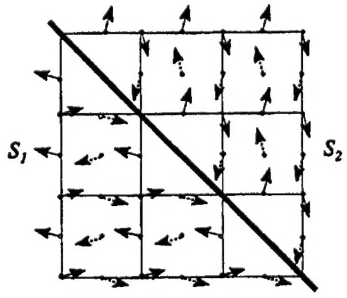


FIG. 5. Twin structure with a domain wall oriented parallel to the $(1\bar{1}0)$ lattice plane.

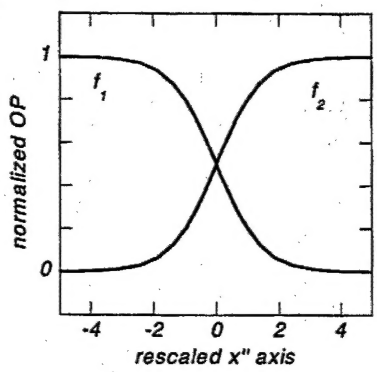


FIG. 6. Numerical solution for the order parameter profile of an orientation twin with $\gamma'=3.0$.

$$f_1=\begin{cases}1, & x'\to-\infty\\ 0, & x'\to+\infty\end{cases},\quad f_2=\begin{cases}0, & x'\to-\infty\\ 1, & x'\to+\infty\end{cases}. \tag{14}$$

We now apply the Euler-Lagrange equations

$$\frac{d}{dx'}\frac{\partial F}{\partial f_{i,x'}}=\frac{\partial F}{\partial f_i}\quad (i=1,2) \tag{15}$$

and obtain a coupled set of ordinary differential equations

$$D\frac{d^2f_1}{dx'^2}=\alpha f_1+\beta f_1^3+\gamma f_1 f_2^2,$$

$$D\frac{d^2f_2}{dx'^2}=\alpha f_2+\beta f_2^3+\gamma f_1^2 f_2, \tag{16}$$

where

$$D=(1+\kappa^2)(D_1+D_3),$$

$$\alpha=(1+\kappa^2)A, \tag{17}$$

$$\beta=p_a^2[4(1+\kappa^2)^2B_1+4(1+\kappa^4)B_2+4\kappa(1-\kappa^2)B_3],$$

$$\gamma=p_a^2[4(1+\kappa^2)^2B_1+24\kappa^2B_2-12\kappa(1-\kappa^2)B_3].$$

In order to meet the boundary conditions in Eq. (14), we must have

$$\alpha+\beta=0. \tag{18}$$

The $x'$ axis can be rescaled to

$$x''=x'\sqrt{\frac{\beta}{D}} \tag{19}$$

to arrive at a simplified set of dimensionless equations

$$\frac{d^2f_1}{dx''^2}=-f_1+f_1^3+\gamma' f_1 f_2^2,$$

$$\frac{d^2f_2}{dx''^2}=-f_2+f_2^3+\gamma' f_1^2 f_2, \tag{20}$$

where $\gamma'=\gamma/\beta$ is temperature independent. Equations (20) have been solved for other systems[14] and the solutions for the choice of $\gamma'=3.0$ are illustrated in Fig. 6.

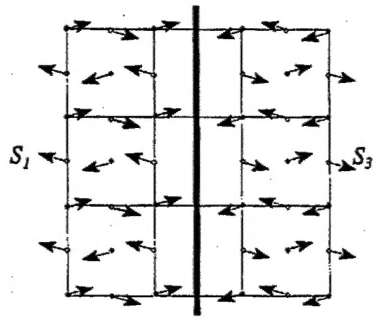


FIG. 7. Dipole arrangement in the vicinity of an antiphase wall between $S_1$ and $S_3$.

For the second type of orientation twin involving domains $S_1$ and $S_4$, the boundary conditions are

$$p_1=\begin{cases}p_a, & x'\to-\infty\\ -p_b, & x'\to+\infty\end{cases},\quad p_2=\begin{cases}p_b, & x'\to-\infty\\ p_a, & x'\to+\infty\end{cases}. \tag{21}$$

We make the following change of variables

$$p_1=p_a f_1-p_b f_2,$$

$$p_2=p_b f_1+p_a f_2. \tag{22}$$

The same set of equations, Eqs. (20), for the functions $f_1$ and $f_2$ can be derived and similar solutions can be obtained.

For the antiphase structures, we cannot use the strain compatibility relations to predict the orientation of the wall since the strain compatibility relations are automatically satisfied. However, we can simplify the equations to quasi-one-dimensional using the same procedure described above. Again, we rotate the coordinate system such that $x'$ is perpendicular to the wall. The derivatives in the gradient part of the free energy can again be expressed in terms of derivatives in the $x'$ direction. By defining the new normalized order parameter $g$,

$$p_1=p_a g,\quad p_2=p_b g \tag{23}$$

and using a rescaling of the space variable similar to Eq. (19) (but dependent upon the specific orientation of the wall), we can simplify the system to a single differential equation for the function $g$,

$$\frac{d^2g}{dx''^2}=-g+g^3. \tag{24}$$

For the antiphase structure formed by domains $S_1$ and $S_3$ (see Fig. 7), the boundary conditions are

$$p_1=\begin{cases}-p_a, & x'\to-\infty\\ p_a, & x'\to+\infty\end{cases},\quad p_2=\begin{cases}-p_b, & x'\to-\infty\\ p_b, & x'\to+\infty\end{cases}, \tag{25}$$

or

$$g=\begin{cases}-1, & x''\to-\infty\\ 1, & x''\to+\infty\end{cases}. \tag{26}$$

Equation (24) has the analytic solution

$$g = \tanh\left(\frac{x''}{\sqrt{2}}\right). \tag{27}$$

## SUMMARY AND CONCLUSIONS

We have proposed a Landau-Ginzburg model based on microscopic symmetry to describe a second-order antiferroelectric phase transition. The OP field used is directly correlated to the local dipole moments of the formula units, instead of the macroscopically averaged polarization. Our model not only can derive the macroscopic model proposed by Kittel but also can address the dipole tilt and cell doubling in the antiferroelectric transition. There is no need to assume separate sublattices in our model.

When the antiferroelectric state is switched to a ferroelectric state by an external electric field, our model predicts a unit cell size twice as large as that of the macroscopic picture obtained from previous investigations.[2] This picture is more consistent with the microscopic picture observed experimentally that the dipoles are actually tilted from the **a** and **b** directions.

There are four domain states in the antiferroelectric phase and they form two distinct orientation twins and one type of antiphase structure. The addition of gradient energy terms in the free energy allows us to model multidomain inhomogeneous structures. Numerical solutions for the inhomogeneous OP profiles describe the gradual change of the dipole amplitude and orientation across the domain walls. We find that if, in the free energy, only the coefficient of the quadratic term is assumed to be temperature dependent, the local dipoles have a fixed orientation independent of temperature, while the amplitude of the dipole moment is a function of temperature.

## ACKNOWLEDGMENTS

This work was sponsored by the Office of Naval Research under the MRUI Grant and the Grant for Piezocrystal Resource.

[1] C. Kittel, Phys. Rev. **82**, 729 (1951).
[2] L. E. Cross, J. Phys. Soc. Jpn. **23**, 77 (1967).
[3] H. Meister *et al.*, Phys. Rev. **184**, 550 (1969).
[4] H. Konwent and J. Lorenc, Phys. Status Solidi B **88**, 747 (1978).
[5] L. Tenzer, B. C. Frazer, and R. Pepinsky, Acta Crystallogr. **11**, 505 (1958).
[6] R. O. Keeling, Jr. and R. Pepinsky, Z. Kristallogr. **106**, 236 (1955).
[7] *International Tables for Crystallography*, edited by T. Hahn (Reidel, Dordrecht, 1983).
[8] R. Blinc, J. Slak, and I. Zupančik, J. Chem. Phys. **61**, 988 (1974).
[9] S. C. Miller and W. F. Love, *Tables of Irreducible Representations of Space Groups and Co-Representations of Magnetic Space Groups* (Pruett, Boulder, 1967).
[10] H. T. Stokes and D. M. Hatch, *Isotropy Subgroups of the 230 Crystallographic Space Groups* (World Scientific, Singapore, 1988). Internet and DOS (PC) versions of this software are available at URL http://www.physics.byu.edu/~stokesh/isotropy.html
[11] J. Sapriel, Phys. Rev. B **12**, 5128 (1975).
[12] J. Fousek and V. Janovec, J. Appl. Phys. **40**, 135 (1969).
[13] K. Aizu, J. Phys. Soc. Jpn. **27**, 387 (1969).
[14] W. Cao and G. R. Barsch, Phys. Rev. B **41**, 4334 (1990).